Investigation of the interaction of ceramide and acyl-coenzyme A with the mitochondrial associated protein, endozepine, using heteronuclear NMR

Ezenwa James Onyemata

A minithesis submitted in partial fulfillment of the requirements for the award of Master of Science degree (Structural Biology) in the Faculty of Science, University of the Western Cape.

Supervisor: Dr. David Pugh

December 2005

Abstract

E. J Onyemata

MSc minithesis, Department of Biotechnology, Faculty of Natural Sciences, University of the Western Cape

Endozepine is an alternative name for the testis-specific isoform of the acyl-CoA binding protein (t-ACBP). Acyl-CoA binding proteins form a highly conserved family of proteins, which bind long chain fatty acid esters with nanomolar affinity. They are also known to be endogenous ligands to the γ-amino butyric acid (GABA) receptor in the central nervous system and to play a role in a wide variety of cellular functions such as vesicular trafficking, fatty acid biosynthesis and gene regulation.
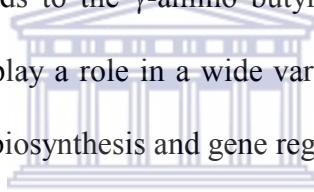
A role for endozepine in apoptosis was suggested through promoter gene trapping studies using CHO22 cells in which 90 % reduction in the expression of endozepine correlated with delayed mitochondrial permeabilization, a reduced activation of caspase-3 (an activator of apoptosis) and a consequent resistance to C_2-ceramide induced apoptosis. Transduction studies using Tat-GFP-ELP fusion protein showed that endozepine restored the sensitivity of mutant CHO22 cells to C_2-ceramide induced apoptosis.

In this thesis, we have investigated two hypotheses for the involvement of endozepine in ceramide-induced apoptosis. The first hypothesis is that endozepine contributes to apoptosis through the transport of palmitoyl-CoA, a substrate required for the *de novo*

synthesis of ceramide. The second hypothesis is that endozepine interacts directly with ceramide leading to interaction with peripheral benzodiazepine receptor and a subsequent opening of the mitochondria permeability transition pore, leading to apoptosis.

^{15}N-labelled endozepine was over-expressed in *E. coli* and purified using the GST purification system. Protein purification was carried out using a combination of affinity, anion and size exclusion chromatography. ^{15}N-HSQC NMR spectra were used to monitor putative interactions between endozepine, C_2-ceramide, C_{16}-ceramide and palmitoyl-CoA. Endozepine was double-labelled with ^{13}C and ^{15}N for CBCA(CO)NH and HNCACB triple resonance NMR experiments in order to carry out backbone resonance assignment. Our results showed no significant binding of endozepine to C_2-ceramide or C_{16}-ceramide, while a strong binding to palmitoyl-CoA was observed. The residues involved in endozepine-palmitoyl-CoA binding have been identified. We have generated a 3 dimensional model of endozepine based on its homology to ACBP and have mapped our NMR binding data onto the model and have shown that the identified binding residues fit into the expected binding pocket.

Our results suggest that endozepine functions as a transport molecule of palmitoyl-CoA, which lends support to out first hypothesis that endozepine is required for the *de novo* synthesis of ceramide.

Investigation of the interaction of ceramide and acyl-coenzyme A with the mitochondrial associated protein, endozepine, using heteronuclear NMR

Ezenwa James Onyemata

December 2005

Keywords:

Endozepine

Apoptosis

Ceramide

Coenzyme-A

Protein

Recombinant

Heteronuclear

NMR

Binding

HSQC

Dedicated to the memory of my father, Onyemata Ucheoma Christian

Declaration

I declare that **"Investigation of the interaction of ceramide and acyl-coenzyme A with the mitochondrial associated protein, endozepine, using heteronuclear NMR"** is my own work, that it has not been submitted for any degree or examination in any other university, and that all the sources I have used or quoted have been indicated or acknowledged by complete references.

Ezenwa James Onyemata   December 2005

Signed……………………………….

Abbreviations

ACBP   Acyl-CoA binding protein

ANT   Adenine nucleotide translocator

APAF-1   Apoptosis activating factor-1

AIF   Apoptosis inducing factor

Bad   Bcl-x_L/Bcl-2-associated death promoter

Bax   Bcl-2-associated x protein

BH   Bcl-2-homology domain

Bid   BH3 interacting death domain

BLAST   Basic local alignment search tool

Bok   Bcl-2-related ovarian killer

bp   Base pair

CAPK   Ceramide-activated protein kinases

CAPP   Ceramide-activated protein phosphatase

Caspases   Cysteine aspartic acid-specific protease

CHO   Chinese hamster ovary

DBI   Diazepam binding inhibitor

DD   Death domain

DED   Death effector domain

DIABLO   Direct IAP-binding protein with low pI

DNA   Deoxyribonucleic acid

DR3   Death receptor 3

DR6   Death receptor 6

DTT	Dithiothreitol
EDTA	Ethylene diamine tetra acetic acid
FADD	Fas associated death domain
Fas	Fabroblast associated
Fas R	Fas receptor
GABA	Gamma-aminobutyric acid
GFP	Green fluorescent protein
GST	Glutathione S-Tranferase
HSQC	Heteronuclear single quantum coherence
IBM	Inhibitor of apoptosis binding domain
IAP	Inhibitor of apoptosis
IMM	Inner mitochondria membrane
IPTG	Isopropyl β-D-thiogalactopyranoside
KDa	Kilo Dalton
LB	Luria Bertani broth
LCA-esters	Long chain acyl-CoA esters
LGA	Longevity assurance gene
MPTP	Mitochondria permeability transition pore
NMR	Nuclear magnetic resonance
OMM	Outer mitochondria membrane
PAGE	Poly acrylamide gel electrophoresis
PBR	Peripheral benzodiazepine receptor
PCR	Polymerase chain reaction

PK11195	1-(2-chlorophenyl-N-methyl-1-methylpropyl)-3-Isoquinolinecarboxamide
PMSF	Phenylmethylsulphonyl fluoride
PRAX-1	PBR associated protein-1
PP1	Protein phosphatase 1
PTP	Permeability transition pore
SDS	Sodium dodecyl sulphate
Smac	Second mitochondria-derived activator of caspases
Smase	Sphingomyelinases
SPT	Serine palmitoyl-CoA transferase
TEMED	*N, N, N', N'*-Tetramethylethylenediamine
TNF	Tumour necrosis factor
TRAIL	TNF-related apoptosis inducing ligand
UV	Ultra violet
VDAC	Voltage-dependent anion channel
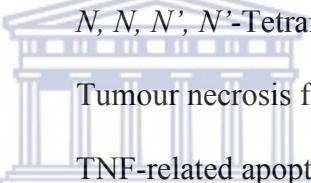
Acknowledgements

Table of contents

Chapter 1: Introduction

1.1 Endozepine

Acyl-CoA binding protein is a highly conserved 10 kDa protein, which binds long chain fatty acids with high specificity and affinity. It was originally identified as an inhibitor of the binding of diazepam to the GABA receptor within the central nervous system, and hence the alternative name "diazepam binding inhibitor". While its precise biological function is not known, it is suggested to be involved in a variety of cellular tasks such as vesicular trafficking, fatty acid biosynthesis and gene regulation. ACBP has evolved in mammals to give rise to several sub-groups including the testis specific isoform (t-ACBP), which is also known as endozepine.
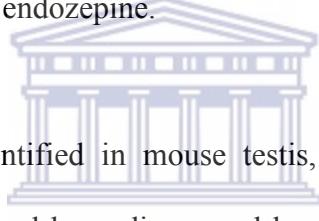
Endozepine was originally identified in mouse testis, encoded by a male germ cell specific gene transcript which had been discovered by differential cloning (Pusch *et al.* 1996). It was shown to have approximately 50 % sequence identity with ACBP, as well as similar lengths and predicted secondary structure. It also contains the binding motif for mid-long chain acyl-CoA esters, conserved in members of the ACBP family (Pusch *et al.* 1996). While several functions have been suggested for endozepine, it is thought to perform ACBP-like functions in maturing spermatozoa (Pusch *et al.* 2000). A role for endozepine in apoptosis has been proposed as a result of studies which revealed that endozepine is one of the proteins released from the mitochondria during permeability transition (Patterson *et al.* 2000). A number of other proteins released from the mitochondria during the permeability transition, including cytochrome c, apoptosis inducing factor (AIF), endonuclease G, Smac/DIABLO, have been implicated in

apoptosis (Van Loo *et al.* 2002). However, no precise role for endozepine in apoptosis has so far been identified.

A role for endozepine in apoptosis has been proposed as a result of promoter gene trapping studies using CHO22 cells (Meyer, 2003). A 90 % reduction in the expression of endozepine was found to correlate with delayed mitochondrial permeabilization, a reduced activation of caspase-3 (an activator of apoptosis) and a consequent resistance to C_2-ceramide induced apoptosis. Transduction of endozepine into mutant CHO22 cells restored the sensitivity of the cells to C_2-ceramide induced apoptosis (Meyer and Rees unpublished). Two hypotheses have been proposed for the role of endozepine in C_2-ceramide induced apoptosis. The first is that endozepine acts as a transport molecule of palmitoyl-CoA, which is a substrate required for the intracellular synthesis of ceramide. The abolishing of palmitoyl-CoA transport would lead to reduction in the intracellular levels of ceramide, reducing the sensitivity of cells to C_2-ceramide-induced apoptosis. The second hypothesis is that endozepine interacts directly with ceramide, facilitating its interaction with the peripheral benzodiazepine receptor (PBR) and leading to opening of the mitochondria permeability transition pore and subsequent apoptosis.

1.2   The Acyl-CoA binding protein family

ACBP is a multifunctional 10 kDa cytosolic protein, which is thought to interact with two different types of receptors, the γ-amino butyric acid (GABA) receptor of the central nervous system and those of peripheral tissues. ACBP was first identified as diazepam (benzodiazepine derivative) binding inhibitor (DBI) due to its ability to

inhibit the binding of diazepam to the α-subunit of the GABA receptor (Guidotti *et al.* 1983). It is thought therefore to be involved in the allosteric regulation of GABA receptors within the central nervous system (Costa and Guidotti 1991). It also interacts with the peripheral type benzodiazepine receptor (PBR), which is located on both cellular and intracellular membranes, including the outer mitochondrial membrane and the glial cells of the central nervous system (Gavish *et al.* 1992). ACBP is a highly conserved protein which is recognized to bind to long chain fatty acids and coenzyme A with high specificity and affinity (K_D 1-10 nM), and is expressed in most eukaryotic species (Kragelund *et al.* 1999a). Although experimental data suggest that the yeast ACBP homologue is involved in a variety of cellular tasks such as vesicular trafficking, fatty acid biosynthesis, gene regulation and protein sorting, the precise biological function of ACBP remains unknown (Faergeman *et al.* 2004; Gaigg *et al.* 2001; Mandrup *et al.* 1992).
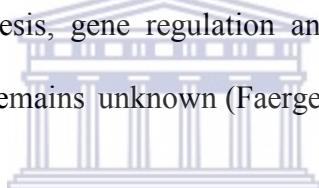
ACBP is reported to occur both as a single domain protein and as a domain within multi-domain proteins (Knudsen *et al.* 1993). A representation of the ACBP family is shown in Fig. 1.1. Phylogenic analysis shows that mammalian ACBP has evolved into a number of subgroups: l-ACBP, t-ACBP, b-ACBP and m-ACBP (Kragelund *et al.* 1999b). The most widely expressed isoform, l-ACBP (the basal isoform), was first isolated from bovine liver (Mogensen *et al.* 1987). It is 86-92 residues in length, highly conserved and is expressed in most tissues. It does not contain cysteine residues and is thought to be the ancestor of other ACBP isoforms. The testis specific isoform, t-ACBP, is expressed at high levels in the post meiotic stages of the male germ cells (Kragelund *et al.* 1999b). It

Generally expressed-ACBP

Brain specific-ACBP

Testis specific-ACBP

ACBP + enoyl-CoA isomarase domain

ACBP + ankyrin binding repeats

Membrane associated ACBP domain

Enoyl-CoA isomerase binding domain

ACBP

Pfam B

Ankyrin binding repeats

Low complexity

Trans-membrane

SMART Domain

Coil coiled region
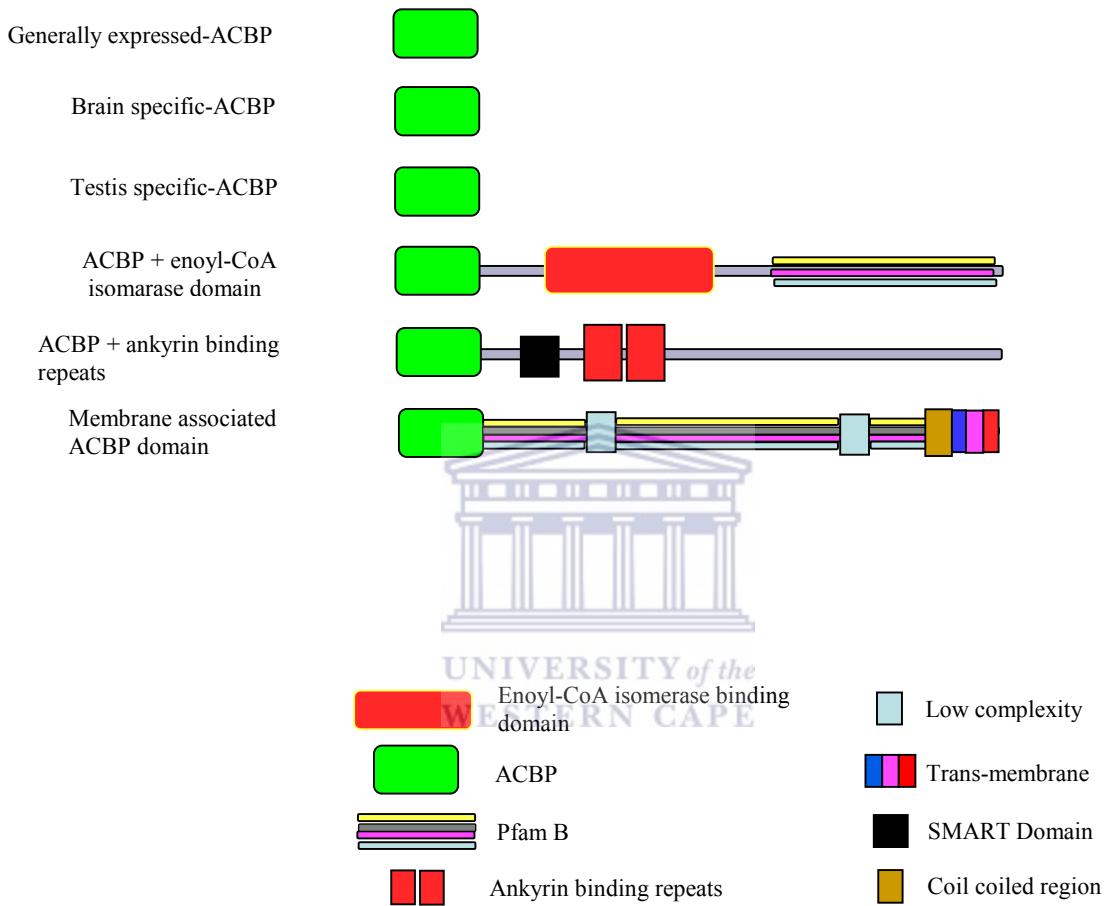
Fig. 1.1: Classification of the ACBP in mammals. ACBP occurs as a single domain protein such as I-ACBP, b-ACBP, t-ACBP or as a single domain in multi-domain proteins such as the ACBP + enoyl-CoA isomerase binding domain, ACBP + ankyrin binding repeats or the membrane associated ACBP. The image was generated using information accessible through http://www.sanger.ac.uk/cgi-bin/Pfam.

contains three cysteine residues and is expressed in rat, mouse and cow (Pusch *et al.* 1996). The gene product of t-ACBP is non-functional in higher primates and humans (Ivell *et al.* 2000). The brain specific isoform b-ACBP is expressed in duck and frog and it contains a single cysteine residue (Metzner *et al.* 2000; Owens *et al.* 1989; Rose *et al.* 1994). The fourth sub-group consists of a group of larger proteins, which have ACBP occurring as a domain, and have been suggested to be the membrane bound isoform (Knudsen *et al.* 2000).

The multi-domain proteins containing ACBP domains have been divided into three groups. The first group consists of the large membrane-associated proteins containing an N-terminal ACBP domain (Chye 1998; Chye *et al.* 1999; Chye *et al.* 2000). The second group are multifunctional enzymes which contain both ACBP and enoyl-CoA isomerase domain (Geisbrecht *et al.* 1999; Suk *et al.* 1999). Although this protein falls under the peroxisomal Δ2-Δ3-enoyl-CoA isomerases, which are known to play a role in peroxisomal β-oxidation of unsaturated fatty acids, the precise role of the ACBP and enoyl-CoA isomerase domain complex is not known. The third group contains both an ACBP domain and one or more ankyrin repeats (Chye *et al.* 2000). The ankyrin binding repeats have been reported to be involved in protein-protein interactions and may therefore target the ACBP-ankyrin repeats to specific cellular sites (Knudsen *et al.* 1993). The precise role of the ACBP domain within these multi-domain proteins is not clear.

1.3 Expression and biological functions of acyl-CoA binding protein

I-ACBP is expressed at all stages of mammalian life and in most tissues, with differential

expression observed among many cell types (Burgi *et al.* 1999; Knudsen *et al.* 1993) differential expression observed among many cell types (Burgi *et al.* 1999; Knudsen *et al.* 1993). High expression levels have been observed in steroid producing cells such as the glomerulosa and fasciculate cells of the adrenal cortex, while lower expression levels have been observed in cells involved in the transport of water and electrolyte such as the intestinal mucosa and distal convoluted tubules of the kidney (Bovolin *et al.* 1990). Expression of ACBP is induced on the stimulation of the growth of human prostate cancer cell line, and is reported to be associated with the stimulation of *de novo* fatty acid synthesis, cholesterol synthesis and lipid accumulation (Esquenet *et al.* 1997). *In vitro* differentiation of 3T3-L1 pre-adipocytes is suggested to lead to the up-regulation of ACBP levels, along with triglyceride accumulation and *de novo* fatty acid synthesis (Hansen *et al.* 1991). These results suggest that ACBP may be involved in secretion, transport, energy metabolism and lipid synthesis. ACBP has also been implicated in a wide range of cellular functions and is suggested to play a role in pool formation and the transport of acyl-CoA esters (Faergeman and Knudsen 1997).

Acyl-CoA esters function as intermediates in lipid biosynthesis, fatty acid degradation, gene regulation and intermediary metabolism (Faergeman and Knudsen 1997). They are amphipathic in nature and are thought to partition into phospholipid vesicles where they inhibit a large number of cellular functions as well as enzymes at very low concentrations (Faergeman and Knudsen 1997). It has been shown that acyl-CoA esters at concentrations as low as 5.5 nM can inhibit acetyl-CoA carboxylase (Knudsen *et al.* 1993). Since the acyl-CoA esters are suggested to be involved in a wide range of cellular

functions and have been shown to inhibit the activity of a number of enzymes, a need for the tight control of their intra-cellular concentration has been suggested (Rasmussen *et al.* 1993; Shirra *et al.* 2001). ACBP is suggested to be an endogenous carrier molecule of the acyl-CoA esters, which mobilize acyl-CoA esters from point of synthesis to point of use (Kragelund *et al.* 1999b). This allows for large amounts of acyl-CoA esters to be readily available for specific purposes such as lipid synthesis while maintaining an overall low free intracellular concentration of acyl-CoA esters (Rasmussen *et al.* 1993).

A role for ACBP in the transport of acyl-CoA esters has been reported in yeast (Schjerling *et al.* 1996). *S. cerevisiae* strains with targeted disruption of the *Acb1p* showed an increase in the intracellular concentration of the long chain acyl-CoA esters but an overall decrease in the intracellular concentration of the short chain acyl-CoA esters. The increase in LCA esters within the mutants did not translate to higher levels of fatty acids due to the supposed inability to incorporate the available LCA esters into the fatty lipid synthetic machinery.

A role for ACBP in the protection of the acetyl-CoA carboxylase, acetyl-CoA synthase and adenylate translocase from inhibition by the acyl-CoA esters has been suggested (Kragelund *et al.* 1999b). Previous studies have shown that acetyl-CoA synthase was activated for the synthesis of acyl-CoA esters but inhibited by the accumulation of LCA esters (Schjerling *et al.* 1996). In *S. cerevisiae*, Acb1p is suggested to protect acetyl-CoA synthase from inhibition by acyl-CoA esters due to the preferential synthesis of short and medium chain length acyl-CoA esters over LCA esters because of

the preference for termination over elongation of the acyl-CoA esters (Schjerling *et al.* 1996). This reported preference for the synthesis of short and medium chain acyl-CoA esters is thought to ensure the uptake of limited amounts of the intermediate chain length acyl-CoA esters into medium chain length fatty acids, resulting in reduced levels of intermediate chain length acyl-CoA esters. This is thought to lead to a shortfall in the synthesis of LCA-esters and thus ensures the non-inhibition of acetyl-CoA synthase. Faergeman and co-workers have suggested that Acb1p plays a role in the synthesis of ceramide in *S. cerevisiae* (Faergeman *et al.* 2004).

ACBP also inhibits the hydrolysis of acyl-CoA esters by the acyl-CoA hydrolases. Acyl-CoA hydrolases function to regulate the intracellular concentration of acyl-CoA esters by serving as scavengers in instances where the pool of acyl-CoA esters is high (Sabri *et al.* 2001). Acyl-CoA hydrolases are thought to be active in the control of pool size of acyl-CoA esters in the presence of the ACBP. Additional functions of ACBP in specific tissues have been suggested. An elegant example is the Midgut ACBP (mg-ACBP), which is exclusively expressed in the mid gut of the larva and the pheromone gland of the adult female fly (Matsumoto *et al.* 2001). The pheromone gland contains a mixture of triglycerides which includes the hexadecadiene-1-ol (bombykol), synthesized from palmitoyl-CoA (Matsumoto *et al.* 2001). This suggests that the mg-ACBP ensures the supply of palmitoyl-CoA and may be implicated in the shuttling of acyl-CoA intermediates in the pheromone synthetic pathway.

t-ACBP (also known as endozepine) is highly expressed within the post-meiotic male germ cells of the testis, with low levels of expression detected in a few other tissues including the ovary (Pusch *et al.* 1999). Expression was limited to elongating spermatids and spermatozoon and is first evident during spermatid elongation (Pusch *et al.* 2000). Immuno-cytochemistry studies have shown that the majority of endozepine is located within the middle piece of the spermatozoon tail, enriched within the mitochondria (Pusch *et al.* 2000). This suggests that endozepine may be involved in spermatid development and metabolism and its presence in the spermatozoa may reflect the usage of fatty acids as a primary source of energy during spermatid metabolism. This is supported by the observation that mice with low expression levels of endozepine lacked later stages of spermatogenic development (Valentin *et al.* 2000). The functional importance of endozepine is suggested by the fact that it is highly conserved with 54 % amino acid identity across 11 different sequences (Ivell *et al.* 2000). A multiple sequence alignment from a number of species is shown in Fig. 1.2. The conserved residues include the acyl-CoA binding motif. Although endozepine has been reported to be non-functional in humans, two closely related but independent human genes h*ELP1* and h*ELP2*, have been identified (Ivell *et al.* 2000). The h*ELP2* is thought to have arisen due to the duplication of a domain in h*ELP1* but maintains an overall 57 % identity to h*ELP1* (Ivell *et al.* 2000).

Comparison of the h*ELP1* and h*ELP2* transcripts with homologues in the rat, mouse and bovine genomes showed that a frame shift mutation had occurred (Ivell *et al.* 2000). The h*ELP1* gene transcript has a single nucleotide insertion which leads to the synthesis of a
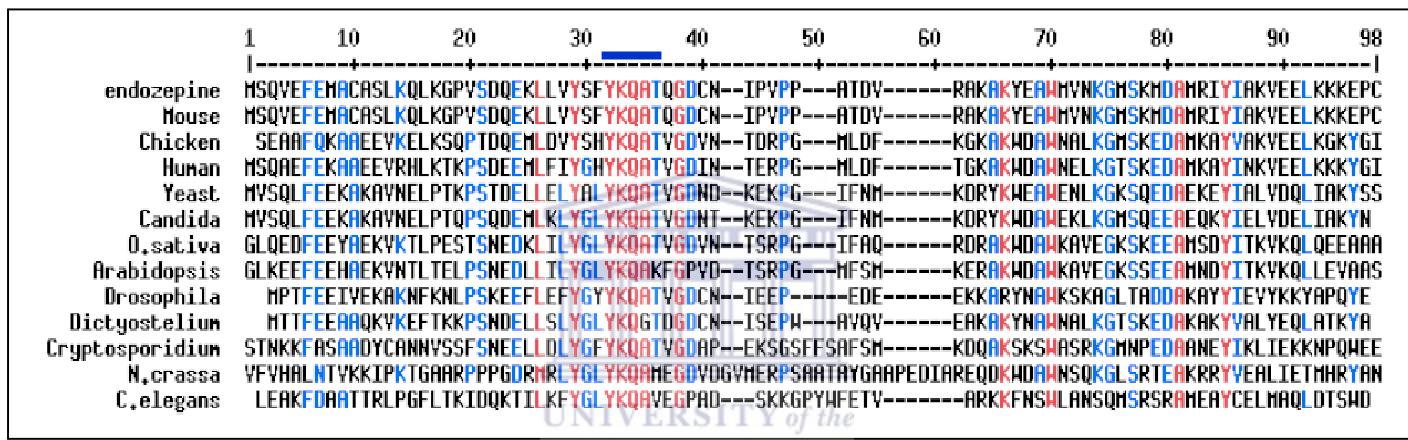
Fig. 1.2: Multiple sequence alignment of ACBP amino acid sequences. Highlighted residues indicate conserved or semi-conserved amino acids. The blue bar above the alignment indicates the binding motif (YKQAT) for the mid-long chain acyl-CoA esters.

truncated protein with 66 amino acid residues (Ivell *et al.* 2000). In h*ELP2* transcript, a single nucleotide insertion gives rise to a new open reading frame (ORF) coding for a protein with 91 amino acid residues (Ivell *et al.* 2000). A BLAST search of the DNA data base using transcripts of h*ELP1* and h*ELP2* showed that the $3'$ un-translated region (UTR) of the h*ELP1* and h*ELP2* included repetitive elements suggesting that the h*ELP1* and h*ELP2* may have arisen from transposition (Ivell *et al.* 2000). Functional analysis of ELP transcripts in other primates showed no frame shift mutations in the marmoset and macaque although mutations were observed in the chimpanzee, gorilla and orangutan. This suggests that the functionality of endozepine homologues may have been lost during primate evolution (Ivell *et al.* 2000). Endozepine homologues in humans and higher mammals transcribe at low levels but have not been detected using Western Blots, which suggest that their gene products are non-functional (Ivell *et al.* 2000). Since endozepine is highly conserved in lower organisms and possibly involved in sperm development and metabolism, it is unclear why the human and higher ape versions are non-functional. One possible explanation for loss of function of endozepine in humans comes from studies suggesting that l-ACBP is preferentially expressed at low levels in somatic cells of the testis (Kolmer *et al.* 1997). Since endozepine and l-ACBP are detected in the testis, it is possible that the loss of function in higher mammals could be compensated for by an up-regulation of other isoforms of ACBP. This may suggest that endozepine is functionally interchangeable with other members of the ACBP family.

1.4 The sphingolipid pathway and acyl-CoA binding protein

1.4.1 Ceramide and the sphingomyelin pathway

The sphingomyelin pathway has been described as a ubiquitous signalling system analogous to conventional systems such as the cAMP and phosphoinositide pathways, conserved from yeast to humans (Hannun 1996). Several enzymes involved in sphingolipid metabolism, such as the sphingomyelinases which function within the sphingomyelin pathway, are now recognized as having an affect on apoptosis through regulation of intracellular ceramide levels. Ceramide is described as a membrane sphingolipid consisting of *N*-acylated carbon chains and sphingosine with bioactive break down products, and is thought to mediate cellular functions such as proliferation, differentiation, growth arrest and apoptosis (Hannun and Luberto 2000; Pettus *et al.* 2002). It serves as a central molecule within the sphingolipid pathway and is recognized to serve as a second messenger molecule for the induction of apoptosis in the extrinsic pathway (Heinrich *et al.* 1999; Pettus *et al.* 2002). Usually the execution of apoptosis involves the activation of specific cysteine proteases termed caspases, a process that may involve ligand-membrane receptor interaction (the extrinsic pathway) or the activation of the mitochondria (the intrinsic pathway) (de Thonel and Eriksson 2005). The extrinsic pathway occurs through the binding of specific protein ligands to trans-membrane receptors belonging to tumour necrosis factor (TNF) super family death receptors, such as the tumour necrosis factor receptors (TNFR), Fas receptors (FasR), death receptors 3 (DR3), TNF-related apoptosis inducing ligand (TRAILR1 or DR4 and TRAILR2 or DR5) and DR6 (Nagata and Golstein 1995). These death receptors have a conserved death domain (DD), which functions as a protein-protein binding module, essential to

convey apoptotic signals (de Thonel and Eriksson 2005). Ligands that bind to these receptors belong to a family of related cytokines, the TNF family, which are the TNFα, lymphotoxin (LTα), Fas-ligand (FasL), Apo-3 ligand (Apo-3L), and TRAIL (de Thonel and Eriksson 2005). The interaction of the ligands with their respective receptors leads to receptor oligomerisation, an event that is required to initiate apoptotic signalling (de Thonel and Eriksson 2005).

A role for ceramide in the induction of the initiation phase of apoptosis was suggested on the basis of the observation that ligands, which bind to the p55 TNF receptor (TR55), interleukin-1 receptor 1 (IL-1 R1) and the Fas receptor result in the activation of the sphingomyelinases (SMase). SMase are enzymes, which are involved in the synthesis of ceramide via the metabolism of the sphingomyelin (Pettus *et al.* 2002). It has been reported that an increase in SMase activity, has a direct bearing on the intracellular levels of ceramide and corresponds to decreases in sphingomyelin in response to agents such as TNFα, Fas ligand, 1α, 25-dihydroxyvitamin D_3, γ-interferon, chemotherapeutic agents, heat stress, ischemia reperfusion and interleukin-1 (Liu *et al.* 1998). Several extracellular agents such as the TNFα, γ-interferon, interleukin-1, and daunorubicin have been suggested to play a role in the activation of the sphingomyelin pathway (Schutze *et al.* 1992; Wiegmann *et al.* 1994). Exogenous cell permeable ceramide analogs and exogenous bacterial sphingomyelinases have been shown to reproduce many biological effects of these agents, suggesting a role for ceramide in mediating and regulating cell responses (Pettus *et al.* 2002). Ceramide induced cell death is characterized by DNA

fragmentation, a feature associated with hallmarks of classical apoptosis (Sakahira *et al.* 1998).

Apoptosis is a highly regulated, genetically encoded molecular cell death program, employed by cells under both normal and in pathological conditions. The execution and regulation of apoptosis is a complex multi-factorial process, controlled by extracellular and intracellular signals and may be accompanied by morphological changes such as cell shrinkage, chromatin condensation and loss of plasma membrane integrity (de Thonel and Eriksson 2005; van Gurp *et al.* 2003). It is a highly coordinated process, orchestrated in three distinct phases: which are; initiation, commitment and effector phases. The initiation phase is thought to involve the assembly of a signalling complex of adaptor proteins through their death domains (DD), dependent on cell line and death inducing-signal.
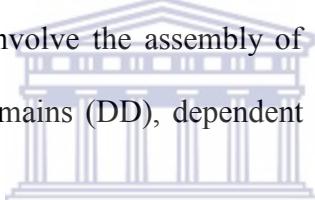
1.4.2 Mitochondria and ceramide-induced apoptosis

Apart from the classical role of the mitochondria in ATP synthesis, additional evidence suggests that the mitochondrion is actively involved in apoptosis. Central to the execution of apoptosis is the activation of a set of proteases (caspases) through receptor-ligand interaction (extrinsic pathway) or the permeabilization of the mitochondria (intrinsic pathway) (de Thonel and Eriksson 2005). Apart from the caspases, apoptosis is known to occur through the activities of other mitochondrial-based proteins, which require release from the mitochondrial inter-membrane space. Some of the proteins released upon the permeabilization of the mitochondria and shown to play a role in apoptosis include

cytochrome c, apoptosis inducing factor (AIF), endonuclease G, Smac/DIABLO, HtrA2/Omi, adenylate kinase 2. Other identified proteins include the acyl-CoA binding protein, poly-pyrimidine tract binding protein, and proteins associated with fatty acid metabolism or protein transport such as the fatty acid binding protein and translocase of the inner mitochondrial membrane (Van Loo *et al.* 2002).

Cytochrome c (cyt c) is synthesized in the cytoplasm as cyt c and translocated through the outer mitochondria membrane (OMM) into the inter-membrane space where it is covalently attached to apocytochrome c (van Gurp *et al.* 2003). Cellular stress induces the release of cyt c from the inter-membrane space, which activates downstream effectors of apoptosis (Li *et al.* 1997). In mammals, cyt c triggers the assembly of the apoptosome, a complex composed of cyt c, apoptosis activating factor-1 (Apaf-1) and dATP. It is thought that cyt c binds to Apaf-1 in the presence of ATP, inducing conformational changes in Apaf-1, leading to the recruitment of procaspase 9 to the complex (apoptosome). The complex activates procaspase 9 to active caspase 9, activating other downstream caspases (Fig. 1.3). Mitochondrial-based apoptosis may be activated independently of cyt c, which implies that cyt c dependent activation of the apoptosome may act as an amplifier and not an essential trigger of apoptosis (van Gurp *et al.* 2003).

Apoptosis Inducing Factor (AIF) is a 57 kDa mitochondrial-based protein, which is thought to act as a free radical scavenger specific for H_2O_2 in normal cells. AIF translocates to the nucleus where it induces chromatin condensation and DNA fragmentation in response to death signals (Daugas *et al.* 2000; Susin *et al.* 1999). AIF
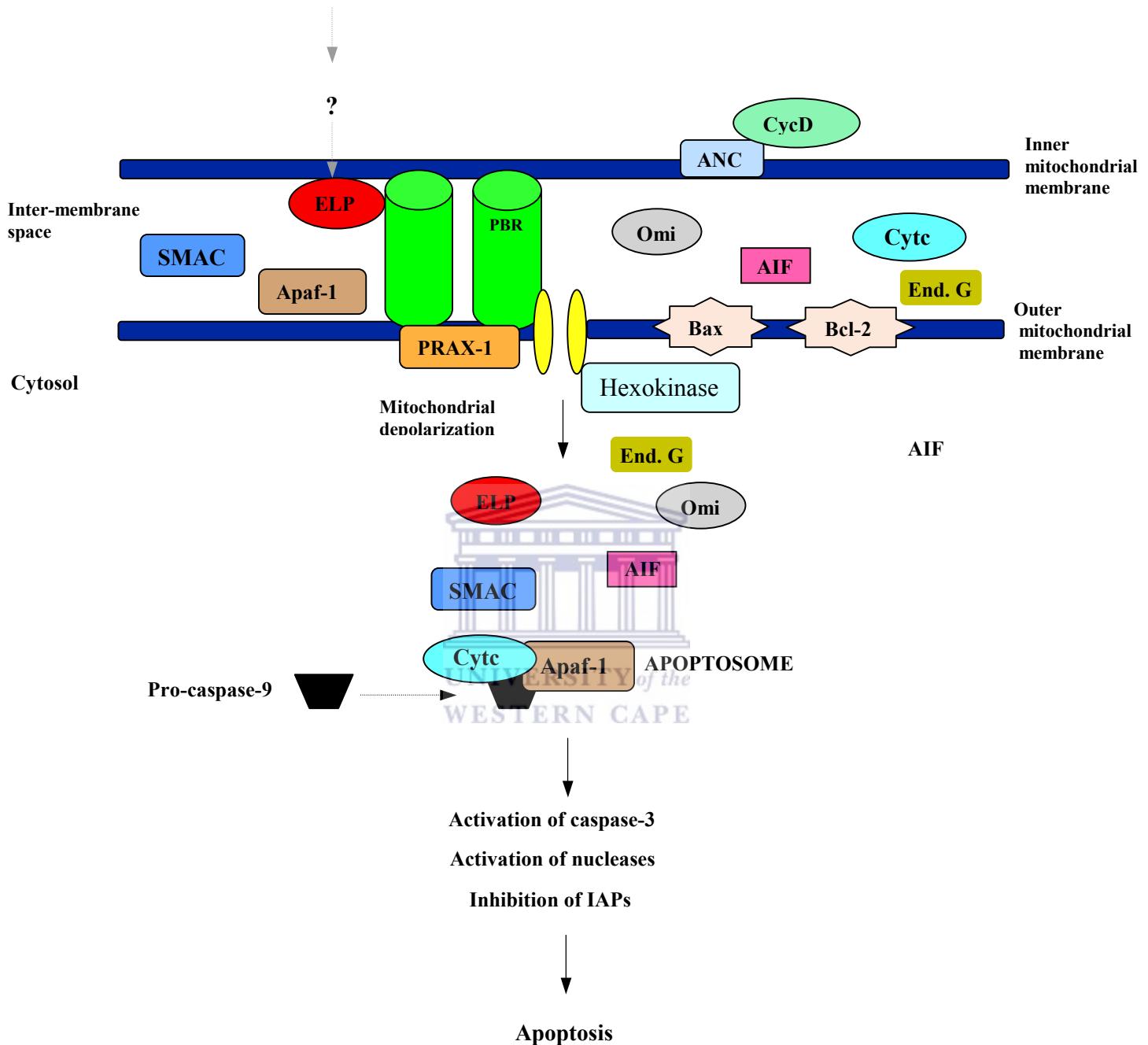
Fig. 1.3: A model for the involvement of endozepine in ceramide induced apoptosis. The model shows endozepine to be one of the proteins released from the mitochondria during mitochondrial permeability transition. This model was adapted from schematic structure of the MPTP (Casellas *et al.* 2002) and the suggested role for endozepine in ceramide induced apoptosis (Meyer 2003).

leads to a drop in the mitochondrial membrane potential and the release of cyt c (Ferri *et al.* 2000). The release of AIF is a caspase independent process and several reports have shown that the mitochondrion releases AIF in response to several agents, including H_2O_2, in a caspase independent manner (Fonfria *et al.* 2002; Susin *et al.* 2000). AIF therefore acts as a lethal caspase independent effector of apoptosis.

Endonuclease G is a mitochondrial inter-membrane protein, which plays a role in replication, repair and degradation of DNA (Donovan and Cotter 2004). In response to death inducing signals, endonuclease G is released from the mitochondria into the cytosol where it translocates to the nucleus and generates oligonucleosomal DNA fragmentation (Li *et al.* 2001). DNA fragmentation by endonuclease G is a caspase-independent process and the release of endonuclease G has been observed upon mitochondrial permeabilization using t-bid (Li *et al.* 2001; van Loo *et al.* 2001). Proteins such as Bcl-2 that regulate the permeabilization of the mitochondria control the release of endonuclease G. This claim is supported by the observation that the release of endonuclease G was not observed in Bcl-2 transgenic mice (van Loo *et al.* 2001). Nematode homologues of endonuclease G have been reported to cleave DNA into nucleosomal sized fragments, a process associated with apoptosis (Parrish *et al.* 2001). The release of endonuclease G into the cytosol when the mitochondrion undergoes permeability transition, its translocation to the nucleus and the associated DNA degradation properties in response to death-inducing signals all implicate endonuclease G in apoptosis.

Smac and its human ortholog, DIABLO, are mitochondrial proteins released from the mitochondrial inter-membrane space during permeability transition (Verhagen *et al.* 2000). Smac/DIABLO is thought to sequester the inhibitors of apoptosis (IAPs), which inhibit the apoptosome complex from the activation of pro-caspase 9. The physiological function of Smac/DIABLO is unknown and Smac/DIABLO knockout mice have been reported to be normal (van Gurp *et al.* 2003). The expression of truncated mutant Smac/DIABLO lacking the IAP binding domain (IBM) induces cell death to the same extent as the full length Smac/DIABLO suggesting an alternative mechanism of Smac/DIABLO that is not dependent on the IBM (Roberts *et al.* 2001). The translocation of Smac/DIABLO upon mitochondrial permeabilization and its role in sequestering IAP suggests a role for Smac/DIABLO in apoptosis.

HtrA2/Omi is a mammalian 49 kDa serine protease that resides within the mitochondrion and released into the cytosol upon mitochondrial permeabilization (Hegde *et al.* 2002; Martins *et al.* 2002). The HtrA2/Omi functions as a chaperone at normal temperatures and a protease at elevated temperatures (Spiess *et al.* 1999). Translocation of the Omi from the mitochondria to the cytosol has been observed in mice liver cells (Hegde *et al.* 2002; Van Loo *et al.* 2002). The sub-cellular localization of HtrA2/Omi is suggested to be under the control of Bcl-2 proteins, which is supported by the observation that t-bid and Bax (pro-apoptotic Bcl-2 proteins) induce the release of HtrA2/Omi, while Bcl-2 (anti-apoptotic Bcl-2) prevents its release (Hegde *et al.* 2002; Spiess *et al.* 1999; Van Loo *et al.* 2002). Omi is thought to play a role in caspase-independent apoptosis through its protease activity, although the exact mechanism of the caspase-independent apoptosis

is not clear. HtrA2/Omi may also contribute to caspase dependent apoptosis through its ability to antagonize the IAPs in a manner similar to that of Smac/DIABLO (Hegde *et al.* 2002).

Other proteins released upon the permeabilization of the mitochondrion include acyl-CoA binding protein and poly-pyrimidine tract binding protein. While no direct involvement of the acyl-CoA binding proteins in apoptosis has been shown, it has been suggested that acyl-CoA binding protein may promote the activation of m-calpain by decreasing calcium ion concentration, which is responsible for activation of m-calpains (Melloni *et al.* 2000). Caspase-dependent and -independent apoptosis have been reported to correlate with calpain activation (Wang 2000).

The permeabilization of the mitochondria is required for the release of mitochondrial-based proteins, which is necessary for the activation of downstream effectors of apoptosis such as caspase 3. Members of the Bcl-2 protein family regulate the integrity of the mitochondrial membrane. The Bcl-2 family of proteins is made up of both pro- and anti-apoptotic members that illicit opposing effect on the mitochondria. Pro-apoptotic members, such as Bax and Bak, induce mitochondrial permeability while the anti-apoptotic members; such as Bcl-2 and Bcl-w preserve mitochondrial membrane integrity, blocking the release of mitochondrial inter-membrane proteins. The Bcl-2 family of proteins may have up to four conserved Bcl-2 homology domains (BH) and is divided into three groups, based on the number of BH domains (Donovan and Cotter 2004). The multi-domain pro-apoptotic members, including Bax, Bok and Bak, contain three BH

domains, BH1, BH2, and BH3. Pro-apoptotic Bcl-2 family members, including Bid, Bad, Bim, Noxa, PUMA and spike, share sequence homology only within the BH3 domain (Donovan and Cotter 2004). The anti-apoptotic Bcl-2 family members such as the Bcl-2, Bcl-xl and Bcl-w share sequence conservation within all four BH domains.

The exact mechanism of action of the Bcl-2 family members in the permeabilization of the mitochondrial outer membrane remains controversial. At least two models have been proposed. The first involves channel formation by Bcl-2 members. Upon the introduction of death inducing signals, Bax is thought to translocate to the cytosol and proposed to interact with t-bid, inducing a conformational change in Bax leading to insertion, oligomerisation and channel formation. Alternatively Bax is proposed to interact with the Voltage-Dependent Anion Channel in the OMM through which pro-apoptotic proteins involved in the caspase-independent apoptosis such as the AIF, exit the mitochondria.
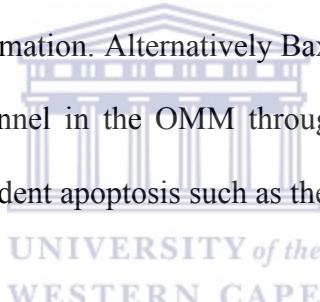
The second model suggests that mitochondrial permeability transition is based upon the opening of the permeability transition pore. The PTP is a multi-protein complex made up of the adenine nucleotide translocator (ANT) in the inner mitochondrial membrane (IMM), hexokinase, the Peripheral Benzodiazepine Receptor (PBR), and cyclophilin D in the matrix and the Voltage-Dependent Anion Channel (VDAC) on the outer mitochondrial membrane (Fig. 1.3) (van Gurp *et al.* 2003). While the VDAC allows most small molecule ions to enter and exit the mitochondria freely, the IMM is highly selective and is thought to ensure that the mitochondrion maintains electron/membrane potential (Corda *et al.* 2001; Gudz *et al.* 1997; van Gurp *et al.* 2003). It is postulated that

opening of the PTP results in the loss of the mitochondrial membrane potential, an influx of fluid into the matrix resulting in the swelling and rupturing of the OMM and release of pro-apoptotic proteins from the inter-membrane space. It is furthermore proposed that pro-apoptotic Bcl-2 proteins such as Bax cause the opening of the PTP while anti-apoptotic Bcl-2 proteins such as Bcl-2 and Bcl-xl favour closure of the channel.

A role for ceramide in mitochondrial-induced apoptosis has been suggested previously. For example, it has been shown that the mitochondrial respiratory chain complex III, which is implicated in oxidative phosphorylation, is inhibited by ceramide, leading to the generation of reactive oxygen species in intact mitochondria (Corda *et al.* 2001; Gudz *et al.* 1997). The known intracellular targets of ceramide such as the ceramide activated protein kinases (CAPK), cathepsin D, and protein phosphatase 1 (PP1) and protein phosphatase 2A (PP2A), seem to converge on the level of the mitochondria. Ceramide-activated protein phosphatase is involved in the de-phosphorylation of both Bcl-2 and the Bcl-2 kinase, with both events occurring in the mitochondria. It is thought that the removal of the inhibitory roles of Bcl-2 and Bcl-X tilts the balance between the pro-apoptotic Bcl-2 proteins such as Bax and the anti-apoptotic Bcl-2 proteins, enabling mitochondrial permeabilization, the release of cyt c and the activation of the down-stream effectors of apoptosis (Kim *et al.* 1997; Sawada *et al.* 2000). In support of the role of ceramide in mitochondrial-mediated apoptosis, studies which involved the targeting of sphingomyelinase GFP fusion constructs to different organelles, showed that only the mitochondrial-targeted constructs were able to induce apoptosis, which could be inhibited by the Bcl-2 proteins (Birbes *et al.* 2001).

1.4.3 The role of acyl-CoA binding protein in ceramide synthesis

Ceramide synthesis can occur through the hydrolysis of the sphingomyelin by the SMase or through the *de novo* synthetic pathway (see Fig. 1.4). The *de novo* synthesis of ceramide begins in the endoplasmic reticulum and continues in the Golgi (Guillas *et al.* 2001). It is initiated through the condensation of serine and palmitoyl-CoA by the serinepalmitoyltransferase (SPT) (Fig 1.4), in which the SPT is the rate-limiting enzyme (Perry *et al.* 2000). The requirement for palmitoyl-CoA pre-supposes the need for an acyl-CoA carrier molecule such as ACBP. Ceramide generated through the *de novo* pathway is thought to exert biological actions; the importance of this pathway in the regulation of apoptosis has been demonstrated using the mycotoxin Fumonisin B1 (Schmelz *et al.* 1998). Fumonisin B1 is a downstream inhibitor of the dihydroceramide synthase and a reported inhibitor of the *de novo* synthetic pathway (Desai *et al.* 2002). It has been suggested that Fumonisin B1 inhibits the formation of ceramide in a variety of cell types, in response to agents such as retinoic acid, TNF, daunorubicin, etopside, angiotensin II and anti-IgM, and contributes to the attenuation of apoptotic response induced by these agent (Kroesen *et al.* 2001; Liao *et al.* 1999). It appears that ACBP contributes to the *de novo* synthesis of ceramide through the introduction of palmitoyl-CoA into the pathway. A recent study involving modelled sphingolipid metabolism supports this view (Alvarez-Vasquez *et al.* 2005). This study suggests that the availability of the acyl-CoA substrate in the *de novo* synthetic pathway is possible through the maintenance of free *in vivo* levels of LCA esters at nanomolar concentrations due to the activity of yeast Acb1p, sterol carrier protein and fatty acid binding protein (Alvarez-Vasquez *et al.* 2005).
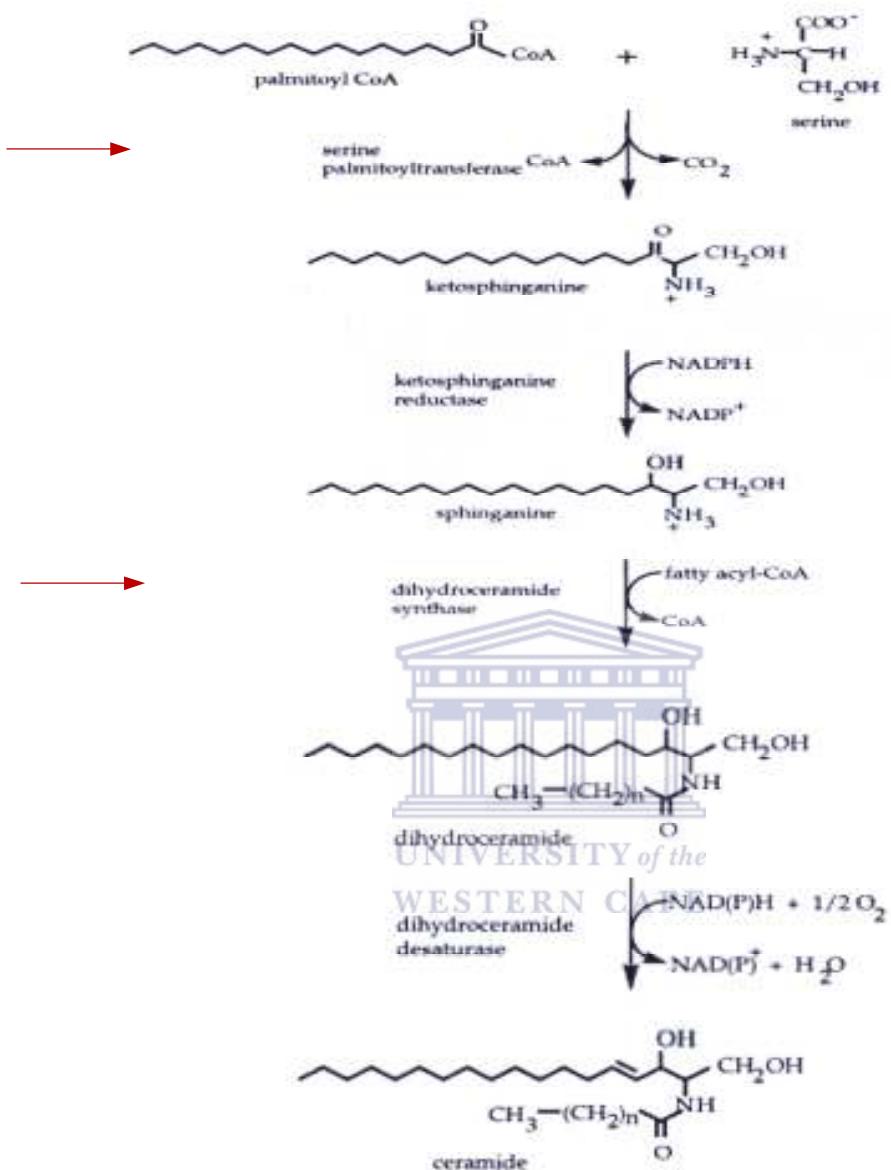
Fig. 1.4: The *de novo* synthetic pathway of ceramide with arrows pointing to steps that require the introduction of the acyl-CoA esters during the intracellular synthesis of ceramide (Hannun 1996)

An examination of the ceramide content of the vacuoles of ACBP-depleted cells in *S. cerevisiae* revealed an increase in the level of glycerophospholipids containing shorter and unsaturated acyl chains. Levels of C_{18}-C_{26} were much lower, and in some cases undetected (Faergeman *et al.* 2004). This supports the view that ACBP is required for the delivery of the *de novo* synthesized palmitoyl-CoA to the initial step in the long chain synthesis, catalyzed in *S. cerevisiae* by the palmitoyl-CoA transferase or the fatty acid elongation system. It appears that the *de novo* synthetic pathway of ceramide is implicated in cancerous conditions. Measurement of the levels of endogenous long chain ceramide in certain carcinoma tissues revealed that the C_{18}-ceramide concentrations were lower in carcinoma cell lines compared to normal cell lines (Koybasi *et al.* 2004). This could be due to de-regulation in the synthesis of LCA-esters and or to in-efficient delivery of the LCA-esters for ceramide synthesis. The over expression of the longevity assurance genes (LGA) was observed to lead to an increase in the cellular levels of C_{18}-ceramide in carcinoma lines (Koybasi *et al.* 2004). Member genes of the LGA have been shown to encode essential components of acyl-CoA dependent di-hydro-ceramide synthase (Schorling *et al.* 2001). Since di-hydro-ceramide synthasis is an acyl-CoA dependent process, one possibility is that the over-expression of LGA may be an ACBP dependent process. Mutational studies suggest that "knockdown" levels of LGA in cells lead to the reduced ability of such cells to transfer long chain acyl-CoA enzymes for the synthesis of dihydrosphingosine or phytosphingosine, which correlated with reduced ceramide content (Guillas *et al.* 2001). This suggests that the ACBP is most likely the link between the synthesis of LCA-esters, the *de novo* synthesis of ceramide and the development of cancerous conditions.

ACBP and endozepine have been reported to have similar lengths, predicted secondary structures and a conserved binding motif for the mid-long chain acyl-CoA esters (Pusch *et al.* 1999), which implies that endozepine could play a role in ceramide synthesis.

1.5 The 3-D structure of acyl-CoA binding protein

The three dimensional structures of ACBP have been determined using NMR and X-ray crystallography. These include bovine ACBP free (PDB code 2ABD; Andersen and Poulsen 1992) and in complex with palmitoyl-CoA (PDB code 1ACA; Kragelund *et al.* 1993) and from *P. falciparum* (PDB code 1HBK; van Aalten *et al.* 2001). The structure of endozepine is yet to be determined. Secondary structure predictions of endozepine (Fig. 5.5) suggest that it should have a structural fold consistent with ACBP. Multiple sequence alignments across the ACBP family (Fig. 1.2) show the presence of amino acid substitutions in endozepine in relation to other ACBP. Since the function of a protein is dependent on the interaction of its residues with other molecules in space, a structural approach is required to provide insight on how amino acid substitutions in endozepine will affect its function.

The backbone conformation of the bovine ACBP structure showed that the protein is an up-down-down-up four α-helix bundle with an overhand loop connecting helix 2 and 3 (Andersen and Poulsen 1992). Its fold is unique because it shows contacts among just four of the helix-helix interfaces instead of the usual six observed in proteins with four-α-helical folds. An adapted representation of the ACBP structure from bovine liver is displayed in Fig 1.5 showing that the ACBP is a flat-disc and α-helical in nature.
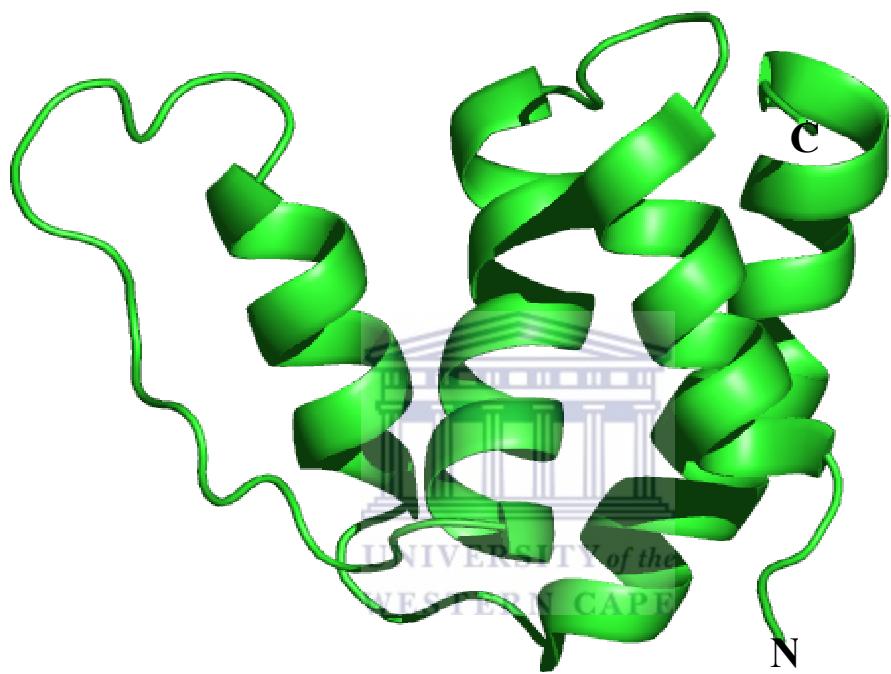
Fig. 1.5: The tertiary structure of bovine ACBP determined by NMR (Andersen and Poulsen 1992). ACBP structure is an up-down-down-up 4 α-helical bundle with an over hand loop connecting helix 2 and 3. This figure was generated using PYMOL Molecular Graphics System (2003) Delano Scientific, San Carlos, CA, USA.

Chemical de-naturation studies on mutant ACBP forms using guanidinium chloride in combination with tryptophan and tyrosine fluorescence have identified the residues in the helix-helix interface of the ACBP structure which are required for the stability of the protein (Kragelund *et al.* 1999a).

1.6 ACBP and ligand binding

In vitro protein-ligand interaction can provide clues to protein function in vivo. NMR has been shown to be a valuable screening tool for the investigation of protein-ligand interactions (Pellecchia *et al.* 2002). A previous study suggested that the bovine, yeast and plant ACBP bound to long chain acyl-CoA esters (LCA esters) or enzymes with high specificity and affinity (Faergeman *et al.* 2004; Kragelund *et al.* 1999a). The structural basis for such interaction was demonstrated through the determination of the ACBP structure from bovine liver in complex with palmitoyl-CoA (Kragelund *et al.* 1993). LCA-CoA esters consist of a hydrophilic head-group, a CoA region and a more hydrophobic region (acyl-chain). The binding sites of ACBP on the LCA-esters have been identified to include the adenine ring, the 3′ phosphate group and the acyl chain of the ligand. Feargeman and coworkers have demonstrated that the 3′ phosphate group contributes 40 % of the total binding energy (Faergeman *et al.* 1996).

An insight into the thermodynamic parameters associated with ligand binding has been gleaned using a combination of single amino acid mutations and free energy changes associated with the exposure of the mutants to the ligand (Kragelund *et al.* 1999b). It has been proposed that the binding of the 3′ phosphate and hydroxyl groups of palmitoyl-CoA

to ACBP involves a network of electrostatic and polar interactions involving the polar parts of side chains of Y28, K32 and K54 (Kragelund *et al.* 1999b). The adenine ring of palmitoyl-CoA is suggested to stack into the hydrophobic pocket formed by the aromatic ring of Y31, and stabilized through the formation of hydrogen bonds between the hydroxyl group of Y71 and proton acceptors (Kragelund *et al.* 1999b). The palmitoyl-containing region of the ligand is suggested to make several non-polar contacts with residues in the hydrophobic cleft of helices 2 and 3 and in particular to the side chains of the M24, L25 and A53 residues (Kragelund *et al.* 1999b).

Length-based ligand preference has been observed for ACBPs isolated from different organisms (Milne and Ferguson 2000). There is evidence that ACBP from *P. falciparum* prefers shorter acyl-CoA chain lengths, where as ACBP from bovine liver prefers longer chain lengths (Milne and Ferguson 2000). The amino acid sequence of *P. falciparum* ACBP compared to that of the bovine ACBP has revealed a number of differences that suggests a possible structural basis for length-based ligand preference. ACBP isolated from *Trypanosoma brucei* (*T. brucei*) is reported to prefer shorter acyl-CoA esters (myristoyl-CoA) (Milne and Ferguson 2000). High resolution structures of ACBP from bovine liver and *P. falciparum*, respectively, suggest that the structural basis for the preference of shorter acyl-CoA chain lengths by *P. falciparum* ACBP may be associated with the insertion of a loop between helices 1 and 2 and tunnel blocking at the terminal position of the acyl-chain (van Aalten *et al.* 2001). This suggests that additional properties and functions may be associated with changes in amino acid sequences where such changes may be host specific, and may have many important biological

implications. This also suggests that while homology modelling may be useful in determining gross structural features, ligand-binding properties and hence function may depend on atomic level features that can not be readily modelled.

1.7 The putative role of endozepine in ceramide induced apoptosis

There are several lines of evidence suggesting a role for endozepine in mitochondrial-induced cell death. Firstly, endozepine has been proposed to act as a putative ligand to the peripheral benzodiazepine receptor (PBR) (Casellas *et al.* 2002). Ligands to the PBR are known to enhance apoptosis initiated by a number of agents including etoposide, doxorubicin and ceramide. They are thought to lead to dissipation of the mitochondria membrane potential, leading to the release of mitochondrial proteins, such as Omi/HtrA2 cytochrome c, endonuclease G, Smac/DIABLO, poly pyrimidine, AIF and endozepine (Patterson *et al.* 2000; Van Loo *et al.* 2002). It is generally accepted that the permeabilization of the mitochondria is the rate-limiting step within the intrinsic pathway of apoptosis. It is also accepted that the release of mitochondrial factors upon mitochondrial permeability transition contributes to apoptosis.

Although direct interaction between endozepine and PBR has not been reported, it has been shown that DBI (the original name given to ACBP) displaces diazepam (a ligand to PBR) from the central benzodiazepine receptor, which suggests that DBI may function as an endogenous ligand to the PBR (Ferrero *et al.* 1984; Guidotti *et al.* 1983). The PBR has been found to be up-regulated in several tumours, which also contain high levels of the anti-apoptotic Bcl-2 protein (de Jong *et al.* 1994; Miyazawa *et al.* 1998;

Venturini *et al.* 1998). Several studies have implicated ligands to the PBR in the regulation of apoptosis and the rescue of corrupted cell death program. It has been suggested that Pk11195 (a ligand of PBR) facilitates the loss of the membrane potential and the release of apoptotic factors such as cytochrome c and abolishes inhibition of apoptosis by anti-apoptotic Bcl-2 proteins (Hirsch *et al.* 1998). Other studies have shown that induction of apoptosis using anti-CD95 receptor antibody in tumour cell lines is enhanced by ligands to the PBR, since detectable mRNA transcripts of the PBR have been found in all tumour cells (Decaudin *et al.* 2002).

A role for ligands of the PBR in the sensitization of tumour cells to apoptosis has been shown using RO5-4864, which is a ligand to the PBR (Decaudin *et al.* 2002). It is possible that death-inducing signals sensitize cells to apoptosis by limiting anti-apoptotic effects, and thereby enabling ligands to the PBR to occupy and bind. This is thought to induce conformational changes in the PT pore, leading to the opening of the PT and the release of other effectors of the downstream apoptotic process. It appears that endozepine may play a role in apoptosis through its interaction with the PBR, which will lead to the permeabilization of the mitochondria. Although endozepine has been observed to be released upon the permeabilization of the mitochondria, there is no direct evidence to demonstrate that its release is not just a consequence of the loss of the mitochondrial membrane integrity with no other role for it in apoptosis.

A role for endozepine in C_2-ceramide induced apoptosis has been suggested (Meyer, 2003). The insertion of modified retroviruses into the promoter region of endozepine in

CHO22 cells using promoter trap mutagenesis led to resistance of the mutants to C_2-ceramide induced apoptosis (Meyer, 2003). These mutants showed approximately 90 % reduction in the expression of endozepine. Transduction of recombinant Tat-GFP-ELP into the promoter-trapped mutants demonstrated that endozepine was able to restore the sensitivity of the mutants to C_2-ceramide death signalling (Meyer and Rees, unpublished data). Various assays showed that the mutants remained viable but displayed a delay in the permeabilization of the mitochondria and a reduced activation of caspase-3 (an activator of apoptosis). A model has been developed which suggests two hypotheses for the involvement of endozepine in ceramide-induced apoptosis. The first hypothesis is that endozepine contributes to apoptosis through the transport of palmitoyl-CoA, a substrate required for the *de novo* synthesis of ceramide. Endozepine shares a conserved binding motif for mid-long chain acyl-CoA esters with the ACBP, which plays a role in the biosynthesis and transport of palmitoyl-CoA. Endozepine may therefore play a role in the synthesis of ceramide in its capacity as an acyl-CoA binding protein. However, since the *de novo* synthetic pathway occurs in the endoplasmic reticulum (ER) and endozepine is mostly expressed within the mitochondria, it would then appear that endozepine could only play a role in the synthesis of ceramide once released from the mitochondrial compartment (Guillas *et al.* 2001; Pusch *et al.* 1996). Endozepine is one of the proteins released from the mitochondria during the permeability transition and may thus serve to amplify death-inducing signals by contributing to a further synthesis of ceramide (Patterson *et al.* 2000).

The second hypothesis is that endozepine interacts directly with ceramide leading to its activation for interaction with the PBR, and a subsequent opening of the mitochondria permeability transition pore leading to apoptosis. It is possible that an interaction between C_2-ceramide, endozepine and PBR contributes to the activation of the mitochondria permeability transition but the exact sequence of such interaction remains speculative. One possibility is that C_2-ceramide directly interacts with endozepine, activating and positioning endozepine to bind and interact with the PBR, leading to induction of conformational changes within the PTP, and a subsequent permeability transition. Reduction in endozepine expression within the promoter-trapped mutants has been shown to correlate with delayed mitochondria permeabilization, suggesting a role for endozepine in the delay (Meyer, 2003).

1.8 Aims of this study

To address the two hypotheses for the involvement of endozepine in ceramide-induced apoptosis, this study is designed to investigate the interaction of endozepine with C_2-ceramide, C_{16}-ceramide and palmitoyl-CoA. Our goal is to investigate if endozepine is an intracellular target of C_2-ceramide, which will provide insight into understanding how endozepine relays death-inducing signals following ceramide signalling. This would support the hypothesis that endozepine contributes to the permeabilization of the mitochondria. Alternatively, we hope to determine whether endozepine contributes to ceramide-induced apoptosis through its role in the transport of acyl-CoA esters, which is required for the intracellular synthesis of ceramide. This will depend on a demonstration,

which shows that the endozepine interacts with palmitoyl-CoA, and thus pulls and donates it into the de *novo* synthetic pathway of ceramide.

1.9 Thesis Outline

The rest of this thesis is organized as follows: Chapter 2 describes the materials and methods applied in this work. Chapter 3 describes the expression and purification of recombinant ^{15}N-labelled and ^{13}C, ^{15}N labelled samples of endozepine for NMR spectral acquisitions. Chapter 4 focuses on the use of ^{15}N-HSQC NMR spectra to monitor putative interactions between endozepine, C_2-ceramide, C_{16}-ceramide and palmitoyl-CoA. Chapter 5 describes the use of triple resonance NMR experiments to assign the ^{15}N-HSQC spectrum and hence identify the residues involved in interaction with palmitoyl-CoA. It goes on to describe the generation of a homology model of endozepine in order to visualize our NMR results in 3 dimensional space. Chapter 6 summarizes our findings and outlines future lines of investigation.
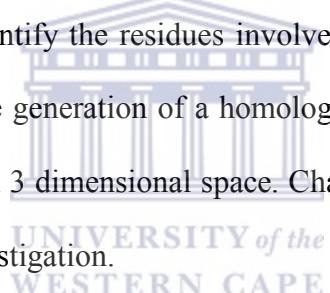
Chapter 2: Materials and Methods

2.1 Bacterial strain used

Escherichia coli (*E. coli*) BL21 (DE3) pLysS: F⁻*omp* T *hsd*S$_B$ (r$_B$⁻m$_B$⁻) *gal dcm rne131*

2.2 General Stock solutions and buffers

10x DNase 1 buffer: 0.1 M MnCl$_2$, 0.5 mg/ml BSA, 0.5 M Tris-HCl pH 7.5 sterilized by filtration, stored at -20 ºC

10x TBE: 0.9 M Tris, 0.89 M boric acid, 25 mM EDTA, pH 8.3

2x Sample treatment buffer: 4 % SDS, 20 % Glycerol, 2 % 2-mercaptoethanol and 0.25 M Tris-HCl pH 6.8 in 10 ml deionised H$_2$O

5x SDS Electrophoresis buffer: 25 mM Tris, 0.1 % SDS and 25 mM glycine

Ammonium persulphate: 10 % stock was prepared in de-ionised water, stored at -20 ºC

Ampicillin: 100 mg/ml stock solution prepared in deionised H$_2$O, sterilized by filtration, stored at -20 ºC

Bradford dye: 100 mg Coomassie Brilliant Blue G 250 dissolved in 50 % concentrated phosphoric acid and 25 % ethanol, stored at 4 ºC

C$_2$-ceramide stock: 20 mM stock prepared in 100 % ethanol, stored at -20 ºC

C$_{16}$-ceramide stock: 20 mM stock prepared in 100 % ethanol, stored at -20 ºC

Chloramphenicol: 35 mg/ml stock solution prepared in ethanol

Coomassie staining solution: 0.025 % Coomassie Blue R-250, 40 % methanol, 7 % acetic acid in 2000 ml deionised H$_2$O

Cleavage buffer: 50 mM Tris pH 7, 0.1 % Triton X-100, 1 mM EDTA, 150 mM NaCl, 1 mM PMSF and 1 mM DTT

De-staining Solution: 15 % (v/v) acetic acid

DNase free RNAse buffer: 0.1 M sodium acetate anhydrate, 0.1 mM EDTA pH 4.8, stored at -20 ℃

DTT: 1 M stock solution prepared in 0.01M sodium acetate pH 5.2, sterilized by filtration, stored at -20 ℃

Ethidium Bromide: 10 mg/ml stock solution prepared in H_2O, stored in the dark at 4 ℃

Equilibration buffer: 137 mM NaCl, 2.7 mM KCl, 8 mM Na_2HPO_4 and 1.5 mM KH_2PO_4, pH 7.4. Sterilized by autoclaving

GTE: 50 mM Glucose, 50 mM Tris-HCl and 10 mM EDTA, pH 8.0

IPTG: 1 M stock solution prepared in deionised H_2O, sterilized by filtration, stored at -20 ℃

L Agar: 10 g/l Tryptone, 5 g/l Yeast extract, 5 g/l NaCl and 14 g/l Bacteriological Agar

Lysis buffer: PBS containing (10 μg /ml DNase1, 100 μg/ml lysozyme, 1 mM EDTA, 1 mM PMSF, 1 mM DTT, 0.1 % Triton-X 100 and Complete EDTA-free protease inhibitor cocktail)

L Broth: 10 g/l Tryptone, 5 g/l Yeast extract and 5 g/l NaCl

Lysis solution: 200 mM NaOH containing 1 % SDS

Minimal media: 3 g/l KH_2PO4, 12.8 g/l $Na_2HPO_4.7H_2O$, 0.5 g/l NaCl, 2 ml 1 M $MgSO_4$ and 0.1 ml 1 M $CaCl_2$ supplemented with 1 g/l NH_4Cl and 2 g/l glucose

Neutralization Solution: 3 M potassium acetate, pH 5

NMR buffer: 50 mM sodium phosphate pH 6.0 (pH adjusted with 0.1 M $NaH_2PO_4.H_2O$ and 0.1 M $Na_2HPO_4.7H_2O$) containing 50 mM NaCl, 10 mM DTT, 0.02 % sodium-azide

Palmitoyl-CoA Stock: 40 mM palmitoyl-CoA solution prepared in NMR Buffer

Phenol: chloroform: isoamylalcohol: 25 parts Tris-saturated, 24 parts chloroform and 1-part isoamylalcohol.

PMSF: 10 mM stock solution prepared in isopropanol, stored at -20 ºC

Protein Elution Buffer: 15 mM glutathione prepared in 50 mM Tris pH 7(containing 1 mM PMSF and 1 mM EDTA)

RNAse (DNase free): 20 mg/ml stock solution prepared in 0.1 M sodium acetate containing 0.3 mM EDTA (pH 4.8 with acetic acid), stored at -20 ºC

Separating Buffer: 1.5 M Tris-HCl pH 8.8, stored at 4 ºC

Stacking Buffer: 0.5 M Tris-HCl pH 6.8, stored at 4 ºC

TE: 10 mM Tris-HCl, 1 mM EDTA, pH 7.4

TFb1 Buffer: 30 mM Potassium acetate, 50 mM $MnCL_2$, 0.1 M KCL and 6.7 mM $CaCl_2$

TFb2 Buffer: 9 mM Mops, 50 mM $CaCl_2$, 10 mM KCl and 15 % glycerol (v/v)

TYM Broth: 20 g/l Trypton, 5 g/l Yeast extract, 3.5 g/l NaCl and 2 g/l $MgCl_2$

2.3 Preparation of competent E. coli BL21 (DE3) pLysS cells

E. coli BL21 (DE3) pLysS cells were streaked out on a Luria agar plate and incubated at 37 ºC for 16 hours. A single colony was picked and used to inoculate 20 ml TYM broth, which was incubated at 37 ºC until the optical density at 550 nm (OD_{550}) reached 0.2. 100 ml of fresh TYM broth was added to the culture and the cells further incubated at 37 ºC until the OD_{550} again reached 0.2. 400 ml of fresh TYM broth was added and the cells incubated at 37 ºC until the OD_{550} reached 0.5. The cells were rapidly cooled by gently swirling of the flask in ice water and the culture transferred to 250 ml polypropylene tubes and centrifuged at 6000 g at 4 ºC for 10 minutes in a Beckman J2-14

centrifuge. The cell pellet was re-suspended in 250 ml ice-cold Tfb1 buffer (Transfer buffer 1) and incubated on ice for 30 minutes, followed by centrifugation at 6000 g at 4 ºC for 10 minutes. The pellet was gently re-suspended in 50 ml Tfb2 buffer (Transfer buffer 2). Re-suspended cells were dispensed in 2 ml aliquots and subsequently snap frozen in liquid nitrogen. Aliquots were stored at - 80 ºC until required.

2.4 Construction of the pGEX-6P-2-endozepine plasmid

Polymerase Chain reaction (PCR) was used to amplify the nucleotide sequence of endozepine (Accession number AF229807) using mouse embryonic DNA as template (Meyer, 2003). The amplified fragment was cloned into the *Bam* HI and *Xho* I sites of the pGEX-6P-2 vector to create the pGEX-6P-2-endozepine expression vector. The expected product was a 37 kDa protein containing endozepine fused to the C-terminus of glutathione-S-transferase (GST), separated by a linker region containing a recognition site for the PreScission Protease (Amersham Biosciences). After removal of GST the expected sequence of endozepine was as follows:

<u>G P L G S</u> M S Q V E F E M A C A S L K Q L K G P V S D Q E K L L V Y S F Y K Q A T Q G D C O I P V P P A T D V R A K A K Y E A W M V N K G M S K M D A M R I Y I A K V E E L K K K E P C

Native endozepine amino acid sequence begins with the residues MSQVEF. The five underlined residues (GPLGS) are artifacts of the expression system. In the remainder of

this thesis the residues will be numbered in such a way that residue 1 corresponds to the initiation methionine of the native protein.

2.5 Preparation of plasmid DNA using the CsCl density gradient method

Plasmid DNA isolation was carried out using the caesium chloride (CsCl) density gradient centrifugation method (Radloff *et al*. 1967). *E. coli* BL21 (DE3) pLysS cells were transformed with pGEX-6P-2-endozepine as described in Section 2.6. Cells were streaked out on a Luria agar plate containing 100 μg/ml ampicillin and incubated at 37 ºC for 16 hours. Single colonies were picked and used to inoculate 1000 ml Luria broth containing 100 μg/ml of ampicillin which were then grown for 16 hours at 37 ºC. Cells were harvested by centrifugation at 6000 g at 4 ºC for 10 minutes. Harvested cells were re-suspended in 15 ml GTE and incubated on ice for 10 minutes. Cells were lysed by the addition of 15 ml lysis solution (200 mM NaOH containing 1% SDS) followed by incubation on ice for 10 minutes. 15 ml neutralization solution (3 M potassium acetate, pH 5.2) was added followed by incubation on ice for 10 minutes. The lysate was centrifuged at 6000 g at 4 ºC for 10 minutes and the resulting precipitate discarded. 0.8 volume of isopropanol was added to the lysate and incubation carried out at -20 ºC for 30 minutes to precipitate nucleic acids followed by centrifugation at 6000 g at 4 ºC for 10 minutes. The supernatant was discarded and pellet re-suspended in 4.5 ml TE. 4 mg of ethidium bromide and 5.75 g of CsCl were added and the mixture centrifuged at 6000 g at 4 ºC for 10 minutes after which the supernatant was collected. The density was adjusted to 1.61 g/ml using TE saturated with CsCl after which the mixture was transferred into Quick Seal tubes (Beckman) and centrifuged in a Nvi 65 rotor at

55000 rpm for 18 hours at 22 °C. The sample was visualized using 360 nm UV illumination and the band containing plasmid DNA drawn off using a 1 ml syringe.

Ethidium bromide was extracted by the addition of an equal volume of salt saturated isopropanol, mixing rigorously and centrifuging to separate the phases after which the top phase was carefully removed using a pipette. This process was repeated until all of the ethidium bromide had been removed. 1 volume of isopropanol and 2 volumes of water were then added and the mixture incubated on ice for 20 minutes followed by centrifugation at 6000 g at 4 °C for 15 minutes. The supernatant was discarded and the pellet washed with 100 μl of 70 % ethanol followed by centrifugation at 13200 rpm for 5 minutes. The supernatant was discarded and the pellet air-dried at room temperature followed by re-suspension in 100 μl TE.
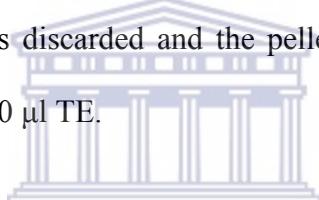
2.6 Transformation of E. coli BL21 (DE3) pLysS cells with pGEX-6P-2-endozepine

Competent *E. coli* BL21 (DE3) pLysS cells were thawed on ice and 100 μl aliquots transferred into two separate eppendorf tubes. 2 μl of plasmid DNA was added to one of the tubes (the experimental tube) but none to the other tube (the control tube). The cells were incubated on ice for 30 minutes after which they were transferred to a 42 °C water bath and incubated for 45 seconds (heat shock) whereafter, they were put back on ice and incubated a further 5 minutes. 900 μl of pre-warmed LB was added to both tubes and the cells incubated at 37 °C for 1 hour after which 50 μl of the transformed cells were plated out on LB plates containing 100 μg/ml ampicillin and incubation carried out at 37 °C for 16 hours.

2.7 Expression screen of transformed E. coli BL21 (DE3) pLysS for recombinant protein expression

E. coli BL21 (DE3) pLysS cells transformed with pGEX-6P-2-endozepine as described in Section 2.6 were plated out on LB plates containing 100 μg/ml ampicillin and grown at 37 ºC for 16 hours. Single colonies were picked and sub-cultured in LB broth containing 100 μg/ml ampicillin and incubated with vigorous shaking at 37 ºC for 4 hours. 1 ml aliquots were transferred into two separate 15 ml tubes with 1 mM isopropyl β-D-thiogalactopyranoside (IPTG) being added to one of the cultures (induced cells), whereas no IPTG was added to the other culture (un-induced cells). Both tubes were incubated for a further two hours at 37 ºC with vigorous shaking.
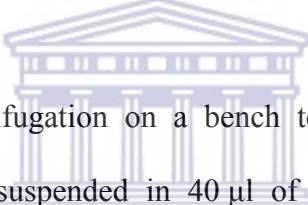
Cells were harvested by centrifugation on a bench top centrifuge at 13200 rpm for 10 minutes and the pellets re-suspended in 40 μl of Sample Treatment Buffer. The suspension was briefly centrifuged on a bench top centrifuge at top speed followed by incubation at 95 ºC for 5 minutes. Samples were analyzed by SDS-PAGE gel electrophoresis as described in Section 2.11. The clone demonstrating the highest level of recombinant protein expression was selected for large-scale expression.

2.8 Recombinant expression of double labelled 13C, 15N-endozepine

50 μl of culture from the highest expressing clone of *E. coli* BL21 (DE3) pLysS cells in Section 2.7 was used to inoculate 100 ml of Minimal Media (3 g/l KH_2PO4, 12.8 g/l $Na_2HPO_4.7H_2O$, 0.5 g/l NaCl, 2 ml 1 M $MgSO_4$ and 0.1 ml 1 M $CaCl_2$) supplemented with 1g/l [15]NH_4Cl and 2g/l ^{13}C-glucose, containing 100 μg/ml ampicillin and 35 μg/ml

chloramphenicol. Cells were incubated with vigorous shaking at 37 ºC for 16 hours. A further 900 ml of Minimal Media containing 100 μg/ml of ampicillin was added to the primary culture and the cells incubated at 37 ºC until the OD_{550} was between 0.4 and 0.6. Expression of recombinant protein was induced by the addition of IPTG to a final concentration of 1 mM and the cells incubated under gentle shaking at 30 ºC for 18 hours. Single and double labelled (^{13}C,^{15}N) endozepine samples were respectively produced by replacing $^{14}NH_4Cl$ with $^{15}NH_4Cl$ (Spectral Gases) and ^{12}C-glucose with ^{13}C-glucose (Spectral Gases) respectively.

Culture were transferred to 250 ml propylene tubes and harvested by centrifugation at 6000 g at 4 ºC for 10 minutes and the pellets re-suspended in 10 ml Lysis Buffer. Cells were lysed effectively using 3 cycles of freezing at -80 ºC, followed by thawing at 37 ºC for 20 minutes, respectively. 20 μg/ml DNase was added to the lysate and incubation carried out at 37 ºC for 45 minutes whereafter the lysate was centrifuged at 6000g at 4 ºC for 30 minutes and clarified through a 0.45 μm filter (OSMONICS). Affinity purification of the GST-endozepine was carried out using a 20 x 1 cm Econo® Column packed with 10 ml glutathione-linked agarose (SIGMA®), operated by gravity flow. The lysate was loaded onto the pre-equilibrated glutathione-agarose column and the flow through collected. The column was then washed with 3 column volumes (CV) of Equilibration Buffer after which the protein was eluted with 3CV's of Elution Buffer (50mM Tris-HCl pH 8, containing 15 mM reduced glutathione, 1 mM EDTA, 1 mM PMSF and 150 mm NaCl). Fractions containing eluted GST-endozepine were placed in a dialysis

bag (Snake Skin, Millipore) with a molecular weight cut off of 3500 Daltons and dialyzed overnight at 4 ºC in Cleavage Buffer.

PreScission[TM] Protease (Amersham Pharmacia Biotech) was added to protein solution according to manufacture's instruction and cleavage allowed to take place overnight at 4 ºC. Following cleavage, GST was removed by loading the protein solution back onto the glutathione agarose column. The flow through, containing endozepine, was taken forward for further purification.

2.9 Anion exchange chromatography

Anion exchange chromatography was carried out using a 1.6 ml column (self packed) containing 20 HQ POROS media (Amersham Biosciences) on a BioCAD® SPRINT[TM] Perfusion Chromatography system (PerSeptive Biosystems) at a flow rate of 10 ml/minute. The instrument was operated using a pre-programmed sequence consisting of the following steps: 10 CV Equilibration Step (50 mM Tris-HCl pH 7 + 10 mM NaCl), Injection of sample, 10 CV Wash Step (50 mM Tris-HCl pH 7.0 + 10 mm NaCl), 15 CV gradient (50 mM Tris, pH 7.0 + 0-0.5 M NaCl), 10 CV Clean Step (50 mM Tris-HCl pH 7.0 + 2M NaCl) and 10 CV Re-equilibration Step (50 mM Tris-HCl pH 7.0 + 10 mm NaCl). Eluted protein was monitored at 280nm using an in-line UV meter and NaCl concentration was monitored using an in-line conductivity meter. The presence of eluted protein was confirmed by subjecting the fractions to SDS-PAGE analysis.

2.10 Size exclusion chromatography

Fractions containing endozepine from the anion exchange step were pooled and concentrated to 900 µl using YM-3 Centriprep devices (Millipore, Bedford, USA). Size exclusion chromatography was carried out using a 100 x 1.8 cm Econo® Column packed with 150 ml Sephacryl S100 gel (Amersham Pharmacia Biotech) on a BioCAD® SPRINT™ Perfusion Chromatography system (PerSeptive Biosystems). The column was equilibrated with 1.5 CV of NMR Buffer at a flow rate of 1.8 ml/minute after which the sample was injected into a 1 ml injection loop using a Hamilton syringe. 1 ml fractions were collected using a Gilson® 203B fraction collector and eluted protein monitored using absorbance at 280 nm. Fractions were collected and subjected to analysis by SDS-PAGE. Fractions containing endozepine were pooled and concentrated to 600 µl using a YM-3 Centriprep device.
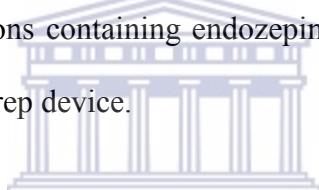
2.11 SDS-polyacrylamide gel electrophoresis (SDS-PAGE)

Proteins samples were separated on SDS-PAGE gels according to Laemmli's method (Laemmli UK.1970), which utilizes a stacking gel to concentrate the proteins into a thin line before they enter the separating gel, which then separates them according to their molecular weight. 8 x 10 cm gels of 1.5 mm thickness were cast using Hoefer Mighty Small™ SE 245 Dual Gel casters (Hoefer), using 40 % premixed acrylamide: bis-acrylamide 37.5:1 solution. 16 % separating gels were made up as follows: 3.2 ml de-ionized H_2O, 2.625 ml 1.5 M Tris pH 8.8, 4 ml 40 % premixed acrylamide: bis-acrylamide 37.5:1, 105 µl 10 % SDS, 60 µl of 10 % ammonium persulphate (APS) and 10.5 µl TEMED (N, N, N', N'-tetramethylenediamine). 4 % stacking gels were prepared

using 3.050 ml de-ionized H_2O, 1.25 ml 0.5 M Tris pH 6.8, 0.75 ml 40 % premixed acrylamide: bis-acrylamide 37.5:1, 50 μl 10 % SDS, 25 μl of 10 % APS and 10 μl TEMED.

Samples were diluted with equal amount of 1 x Sample Treatment Buffer and boiled at 95 ºC for 5 minutes followed by centrifugation on a bench top centrifuge at 13200 rpm for another 5 minutes. Pre-mixed protein molecular range marker was diluted 20 times before being subjected to the same treatment. Electrophoresis was carried out in 1x SDS Electrophoresis Running Buffer at a field of 10 V/cm using a Mighty Small II Gel Electrophoresis System (Hoefer). The voltage was adjusted to 15 V/cm when the Bromophenol blue dye reached the separating gel. Electrophoresis was stopped when the dye reached the bottom of the separating gel after which the gel was stained in Coomassie Staining Solution and de-stained in De-staining solution for visualization.

2.12 Determination of protein concentrations

Protein concentrations were determined using two independent methods: UV absorption and the Bradford colourimetric assay method (Bradford 1976). UV absorption measurements were carried out at 280nm using a NanoDrop® *ND-1000* Spectrophotometer (NanoDrop Technologies Inc.). Bradford dye stock was prepared by dissolving 100 mg of Coomassie brilliant blue G250 in 25 % ethanol, 50 % phosphoric acid and 25 % H_2O. The Bradford dye stock was diluted 5 fold immediately prior to use and 500 μl of 0.1 N NaOH added per 10 ml of the diluted dye solution. The Bradford dye solution was filtered through a 0.45 μm filter (OSMONICS) while

incubated on ice. Serial dilutions of lysozyme (0.25 mg/ml) were prepared in NMR Buffer until a final concentration of 0.0039 mg/ml was obtained to serve as standards. 20 μl each of the standards, blank and protein samples were aliquoted into separate wells of a 96-well plate. 180 μl of the filtered Bradford assay reagent was aliquoted into each well and the plate incubated at room temperature for 5 minutes. The absorbance of lysozyme at 620 nm (A_{620}) was measured using a Labsystems Multiskan® BIOCHROMATIC Spectrophotometer. Microsoft Excel software (Microsoft Corporation) was used to generate a plot of A_{620} against [lysozyme] and to construct a straight line through the data.

The UV absorption method involved measurement of the absorbance at 280 nm, A_{280}, using a NanoDrop® *ND-1000* Spectrophotometer (NanoDrop Technologies Inc.). The protein concentration was determined using the Beer-Lambert Law, $A_{280} = ECL$, where E = is the molar extinction coefficient and L = 1cm, is the path length. E was estimated from the amino acid sequence of endozepine using the Expert Protein Analysis System server (http://www.expasy.ch/cgi-bin/pi_tool) and found to be 10.930 mM^{-1} cm^{-1}.

2.13 NMR Analysis

Samples were exchanged into NMR Buffer (50 mM Sodium Phosphate pH 6.0, 50 mM NaCl, 10 mM DTT and 0.02 % Sodium Azide), concentrated to 600 μl using YM-3 Centriprep devices (Millipore, Bedford, USA) and transferred to a 5 ml NMR tube (Wilmod) for NMR analysis. 7 % D_2O was added to act as internal reference frequency to lock the spectrometer carrier frequency.

NMR spectra were recorded at 25º C on the Varian Unity Inova 600 MHz spectrometer in the Department of Chemistry at the University of Stellenbosch, South Africa. Spectra were processed using nmrPipe (Delaglio *et al.* 1995) and visualized using NMRView (Johnson 2004). All spectra were recorded using a triple resonance probe equipped with Z-gradients using pulse sequences configured using the Varian BIOPACK software suite (Varian Inc., Palo Alto, USA). For triple-resonance experiments, 128 increments in the carbon dimension, 64 increments in the Nitrogen dimension and 4 transients per FID were used. Strip plots were generated in NMRView (Johnson 2004) using a peak list picked from an HNCO spectrum.

2.14 Analysis of NMR-based binding experiments

Protein-ligand binding studies were based on the fact the binding of a small molecule ligand to a large receptor protein follows a biomolecular association reaction with second order kinetics. The binding of ligand $[L_{free}]$ to a large receptor protein $[P_{free}]$ leads to the formation of a complex $[PL]$, represented by the expression in Eqn.1 below

$$[P_{free}] + [L_{free}] \underset{k_{off}}{\overset{k_{on}}{\rightleftarrows}} [PL]. \tag{1}$$

The rate of binding (association) is given by the product $k_{on}[P_{free}][L_{free}]$ and the rate of dissociation is given by $k_{off}[PL]$. Under equilibrium conditions these two rates are equal, and we have

$$k_{on}[P_{free}][L_{free}] = k_{off}[PL],$$

which can be written as

$$K_D \equiv \frac{k_{off}}{k_{on}} = \frac{[P_{free}][L_{free}]}{[PL]}$$

where we have defined the dissociation constant

$$K_D = \frac{k_{off}}{k_{on}} \tag{2}$$

Since
$$[L_{free}] = [L_{total}] - [PL]$$
$$[P_{free}] = [P_{total}] - [PL]$$

Eqn.1 can be expressed in the form

$$\theta_L \equiv \frac{[PL]}{[P_{total}]} = \frac{[P_{total}] + [L_{total}] + K_D - \sqrt{([P_{total}] + [L_{total}] + K_D)^2 - 4[P_{total}][L_{total}]}}{2[P_{total}]} \tag{3}$$

as shown in Appendix 1, where θ_L is the fraction of the protein that is bound
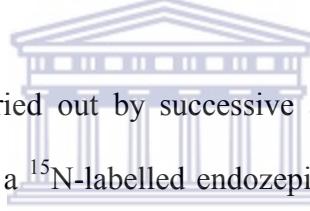
Binding experiments were carried out by successive additions of small aliquots of a concentrated ligand solution to a ^{15}N-labelled endozepine sample. After each addition a ^{15}N-HSQC spectrum was recorded, consisting of 1024 complex points in the ^{1}H dimension, 256 complex points in the ^{15}N dimension and 4 transients per FID. For each ligand concentration, the volumes of the bound peak (V_b) and the unbound peak (V_f) were measured from the corresponding ^{15}N-HSQC spectrum using NMRView (Johnson 2004). Using these values, the bound fraction $\theta_{[L]}$ was calculated using Eqn (4):

$$\theta_{[L]} = \frac{V_b}{V_b + V_f} \tag{4}$$

A graph of θ_L as a function of [L] was generated using MATLAB$^{\circledR}$ (Math Works, Inc.) and the data fit to Eqn. (3), expressed as below

$$\theta_L = \frac{[P_{total}] + [L_{total}] + K_D - \sqrt{([P_{total}] + [L_{total}] + K_D)^2 - 4[P_{total}][L_{total}]}}{2[P_{total}]}$$

where [P] is the fixed protein concentration, [L] is the variable ligand concentration and K_D is the dissociation constant whose value is to be determined. Since we did not expect the values of $[P]$ and K_D to be strongly correlated, we allowed both $[P]$ and K_D to vary freely during the fitting.

We note that

$$\theta_L = \frac{[P_{total}] + [L_{total}] + K_D - \sqrt{([P_{total}] + [L_{total}] + K_D)^2 - 4[P_{total}][L_{total}]}}{2[P_{total}]}$$

can also be expressed as

$$\theta_L = \frac{1 + \frac{[L_{total}]}{[P_{total}]} + \frac{K_D}{[P_{total}]} - \sqrt{\left(1 + \frac{[L_{total}]}{[P_{total}]} + \frac{K_D}{[P_{total}]}\right)^2 - 4\frac{[L_{total}]}{[P_{total}]}}}{2}$$

$$\theta_L = \frac{1 + [L]' + K_D'' - \sqrt{(1 + [L]' + K_D'')^2 - 4[L]'}}{2}$$

Where $[L]'$ respresents the ligand concentration in units of protein concentration and K_D'' represents the dissociation constant in units of protein concentration. In Fig. 4.4, K_d is such that $K_d \equiv K_D''$.

Table 2.1: NMR experiments performed on endozepine

Experiment	Spectrophotometer field strength	Purpose
1D ^{1}H homonuclear	600MHz	To evaluate sample integrity and folding
^{15}N-HSQC	600MHz	To evaluate sample integrity and state of folding; ^{1}H and ^{15}N chemical shifts; binding experiments
CBCA(CO)NH	600MHz	Sequential assignment of backbone resonances; ^{13}C$_\alpha$ and ^{13}C$_\beta$ chemical shifts
HNCACB	600MHz	Sequential assignment of backbone resonances; ^{13}C$_\alpha$ and ^{13}C$_\beta$ chemical shifts
HNCO	600MHz	Carbonyl carbon chemical shifts
H(CCO)NH	600MHz	Side chain proton shifts
TOCSY-HSQC	600MHz	Side chain proton shifts

2.15 Model building

The templates used for model building were identified based on predictions by mGenTHREADER (Jones *et al.* 1999). Secondary structure predictions were generated using PSIPRED (McGuffin *et al.* 2000) and used as a guide in structure-based alignments of endozepine and ACBP sequences from *M. bovis* and *P. falciparum*. The structure file used for model building was generated by superimposition of the templates in MODELLER (Sali and Blundell 1993). Superimposed structures were viewed using the PYMOL Molecular Graphics System Delano Scientific, San Carlos, CA, USA (www.pymol.org 2003). Endozepine models were generated by MODELLER, using a Probability Density Function constrained from the structure-based alignment (Sali and Blundell 1993). The generated models were evaluated using RAMPAGE (Lovell *et al.* 2003) accessible through an on-line server (http://raven.bioc.cam.ac.uk/rampage.php), to ascertain whether the protein stereo-chemical requirements were satisfied. Several

49

models were generated through a series of iterations until the most energetically stable

model was obtained.

Chapter 3: Expression and purification of endozepine

3.1 Introduction

Nuclear Magnetic Resonance spectroscopy (NMR) is an inherently insensitive technique that requires highly concentrated samples (0.5 mM and above) in order to generate spectra with sufficiently high signal-to-noise ratio in a reasonable length of time. The samples need to be enriched with ^{15}N in order to perform NMR-based binding assays, and additionally with ^{13}C in order to assign the spectra and therefore identify amino acids directly involved in the binding site. Molecular biology has provided us with the tools for producing milligram quantities of proteins by over-expression in bacteria, as well as enriching them with ^{15}N and ^{13}C by growing the bacteria on suitably enriched media. This Chapter describes the exogenous expression of isotopically enriched recombinant endozepine and its purification to homogeneity for NMR analysis.
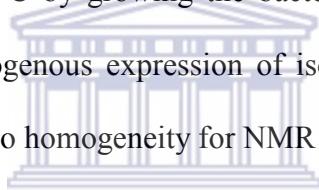
Endozepine was expressed as a C-terminal fusion with the 26 kDa Glutathione S-transferase (GST) using the pGEX-6P-2 system (Amersham Biosciences). The GST tag allowed for separation of the GST-endozepine fusion protein from bacterial proteins using a glutathione-linked agarose column. The pGEX-6P series of plasmids contain a *tac* promoter, which drives high levels of IPTG inducible expression of the recombinant fusion protein in *E. coli*, as well as a recognition sequence for the PreScission^{TM} Protease (Amersham Pharmacia Biotech), which allows for separation of the GST domain from endozepine after purification. PreScission^{TM} Protease (Amersham Pharmacia Biotech), a fusion of GST and human rhinovirus 3C protease, was removed along with the cleaved GST domain using the glutathione affinity method.

3.2 Recombinant production of 13C, 15N enriched endozepine

E. coli BL21 (DE3) pLysS cells were transformed with pGEX-6P-2-endozepine, as described in Section 2.6. Transformed cells were screened for recombinant protein expression, as described in Section 2.7. Fig. 3.1 shows SDS-PAGE analysis of bacterial lysates from 1 ml cultures from four different clones. Lane 1 is the molecular range marker, lanes 2, 4, 6 and 8 correspond to un-induced lysate. Lanes 3, 5, 7 and 9 correspond to induced lysate. The recombinant GST-endozepine fusion protein corresponding to approximately 37 kDa can be seen in all four induced lysates. Large-scale expression was carried out using 50 μl from the culture shown in lane 2 of Fig. 3.1.

Cell lysis, extraction and affinity purification of GST-endozepine were carried out as described in Section 2.8. SDS-PAGE analysis of the expression and purification is shown in Fig. 3.2. It is evident from lane 6 that a very high yield of recombinant GST-endozepine fusion protein was achieved.

The recombinant protein was cleaved for 24 hours at 4º C using PreScission^{TM} Protease (Amersham Pharmacia Biotech) as described in Section 2.8. After cleavage the sample was returned to the glutathione-linked agarose column in order to remove most of the GST, with the target protein being collected in the flow through. The results of the cleavage and purification were analysed using SDS-PAGE, as shown in Fig. 3.3. Lane 3 shows a band corresponding to GST (26.6 kDa) and a band corresponding to endozepine (10.5 kDa). Only trace amounts of the original fusion protein (37.1 kDa) remain, indicating that cleavage was almost complete within 24 hours. The intensities of
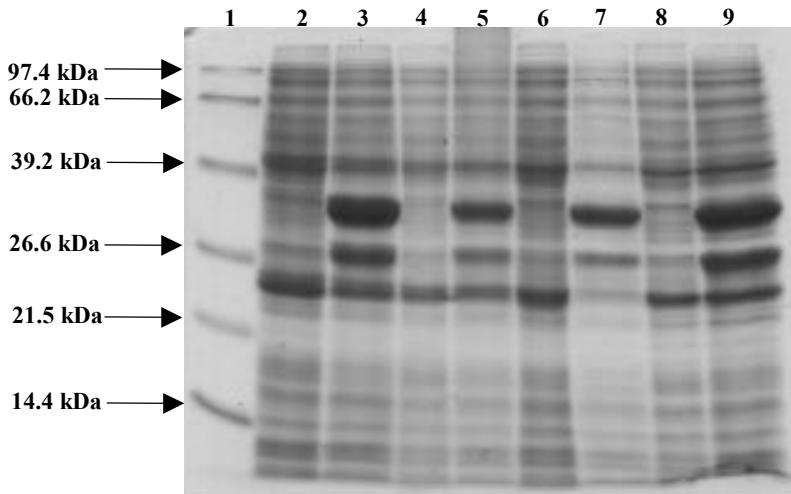
Fig. 3.1: Screening of colonies transformed with pGEX-6P-2-endozepine for the expression of GST-endozepine fusion protein. Lane 1 shows molecular range maker, lanes 2, 4, 6 and 8 show un-induced samples. Lanes 3, 5, 7 and 9 show induced samples. All induced samples demonstrate the presence of a strong band of approximately 37 kDa, corresponding to the expected combined size of GST and endozepine. The co-expression of an un-identified protein corresponding to approximately 27 kDa was observed in the induced samples.
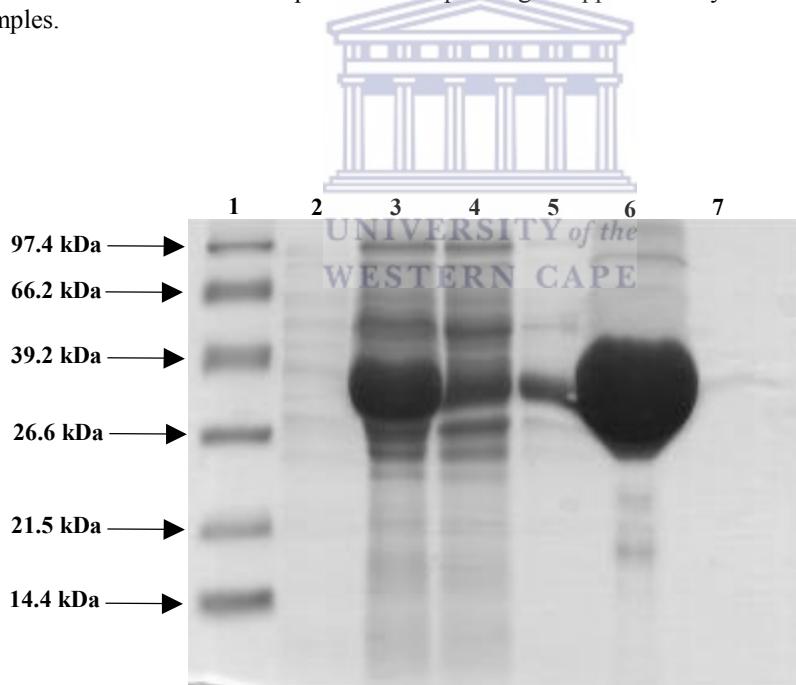
Fig. 3.2: Expression and affinity purification of GST-endozepine fusion protein. Lane 1 shows molecular range maker, lane 2 shows total protein extract from un-induced sample, lane 3 shows total protein extract from induced sample, lane 4 shows GST column flow through, lane 5 shows GST column wash (1), lane 6 shows GST column elute and lane 7 shows GST column wash (2).

the band corresponding to GST and endozepine are consistent with the relative sizes of the two proteins, suggesting that there was little loss of endozepine following the removal of GST. The result of the removal of GST using a second glutathione affinity step is shown in lanes 4 and 5.

An alternative method of removing GST was also developed, using anion exchange chromatography at pH 7.0, as described in Section 2.9. The chromatogram is shown in Fig. 3.4 and an SDS-PAGE analysis of the corresponding fractions is shown in the insert. The top left insert shows the presence of endozepine in the column flow through while the top right insert shows that the residual GST from the affinity purification step was immobilized onto the anion exchange column and eluted with increased salt gradient. Anion exchange therefore resulted in significant purification of the endozepine by removing the residual GST. Fractions containing endozepine were pooled and concentrated to 900 μl using YM-3 Centriprep devices (Millipore, Bedford, USA).

Size exclusion chromatography was carried out using a 100 x 1.8 cm Econo® Column packed with 150 ml Sephacryl S100 gel operated using a BioCAD® SPRINT^TM Perfusion chromatography system (PerSeptive Biosystems), as described in Section 2.10. The chromatogram is shown in Fig. 3.5, containing 1 major Peak. Fractions across the peak (see Fig. 3.6) show that it corresponds to highly purified endozepine. Fractions containing endozepine were pooled and concentrated using YM-3 Centriprep devices (Millipore, Bedford, USA) to a final volume of 600 μl. SDS-PAGE analysis of the concentrated endozepine sample is shown in Fig. 3.7. Lane 1 shows molecular range
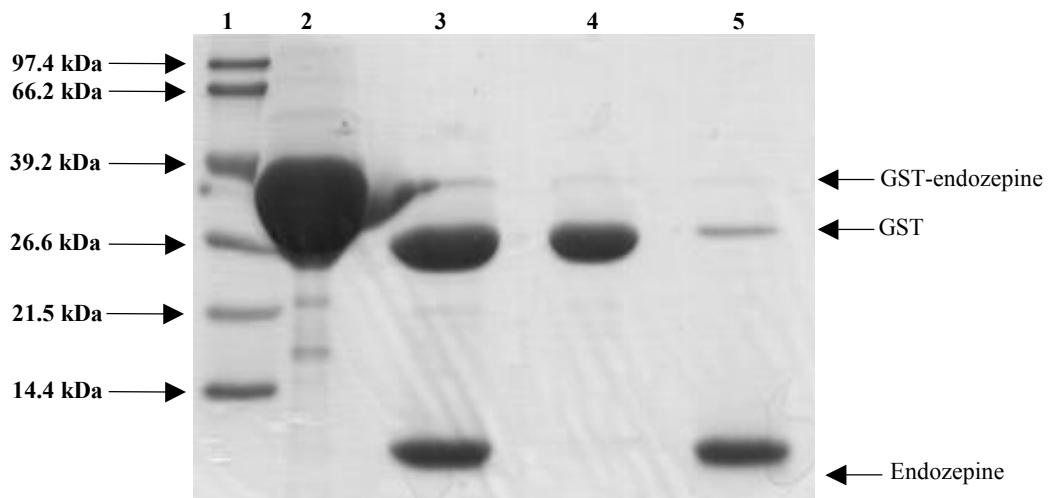
Fig. 3.3: PreScission^TM protease cleavage of GST-endozepine fusion protein. Lane 1 shows molecular range marker, lane 2 shows the un-cleaved fusion protein, lane 3 shows fusion protein after cleavage, lane 4 shows eluted GST from the gravity fed glutathione agarose column and lane 5 shows endozepine after affinity purification of the cleaved sample. Lane 5 shows the presence of residual GST within the fractions containing endozepine.
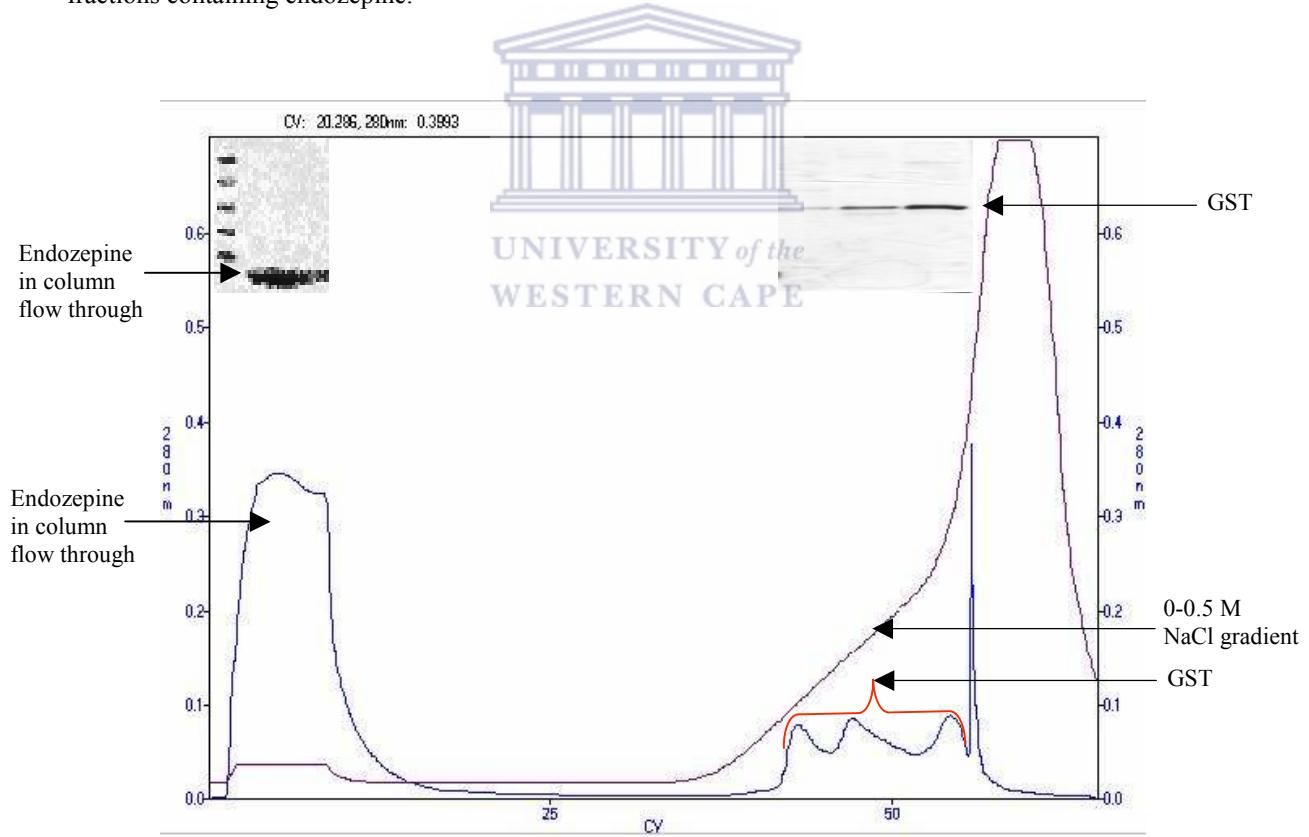
Fig. 3.4: Chromatogram showing anion exchange chromatography of the affinity purified endozepine sample (Fig. 3.3, lane 5). SDS-PAGE analysis of the corresponding peaks in the chromatogram is shown in the insert. The top left insert shows the presence of endozepine in the anion exchange column flow through while the top right insert shows that GST was immobilized to the anion exchange column and eluted using a salt gradient.
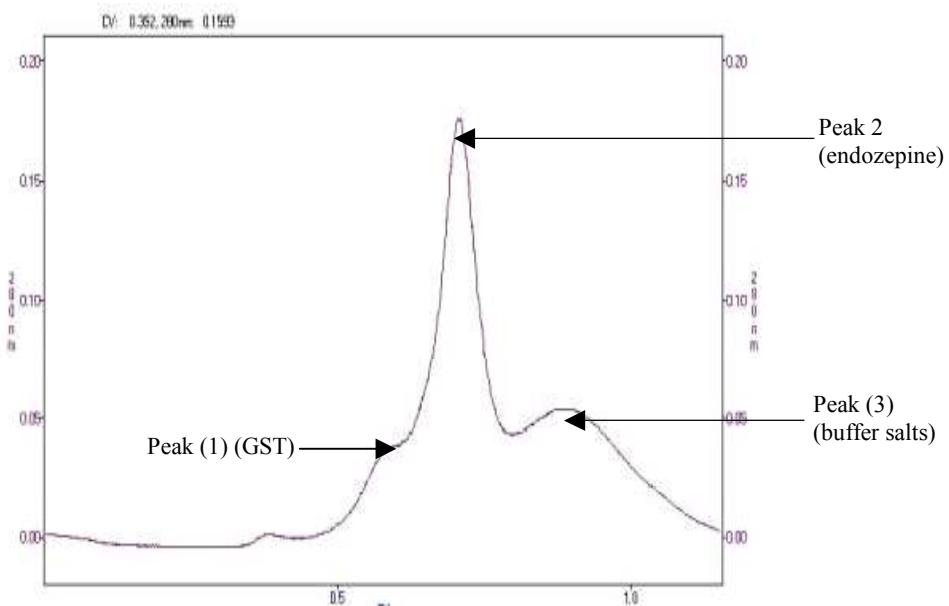
Fig. 3.5: Chromatogram showing size exclusion chromatography of anion exchanged endozepine sample. The chromatogram shows three peaks, corresponding to GST, endozepine and sample buffer salts respectively.
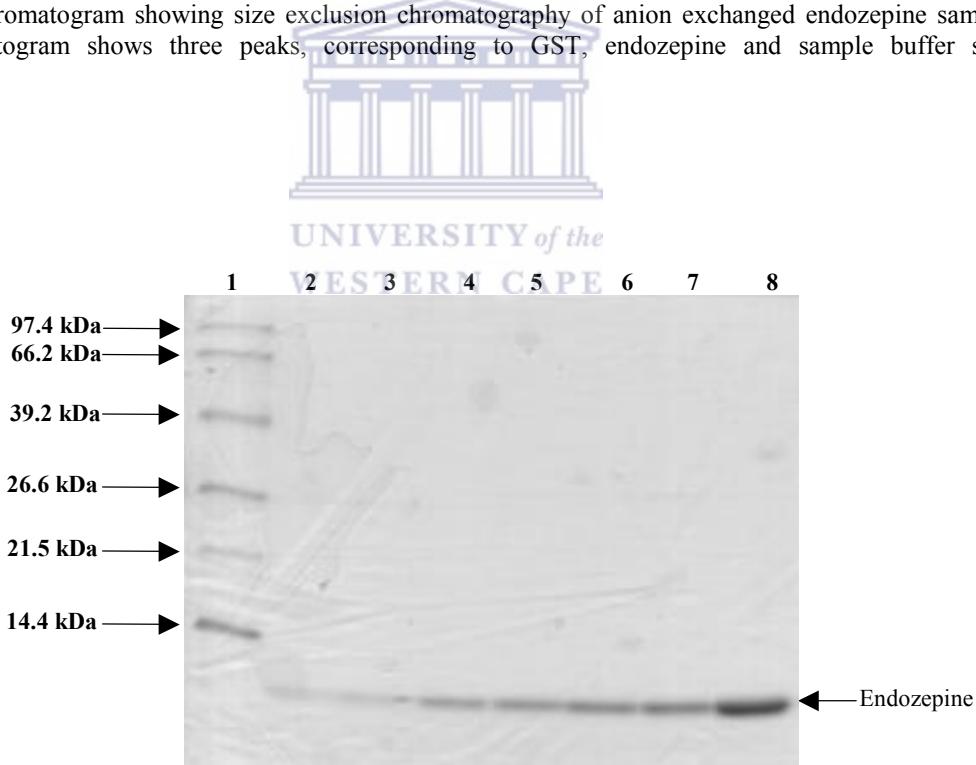
Fig. 3.6: SDS analysis of fractions across peak (2) of the size exclusion chromatogram (Fig 3.5). Lane 1 shows molecular range marker, lanes 2-8 show that peak (2) of the size exclusion chromatogram corresponds to highly purified endozepine.
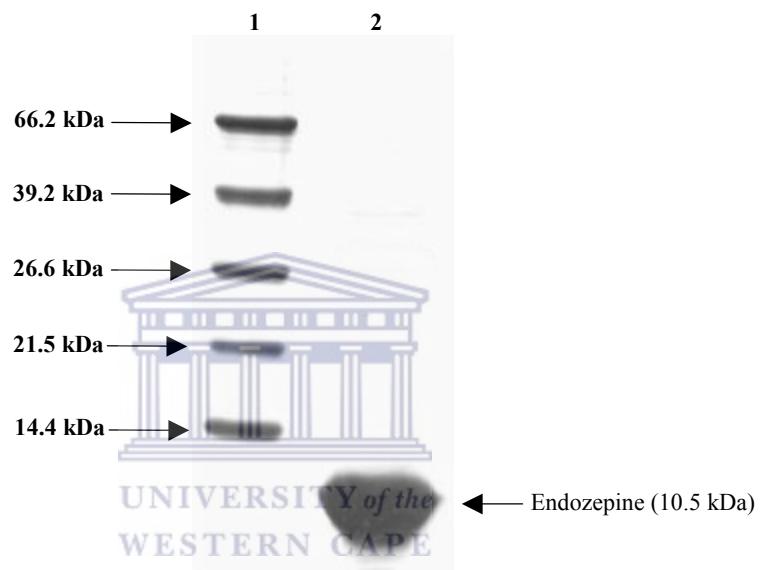
Fig. 3.7: SDS-PAGE analysis of a concentrated sample of endozepine. Lane 1 shows molecular range marker and lane 2 shows a concentrated sample of endozepine.

and lane 2 shows a concentrated sample of endozepine.

3.3 Physical analysis of 13C, 15N endozepine

3.3.1 Determination of protein concentrations

Endozepine concentrations were calculated using two independent methods: the Bradford calourimetric assay and the UV absorption method. For the Bradford assay (see Section 2.12), Bradford reagent was added to five different concentrations of lysozyme and the absorbance at 620 nm used to construct a plot of absorbance as a function of the lysozyme concentration (see Chart 3.1), to construct a straight line through the data of the form

$$A_{620} = 1.7741 \ [\text{lysozyme}] + 0.0003 \tag{5}$$

The absorbance of the endozepine sample at 100-fold dilution recorded under the same condition was found to be 0.224. The horizontal dashed line, in Chart 3.1, indicates this value. The corresponding concentration, determined using Eqn (5), is 12.61 mg/ml. Since the molecular weight of the protein is 10.5 kDa, this corresponds to a molar concentration of 1.2 mM.

The protein concentration was measured independently using a NanoDrop® *ND-1000* Spectrophotometer (NanoDrop Technologies Inc.). The UV absorption spectrum of the sample is shown in Fig. 3.8. The large broad peak at 280 nm is indicative of very concentrated protein. The concentration (C) is related to the absorbance at 280 nm (A_{280}), the optical path length (L), and the molar extinction coefficient (E) by the Beer Lamberts

Table 3.1: Absorbance values of lysozyme at 620nm

Concentration in mg/ml	Absorbance at 620 nm
0.015625	0.0080
0.03125	0.0525
0.06250	0.1225
0.12500	0.2485
0.25000	0.4295
endozepine : 1/100	0.2240

Chart 3.1
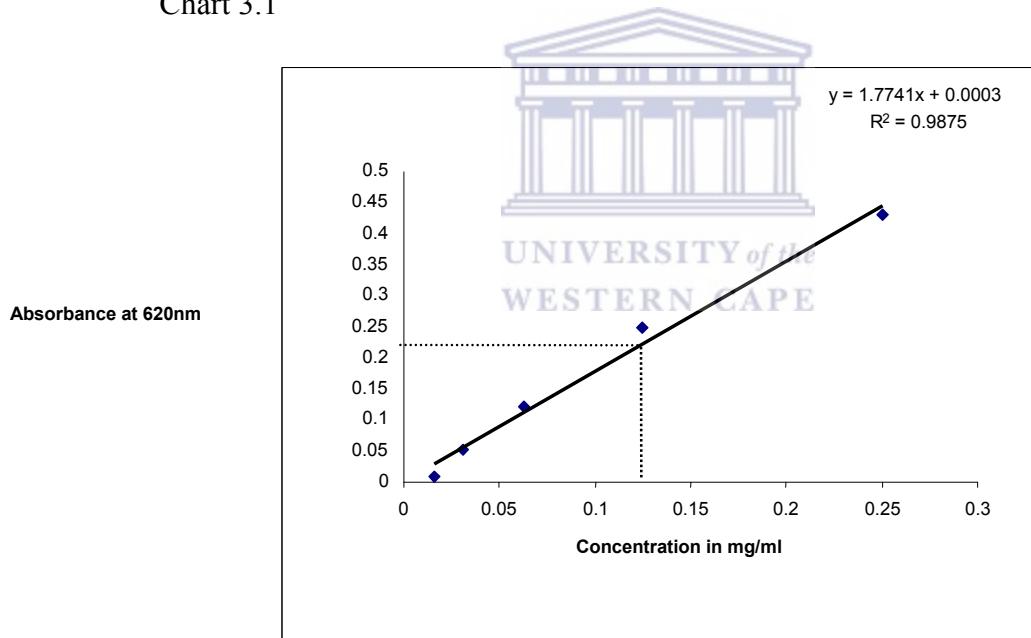
Table 3.1 shows the absorbance values obtained at 620 nm (A_{620}) and the corresponding concentrations of lysozyme. Chart 3.1 shows the standard curve fit to the data in Table 3.1. The absorbance of the endozepine sample (0.224) at 100-fold dilution is indicated by the horizontal dashed line. The corresponding concentration (vertical dashed line) is 12.60 mg/ml, which corresponds to 1.2 mM.
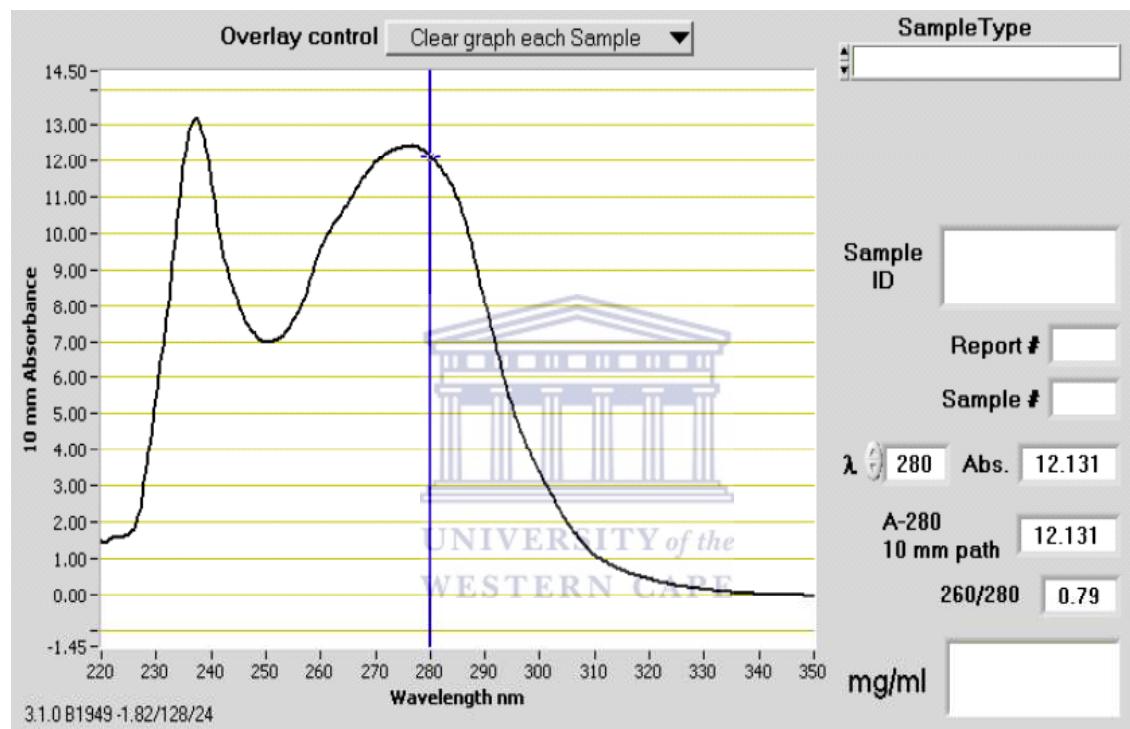
Fig 3.8: The UV absorption spectrum of a concentrated endozepine sample at 280 nm, recorded using NanoDrop®*ND1000* Spectrophotometer (NanoDrop Technologies Inc.).

Law.

$$A_{280} = ECL \qquad\qquad (6)$$

The extinction coefficient was predicted on basis of the amino acid sequence of endozepine to be $E = 10.930$ mM^{-1} cm^{-1}. Using the values of $A_{280} = 12.13$ and $L = 1$ cm, C was calculated using (6) to be $C = 1.12$ mM.

Although the UV absorption method relies on the prediction of the extinction coefficient from the amino acid sequence, it gives a value for the concentration of endozepine, which is consistent with the value, calculated using the Bradford assay. We conclude that the concentration is in the range 1.1-1.2 mM. NMR experiments require a high sample concentration in the range of 0.5 mM and above, to generate spectra with sufficiently high signal to noise ratio in a reasonable length of time. We concluded therefore that our sample concentration was adequate for conducting NMR experiments.

3.3.2 Assessment of folding and sample integrity using NMR

Samples used for spectral acquisition were prepared as described in Section 2.13. 7% D_2O was added to the NMR sample to act as internal reference frequency on which to lock the spectrometer frequency, thus providing stable conditions for extended NMR experiments. Suppression of the water resonance at 4.73 ppm was effected using pre-saturation. NMR analysis was carried out in H_2O rather than D_2O because exchange of the labile amide protons would lead to the suppression of their NMR resonances, which are required for ^{15}N-HSQC experiments.

1D proton spectrum

The 1D proton spectrum of endozepine is shown in Fig. 3.9. A 1D ^{1}H-NMR experiment is an established and sensitive method for investigating the state of folding of a protein (Rehm *et al.*, 2002). The degree of folding can be predicted on the basis of the chemical shift dispersion of proton signals. In unfolded proteins proton chemical shifts correspond to random coil values; i.e, backbone H^N resonances appear clustered around 8.3 ppm, methyl groups appear between 0.8 and 1.1 ppm (Wüthrich 1986) and H^{α} resonances protons appear in the region 4.1-4.4 ppm (Cavanagh 1996). In folded proteins these chemical shifts become significantly shifted away from random coil values due to structural diversity and the presence of different chemical environments and shielding effects, in particular from ring currents caused by aromatic side chains (Rehm *et al.* 2002). It can be seen from Fig. 3.9 that a number of H^N resonances are shifted significantly up-field into the range 8-11 ppm. A number of methyl group resonances have been down-shifted into 0.5-(-1.0 ppm); in particular, the peak observed at -0.35 ppm. All of these resonances correspond to groups that are in chemical environments significantly different from what they would be if the protein were unfolded. We conclude therefore that endozepine is properly folded and suitable for structural analysis.

2D ^{15}N-HSQC spectrum

The state of folding and integrity of endozepine sample were confirmed using a 2-dimensional ^{1}H, ^{15}N-heteronuclear single quantum coherence (^{15}N-HSQC) spectrum (see Fig 3.11). Each peak represents the backbone NH group of a single amino
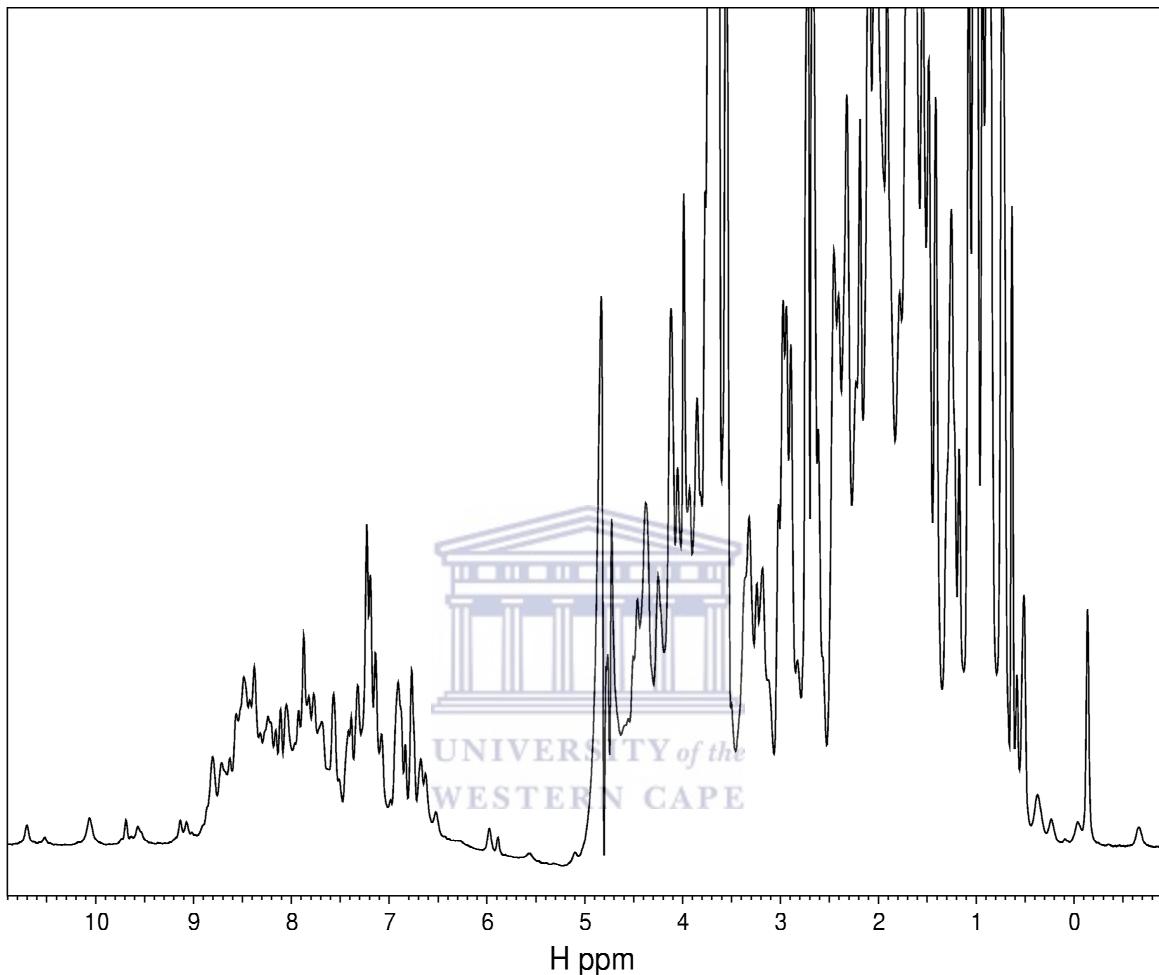
Fig 3.9:1D ^{1}H spectrum of endozepine at pH 6.0, 25 ºC recorded at 600 MHz. Spectrum shows a good dispersion of resonances (amide protons in the region of 8-11 ppm, alpha protons in the regions of 4.0-6.0 ppm and methyl protons in the region of 0.5 to -1 ppm). The peak observed at -0.35 ppm within the methyl group region and the overall spread of peaks indicates that the protein is folded and ideal for structural studies.
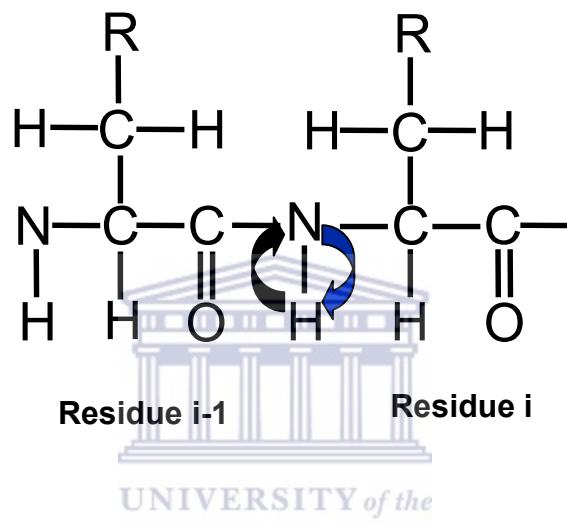
Fig. 3.10: The magnetization transfer in a ^{15}N-HSQC-experiment depicting through-bond transfer between the backbone nitrogen nuclei and the attached amide proton, using the 95 Hz scalar coupling between them.

acid (see Fig.3.10), horizontal coordinates corresponding to the H^N chemical shift and the vertical coordinate to the chemical shift of the attached nitrogen. The only exceptions are the pair of peaks (shown joined by horizontal lines in Fig 3.11), which correspond to backbone NH_2 groups of arginine and glutamine residues. Proline residues do not appear in a ^{15}N-HSQC spectrum since they lack an NH group. The spectrum is well dispersed in both dimensions, indicating that the protein is well folded (Woestenenk *et al.* 2003).

In the ^1H dimension, a number of resonances are shifted significantly up-field, including those at $(^{15}N, {}^1H) = (112, 9.57)$, $(118, 10.1)$, $(125.8, 10.7)$, $(126, 9.7)$, $(130, 10.1)$. These provide good evidence that the protein is folded, as these resonances must experience a chemical environment leading to anti-shielding of the B_0 field (magnetic field). The resonances are also very sharp indicating that the protein tumbles rapidly in solution, which suggests that it adopts a compact, globular shape in solution. Unfolded proteins tend to have broad line shapes due to slow tumbling resulting from aggregation and their large apparent size (Larsson *et al.* 2003).

Despite the up-shifted resonances mentioned above, the majority of the resonances are clustered in quite a narrow range on either side of 8.3 ppm. However, the sharpness of the line indicates that this is due to high α-helical content, rather than to unfolding, consistent with the secondary structure expected on the basis of homology modelling. The high degree of symmetry of the α-helical conformation leads to clustering of chemical shifts around 8.3 in the ^1H dimension (Vadrevu *et al.* 2003). Despite the low levels of dispersion, the narrowness of the lines means that at 600 MHz the degree of overlap in the
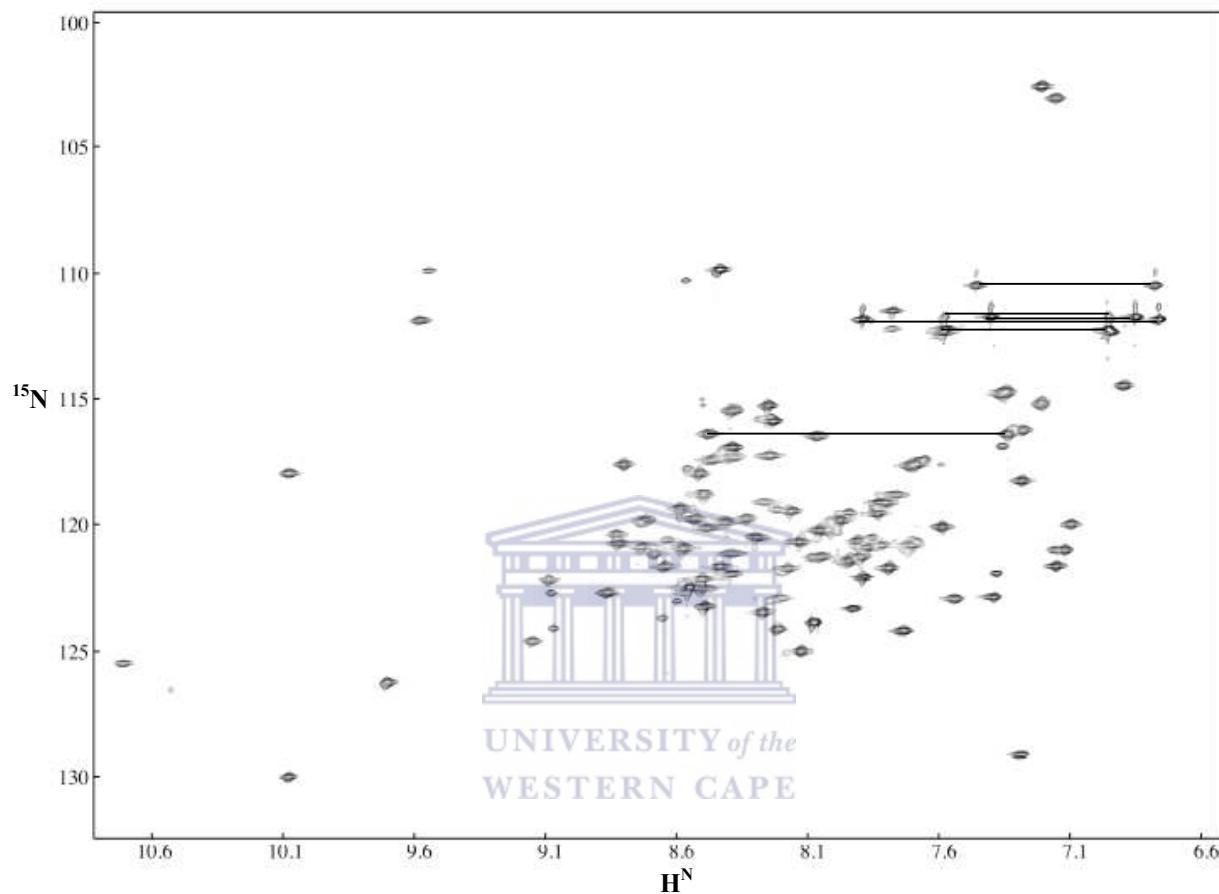
Fig. 3.11: ^{15}N-HSQC spectrum of endozepine at pH 6.0, 25 ºC, recorded at 600 MHz. The expressed sample including the artifactual residues contains 92 residues. Excluding the six prolines and the N-terminal residue for which no peaks are expected we expect a total of 85 resonances. Excluding the NH$_2$ resonances and the tryptophan NH group, a total 82 resonances can be identified. The resonances unaccounted for are either not visible or overlapped by others. Six of the seven expected NH$_2$ groups are shown connected by horizontal lines. The seventh NH$_2$ group, which is in the vicinity of 6ppm, is not shown in this spectrum. These evidences support the conclusion that the spectrum shown above, corresponds to endozepine.

^{15}N-HSQC spectrum is small.

A number of side-chain NH_2 group resonances have been indicated using horizontal lines at the top of the spectrum in Fig. 3.11. These take the form of a pair of peaks with a single nitrogen shifts and two different proton shifts, corresponding to the two protons respectively. Endozepine contains seven amino acids bearing side chains NH_2 groups; five glutamines and two asparagines. Of these, six are visible in Fig. 3.11. The seventh, which is shifted far downfield to (^{15}N, ^{1}H) = (116, 6.1) and (116, 5.5), is not shown. The resonances (^{15}N, ^{1}H) = (130, 10.1) appears in the ^{15}N-HSQC spectrum, but not in the HNCO (data not shown), from which we deduce that it corresponds to the H$^\varepsilon$ side chain proton of Trp 59, which is the only Trp in the sequence. The absence of an attached C=O in the tryptophan ring means that the resonance will not appear in the HNCO, although that will not prevent it from appearing in the ^{15}N-HSQC.

With the inclusion of the five artifactual residues at the N-terminus, the expressed sample of endozepine is expected to contain 92 amino acid residues. Excluding the six prolines and the N-terminal residue, none of which could give rise to resonances, a total of 85 resonances would be expected. With the inclusion of the fourteen NH_2 resonances and the tryptophan side chain, the number of resonances identified (see Fig. 5.4) is infact 82. Some of these turn out to be duplicates due to the presence of more than one conformation of a few residues (see Fig. 5.4); on the whole the spectrum appears to be a good representation of the protein and therefore a suitable indicator for ligand binding.

Chapter 4: Investigation of the binding of endozepine to palmitoyl-CoA, C16-ceramide and C2-ceramide

4.1 Introduction to NMR-based binding studies

An understanding of protein-ligand interactions provides clues to the functions of proteins in their physiological states. NMR has been shown to be a valuable tool for the investigation of protein-ligand interactions (Pellecchia *et al.* 2002). NMR-based binding studies employ the fact that when a ligand binds to a macromolecule it affects the chemical environment around the binding site leading to perturbations of NMR precession frequencies. Those perturbations are particularly significant for the backbone NH groups, which are typically involved in hydrogen bond formation. Ligand binding often involves re-arrangement of hydrogen bonding networks, which have large effects on H^N and N chemical shifts. These chemical shift changes can be conveniently observed in ^{15}N-enriched proteins with the aid of a ^{15}N-HSQC spectrum. In this study, ^{15}N-enriched endozepine samples were used to record ^{15}N-HSQC NMR spectra, which were employed to probe the binding of endozepine to palmitoyl-CoA, C_2 and C_{16}-ceramide. The identity of the resonances implicated in binding was subsequently determined through sequence specific resonance assignment, which was accomplished with the aid of ^{15}N, ^{13}C-enriched proteins using triple resonance experiments. Residues identified as being involved in binding were mapped onto a modelled structure in order to gain better insight into their spatial arrangement.

Two quantitatively different effects are observed in the NMR spectrum when a ligand is titrated into a protein sample, depending on the strength of the interaction and the

difference between the chemical shifts of a particular resonance in the bound and unbound states respectively. The strength of binding is characterized by

$$K_D \equiv \frac{k_{off}}{k_{on}},$$

where K_{off} and K_{on} are the off-rate and on-rate respectively.

Small values of K_D are indicative of strong binding whereas large values are indicative of weak binding (Fig. 4.4). Strong binding typically corresponds to slow off-rates whereas weak binding corresponds to fast off-rates. The difference in chemical shifts of bound and unbound resonances is given in Hz. If the off-rate is slow compared to the difference in chemical shift between the bound and un-bound forms of the protein, the bound and unbound molecules appear as separate species from the point of view of NMR, and two separate peaks are observed. The volume under each peak is proportional to the number of molecules in each state. During a titration the volume of the unbound peak therefore decrease and the volume of the bound peaks increases; the fraction of molecules in the bound state can be inferred from Eqn. (4) in Section 2.14.

Alternatively, if the off-rate rate is fast compared with the difference in the chemical shifts, a single peak is observed at a position corresponding to the weighted average of the positions of the bound and un-bound peaks, where the weighting is proportional to the fraction of the molecules in each state (Pellecchia *et al.* 2002). Correspondingly, during a titration a single peak moves from the position of the unbound to the bound state, and the bound fraction can be inferred from the position of the peak.

4.2 Interaction of palmitoyl-CoA with endozepine

The binding of ^{15}N-enriched endozepine to palmitoyl-CoA was investigated using a 1.2 mM sample of ^{15}N-labelled endozepine. Successive aliquots of palmitoyl-CoA were added to the sample to final concentrations of 0.11 mM, 0.22 mM, 0.37 mM, 0.6 mM, 0.82 mM, 1.0 mM, 1.2 mM, 1.4 mM and 2.0 mM respectively and a ^{15}N-HSQC spectrum acquired following each addition. A large number of changes were observed, as can be seen in Fig. 4.1. More than half of the resonances showed a decrease in amplitude accompanied by the appearance of new resonances nearby. The remaining resonances were unaffected. We conclude that palmitoyl-CoA binds strongly to endozepine. Figs. 4.2 and 4.3 show expanded views of two resonances later determined to correspond to K17 and G18 respectively, displaying a decrease in the amplitude of one peak and an increase of the other peak during the course of the titration. The volumes of the bound and unbound peaks were measured using NMRView (Johnson 2004) and used to calculate the bound fraction θ using Eqn. (4) in Section 2.14.

θ was plotted as a function of total added ligand for resonances corresponding to residues K17 (Fig 4.2) and G18 (Figs. 4.3). In both cases it can be seen that θ increases almost linearly with increasing ligand concentration until it levels off sharply at $\theta = 1$, at a ligand concentration roughly equal to that of the protein. The protein sequesters all of the available ligand until it becomes saturated, from which we conclude that the protein has a high affinity for palmitoyl-CoA. The experimentally determined values of θ were fit to the theoretical expression (Eqn. (4), Section 2.14), from which values for K_D and the total protein concentration $[P_{total}]$ were extracted (see Table 4.1). The raw data can be found in Appendix II.
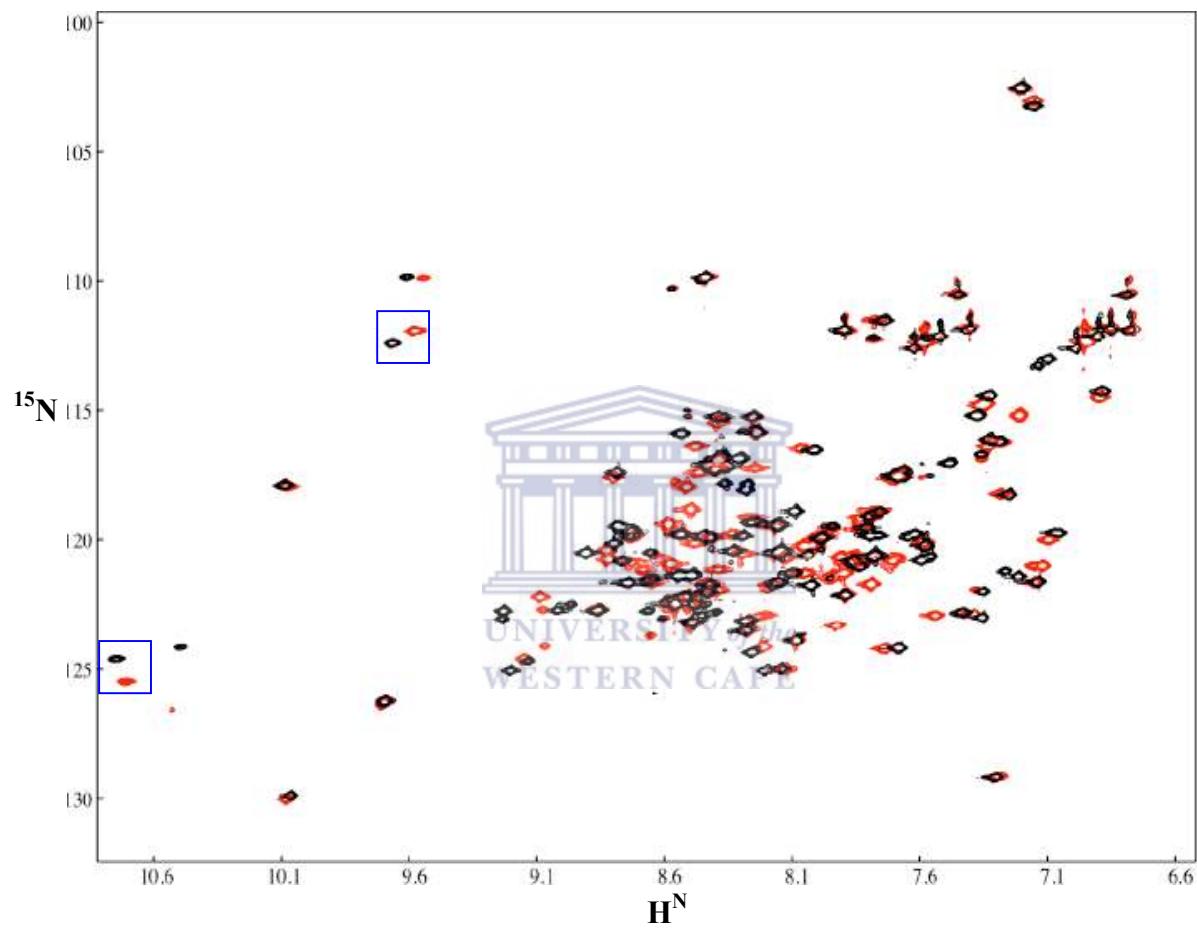
Fig. 4.1: Overlay ^{15}N-HSQC spectra of 1.2 mM un-liganded spectra of endozepine (red) and endozepine fully saturated with 2 mM palmitoyl-CoA (black). Perturbations to more than half of the resonances indicate that palmitoyl-CoA interacts with endozepine. Squares indicate pairs of resonances used to calculate K_D .
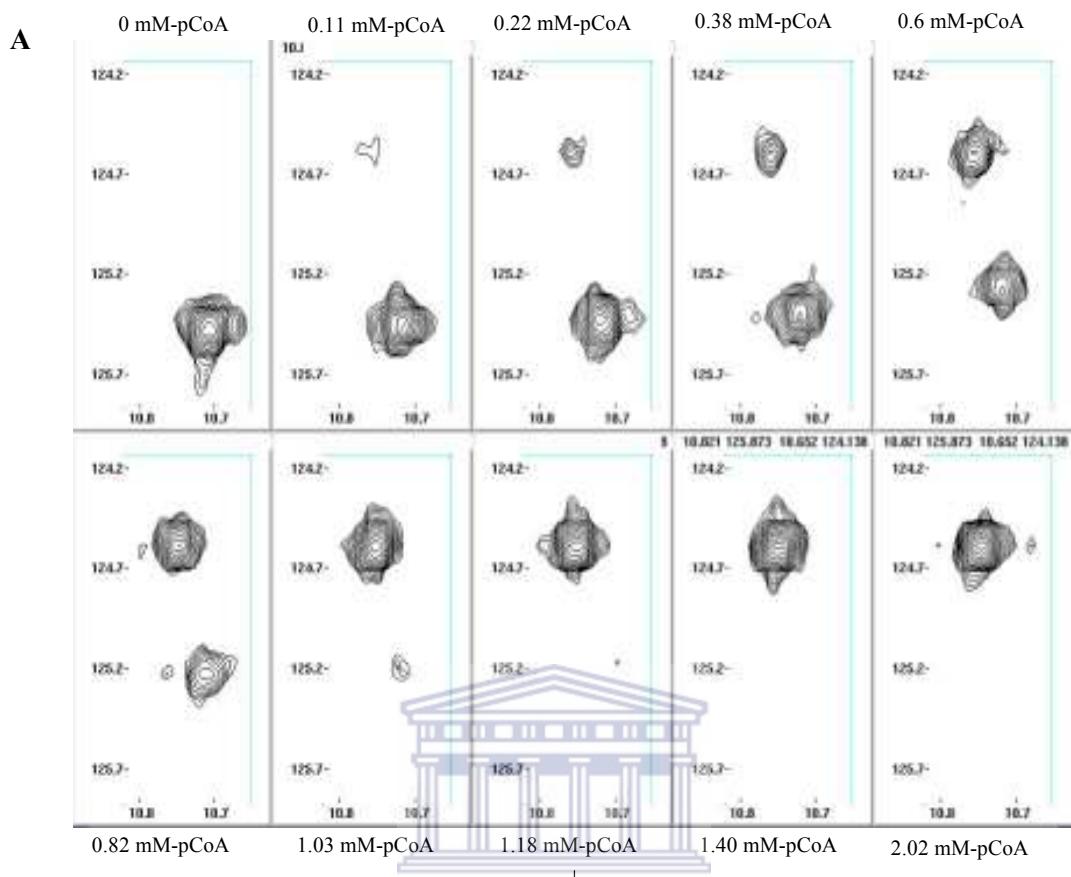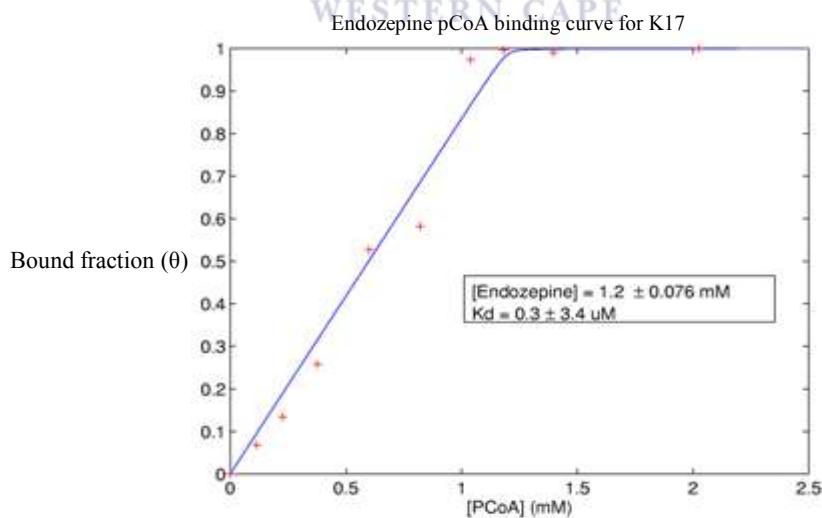
Fig. 4.2 (A): A close up of region around K17 displaying resonance changes during titration binding experiments. (**B**) A plot of θ as a function of ligand concentration (crosses), fit to the theoretical expression of θ (see Section 2.14). Experimental data (crosses in B) were extracted from volumes shown in A.
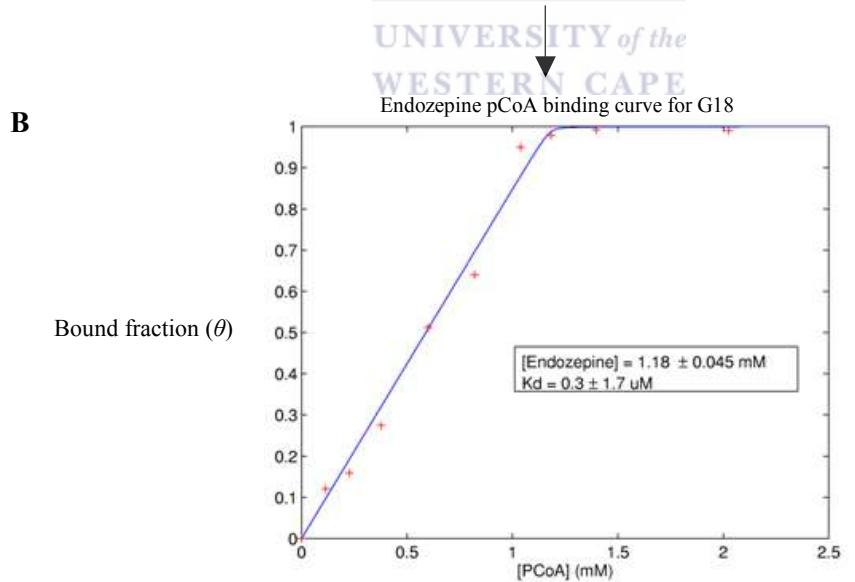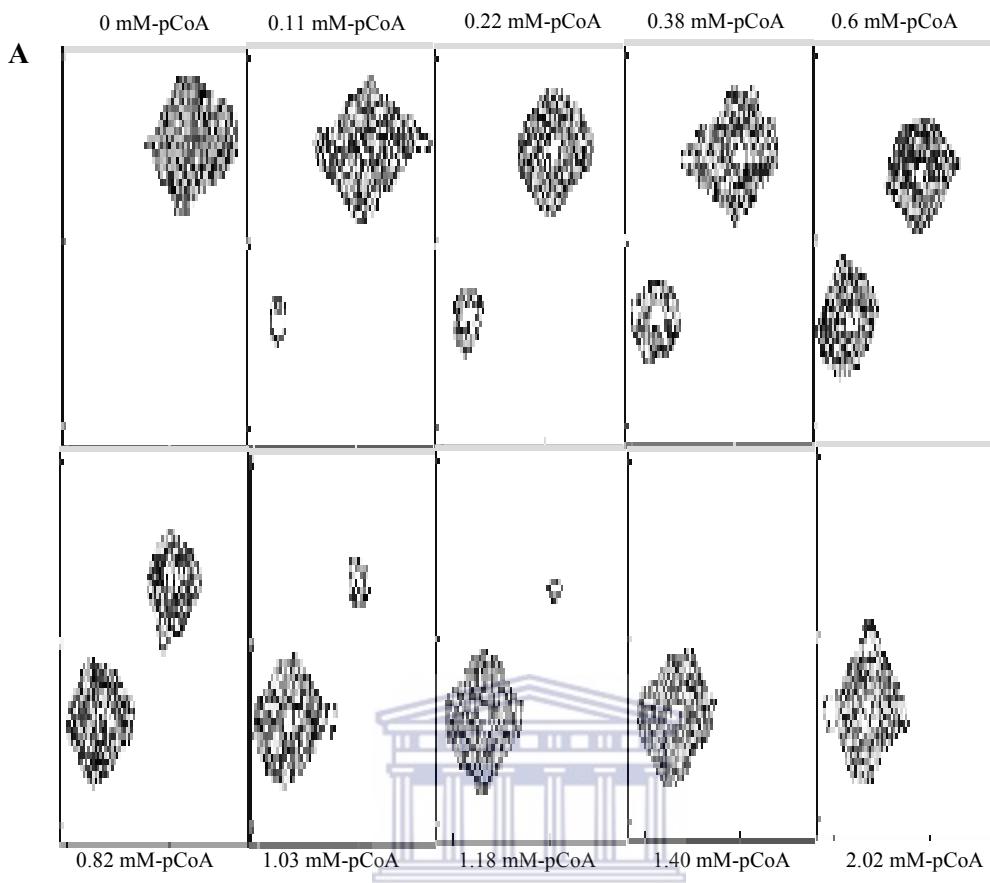
Fig. 4.3 (A): A close up of region around G18, displaying resonance changes during titration binding experiments. (**B**) A plot of θ as a function of ligand concentration (crosses) to the theoretical expression of θ (see Section 2.14). Experimental data (crosses in B**)** were extracted from volumes shown in A.

The expression in Eqn. (3) Section 2.14 can be used to generate a series of binding curves as a function of difference in their K_D values (Fig. 4.4). The value of K_D is indicative of the strength of interaction between two molecules with very small K_D values (in the micromolar range) typically corresponding to strong binding (Nietlispach *et al.* 2004). The method employed in this work for studying interaction of small molecule ligand to large receptor protein has the limitation of being inadequate to discriminate between strong and very strong binding because at smaller values of K_D, the corresponding binding curves will differ negligibly around the "turnover point" leading to the sharpening of the "turnover point" (Fig. 4.4). The value of K_D = 0 corresponds to infinitely strong binding and is observed to show the effect of a sharpened "turnover point" in Fig. 4.4. Furthermore, from Fig. 4.4, we observe that at smaller values of K_D (the typical scenario during strong and very strong binding), the bound fraction (θ) increases linearly until it levels off, at a point were protein concentration is approximately equal to the ligand concentration.
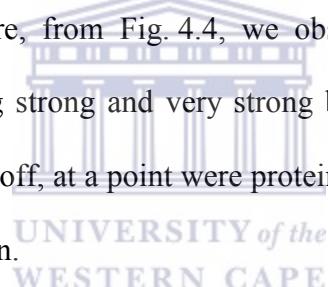
The values of K_D obtained from the fitting are both in the region of $0 - 1$ μM, which corresponds to strong binding (Nietlispach *et al.* 2004). However, the size of the error bars suggests that K_D is actually consistent with zero. In terms of the fitting procedure, values of K_D smaller than 3 μM would only have the effect of "sharpening the turnover" (Fig. 4.4) in Figs. 4.2 and 4.3, which is beyond the accuracy of our data. Our data is therefore not comprehensive enough in this region to distinguish between values of K_D less than ~3 μM. Our data is therefore consistent with both strong and very strong binding.

$K_D[P]$
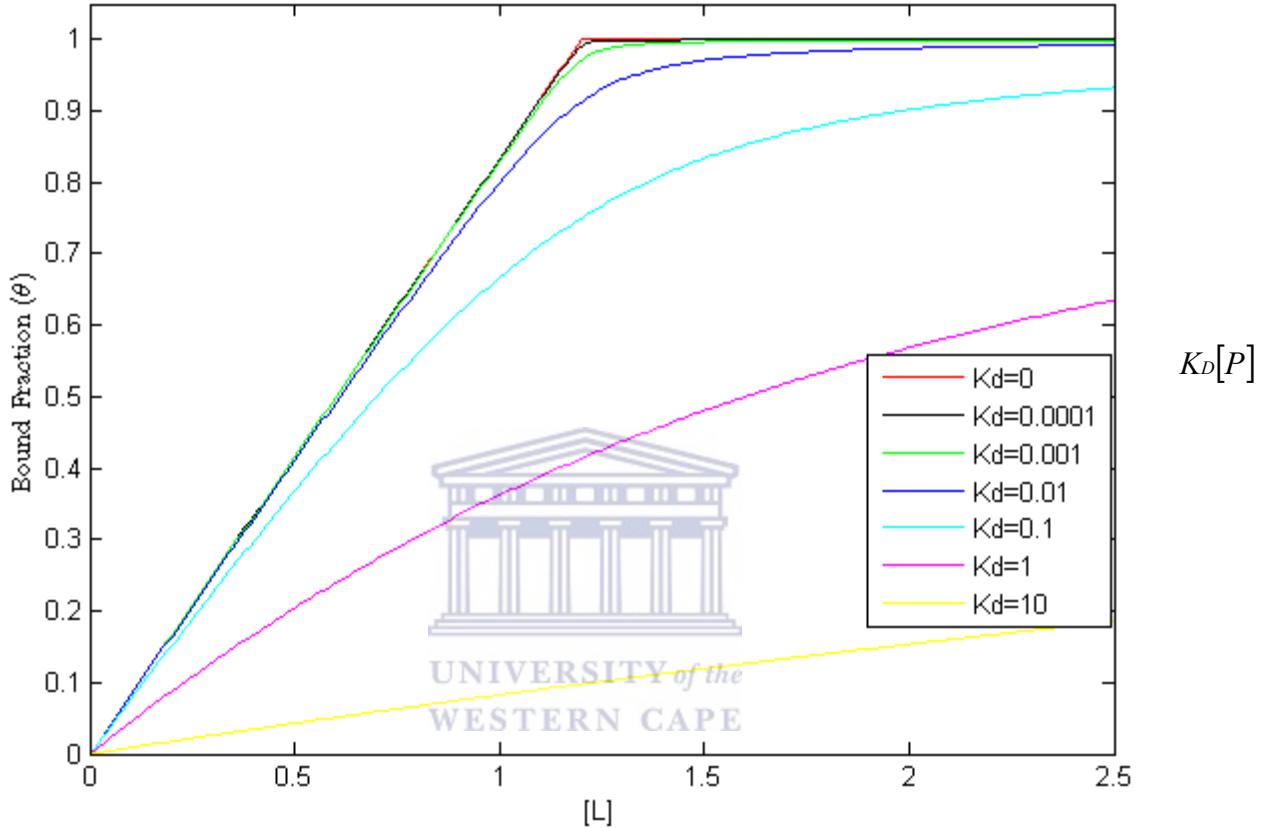
Fig. 2.1: Binding curves of different K_d values generated using Eqn. (3), Section 2.14. The figure shows that at low K_d values (strong binding), the bound fraction (θ) increases linearly and levels off at a point where protein concentration is approximately equal to ligand concentration. The figure also shows the sharpening of "turnove point" at lower K_d values and a sharp "turnover point" at $K_d = 0$. Curves were generated using MATLAB® (Math Works, Inc.). Note K_d is expressed in units of protein concentration ($[K_d \equiv K_D"]$), see Section 2.14.

The use of Eqn. (3) Section 2.14, to generate binding curves is most useful for discriminating between strong and weak binding and may not be ideal for differentiating between strong and very strong binding. At lower values of K_D a change in "turnover point" occurs however we can not tell with accuracy the exact point of turnover. Our data therefore establishes an upper limit of 3 μM on the value of K_D; although the value may be lower than 3 μM, we cannot decide on the basis of our data. In order to discriminate between strong and very strong binding, it may be useful to employ tools that that can readily work with protein concentrations in the micro to nanomalar range since this will provide more accurate values for the "turnover point" and thus provide more precise measurements of K_D. NMR technique requires that the protein concentration be the range of 0.5 mM and above. We conclude therefore that our approach is not the most ideal for differentiating between both possibilities.

Table 4.1 gives the values of the dissociation constant K_D and the total protein concentration.
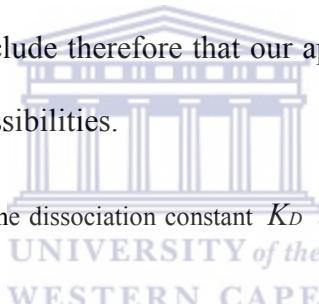
Residues	Dissociation constant (K_D)	Protein concentration [P]
K17	$0.3 \pm 3.4 \, \mu M$	$1.2 \pm 0.076 \, mM$
G18	$0.3 \pm 1.7 \, \mu M$	$1.18 \pm 0.045 \, mM$

The values for [P] in Table 4.1 provide an independent measurement of protein concentration. We observe nevertheless that the values are consistent with the values obtained using both the Bradford assay and UV absorption methods (see Sections 2.12 and 3.3.1).
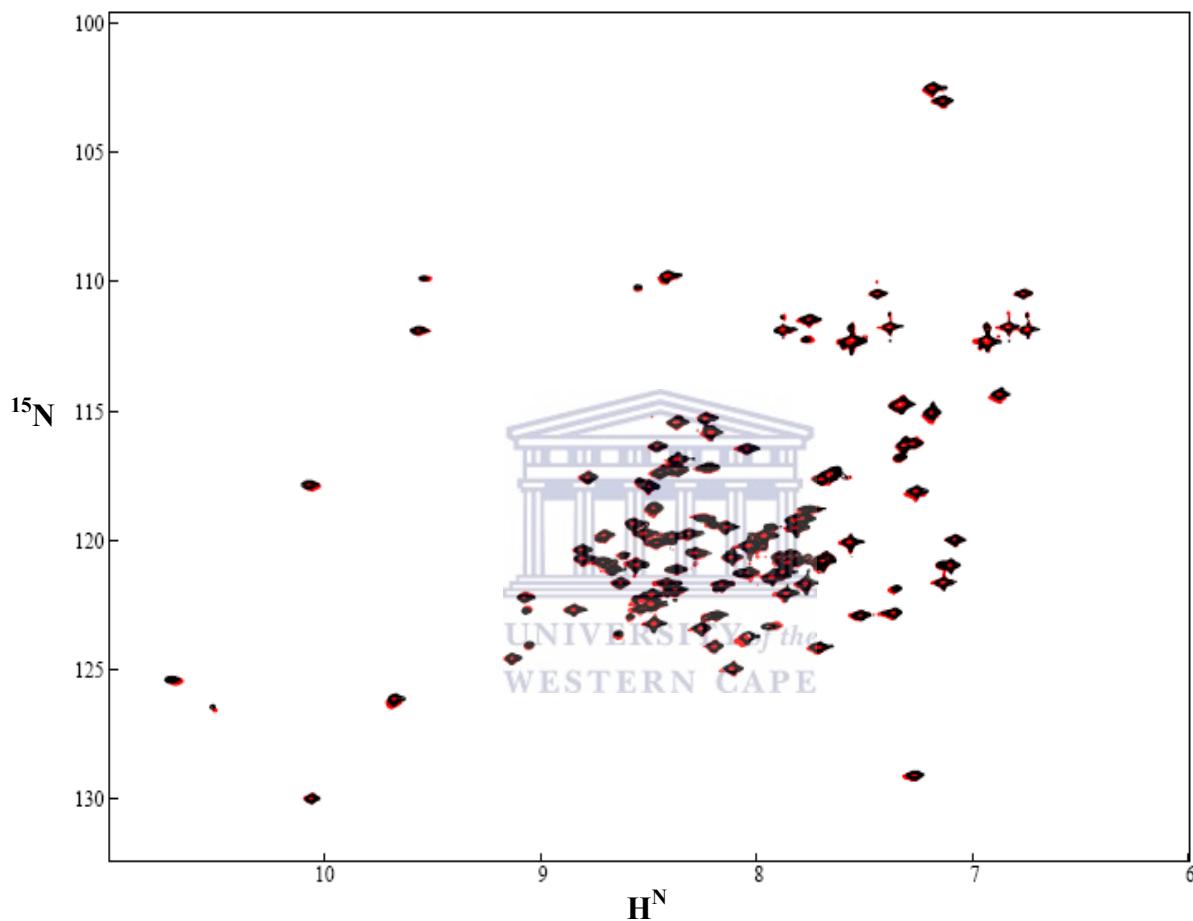
Fig. 4.4: Overlay ^{15}N-HSQC spectra of 1.2 mM un-liganded spectra of endozepine (red) and endozepine fully saturated with 2 mM C_2-ceramide (black). The non-shifting of endozepine resonances when saturated with C_2-ceramide indicates that endozepine does not interact directly with C_2-ceramide.

4.3 Interaction of C2-ceramide and C16-ceramide with endozepine

The binding analysis in the previous section suggests that strong binding occurred between endozepine and palmitoyl-CoA. Similar studies carried out using C_2-ceramide (Fig. 4.5) and C_{16}-ceramide (data not shown) produced no changes to the ^{15}N-HSQC spectra of endozepine. We conclude from this that C_2-ceramide and C_{16}-ceramide do not interact directly with endozepine.

Chapter 5: Investigation of the site of binding of palmitoyl-CoA to endozepine using heteronuclear NMR

5.1 Sequential assignment of Cα and Cβ backbone resonances using CBCA(CO)NH and HNCACB experiments

In the previous chapter we showed that the binding of palmitoyl-CoA to endozepine led to perturbations of many resonances in the ^{15}N-HSQC spectrum of endozepine. These correspond to backbone amide groups that are likely to be in close proximity to the binding site of palmitoyl-CoA. In order to identify the position of the binding site, we need to identify the residues to which the resonances correspond. These can then be mapped onto a molecular model of endozepine, generated on the basis of its homology to other members of the ACBP family. To correlate the signals with the endozepine amino acid sequence and thus obtain sequence specific information, ^{15}N-HSQC has to be assigned. Backbone resonance assignments were carried out using the "sequence guided" strategy (Wüthrich 1986).

This section describes the use of triple resonance coherence transfer experiments to sequentially assign the backbone NH groups of endozepine. In effect this means assigning a residue number to each resonance in the ^{15}N-HSQC spectrum shown in Fig. 3.11. The process is known as "sequential assignment" in that it establishes the resonance corresponding to a particular amino acid and the resonance corresponding to the preceding amino acid. By joining together the resulting pairs of amino acids it is possible to complete the entire chain. The experiments are known as "triple resonance" because they involve the manipulation of the magnetic states of proton (^{1}H),

nitrogen (^{15}N) and carbon (^{13}C) nuclei simultaneously in order to transfer magnetic energy from one amino acid to the preceding one. This requires the use of spectrometer probes simultaneously tuned to 600 MHz, 60 MHz and 150 MHz, so called "triple resonance" (or HCN) probes. They also require proton samples enriched with ^{13}C as well as ^{15}N.

Various triple resonance experiments offer alternative ways of establishing sequential backbone connectivity. In CBCA(CO)NH and HNCACB experiments, the start point is a large proton magnetization of the H^{N} proton. The signal is then transferred to the nitrogen nuclei and then either to the C$_\alpha$ and C$_\beta$ nuclei of the same residue, referred to here as the "in-residue" i or to the C$_\alpha$ and C$_\beta$ of the preceding residue i-1. During the first evolution period, t_1, the signal is frequency modulated by the precession frequency of the C$_\alpha$ and C$_\beta$ nuclei. During the second evolution period, t_2, the signal is transferred back to the nitrogen nucleus and frequency modulated by the precession frequency of the ^{15}N nucleus. The signal is subsequently transferred back to the H^{N} proton and modulated by the precession frequency of the amide proton during the acquisition time, t_3. Fourier transformation of the data results in a three dimensional spectrum in which the ω_1 dimension corresponds to the ^{13}C chemical shifts, the ω_2 dimension corresponds to the ^{15}N chemical shifts and the ω_3 dimension corresponds to the H^{N} chemical shifts.

The magnetization transfer pathways of the CBCA(CO)NH and HNCACB experiments are shown in Fig. 5.1. They differ in the sense that in the CBCA(CO)NH experiment the transfer of signal from the C$_\alpha$ and C$_\beta$ is forced to go via the CO group and then onto the N

CBCA(CO)NH
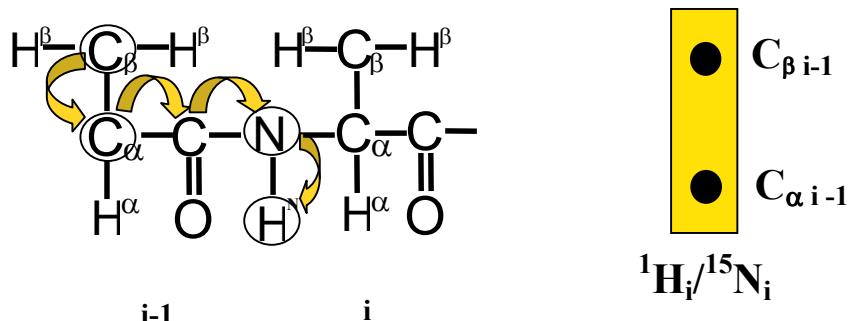
HNCACB
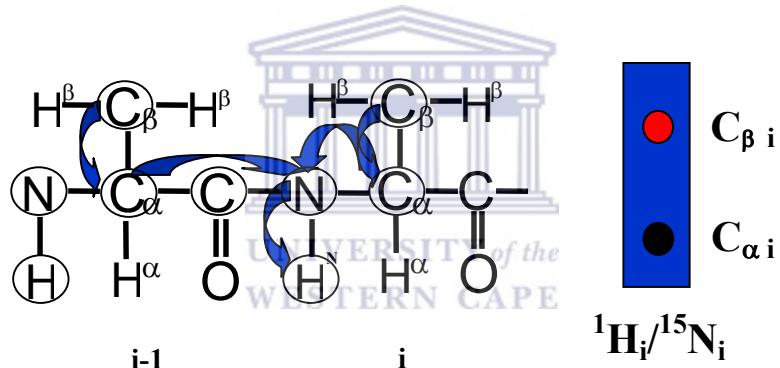
Fig. 5.1: Coherence transfer in CBCA(CO)NH and HNCACB experiments for a pair of consecutive residues. In the CBCA(CO)NH, magnetic energy is transferred from the C_β to the C_α of the preceding residue to the N and H^N proton of the in-residue through the CO group of the preceding residue. In the HNCACB experiment magnetic energy is transferred from the C_β and C_α of both the preceding and in-residue to the N and H^N proton of both the preceding and in-residue. The carbon shifts (C_β and C_α) of the preceding residue is generally weaker in the HNCACB and normally of the opposite phase, shown in red.

and H^N of the following residue. In order words, the N and H^N of residue i are correlated with the C_α and C_β of residue i-1, the preceding residue. However, the precession frequency of the CO nuclei is not allowed to modulate the signal, which is why the "CO" is written in brackets in "CBCA(CO)NH". In the HNCACB experiment, the transfer of signals from the C_α and C_β nuclei does not go through the CO group but instead is transferred directly to the HN group of the same residue. In other words, the H^N and N of residue i are correlated with the C_α and C_β of residue i. In addition the HNCACB may also yield correlations to C_α and C_β of residue i-1, but these signals are generally weaker compared to signals from the "in-residue" carbons, residue i. A combination of the CBCA(CO)NH and HNCACB experiments can be used to identify C_α and C_β of both the preceding residue and the in-residue and makes it possible to identify the backbone C_α and C_β chemical shifts of residues along the amino acid main chain. HNCO and HN(CA)CO experiments are very similar to the CBCA(CO)NH and HNCACB respectively, except that the H^N and N of residue i are correlated with the CO chemical shift of residue i-1, in the case of HNCO, and residue i, in the case of HN(CA)CO. The advantage of CBCA(CO)NH and HNCACB experiments is that they provide two frequencies (C_α and C_β) to match successive residues, rather than just one and thereby reduce ambiguity in the assignment process.

Many triple resonance experiments are built on the ^1H, ^{15}N-HSQC spectrum in the sense that the H^N and N of residue i are correlated with a third nucleus in the 3rd frequency dimension. Projecting the 3-dimensional spectrum along the 3rd dimension gives rise to a

2-dimensional spectrum, which is essentially the ^{15}N-HSQC spectrum of the protein. The HNCO spectrum is similar to the ^{15}N-HSQC spectrum, except that in the HNCO spectrum the resonances are spread out into the 3rd dimension by the ^{13}C chemical shifts of the attached CO, thereby reducing the amount of overlap. The resulting peaklist has coordinates (δ^1H, δ^{15}N and δ^{13}C), of which only the δ^1H and δ^{15}N values are used to split the CBCA(CO)NH and HNCACB. A two-dimensional strip plot was generated from the CBCA(CO)NH and HNCACB spectra by extracting tubes centered on each HN resonance and extending across the full ^{13}C spectral width. Two dimensional strip plots were generated using a peaklist picked from a HNCO spectrum. The tubes were reduced to two-dimensional strips by taking cross sections through the tubes in either the ^{1}H or the ^{15}N dimensions. Fig. 5.2 shows a "double strip plot", generated by interlinking strips from the CBCA(CO)NH (gold) with strips from the HNCACB (blue). In the HNCACB spectrum, correlations from the β carbon (shown in red) can be distinguished from those of α carbons (shown in black) since they are of the opposite phase. The gold coloured strips contain peaks that correspond to the C$_\alpha$ and C$_\beta$ resonances of the preceding residue (i-1) and the blue coloured strips contain the C$_\alpha$ and C$_\beta$ resonances of the in-residue (i). The black arrows correspond to C$_\alpha$ and C$_\beta$ resonances of residue i while the green arrows correspond to C$_\alpha$ and C$_\beta$ resonances of residue i-1. The C$_\alpha$ and C$_\beta$ resonances in the HNCACB spectrum which has no corresponding resonances in the CBCA(CO)NH spectrum, with reference to identical residues, corresponds to C$_\alpha$ and C$_\beta$ resonances of the in-residue i (see Fig. 5.2). To link the assigned C$_\alpha$ and C$_\beta$ resonances to
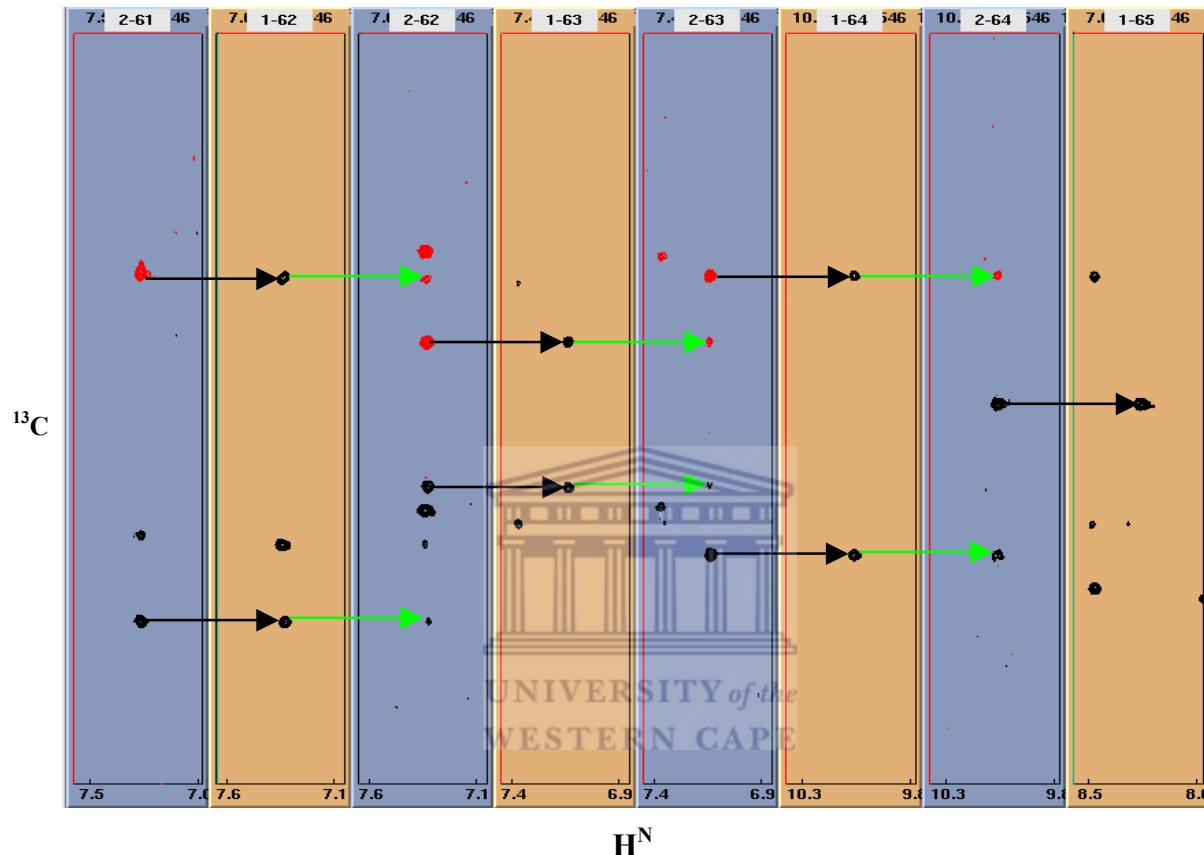
Fig. 5.2: Strip chart showing the backbone sequential connectivities of residues 61-64 of endozepine. The golden coloured strips were taken from CBCA(CO)NH spectrum while the blue coloured strips were taken from HNCACB spectrum. Black arrows indicate transfer of magnetic energy from C_α or C_β resonance to adjacent H-N groups of the in-residues, while green arrow indicate transfer of magnetic energy from the C_α or C_β resonance to adjacent H-N groups of the preceding residue, allowing sequential relationships to be established.

specific amino acid residues, the ^{13}C chemical shift values obtained were compared with the chemical shift references shown in Fig. 5.3. The strategy involved looking for sets of C_α and C_β shifts characteristic for particular amino acids. Alanines have very high C_β resonances (low ppm values). Serines and threonines are the only amino acids in which the C_β is below the C_α resonance. Prolines do not appear in the HNCACB because they do not have an "in-residue" HN group. However they do appear in the CBCA(CO)NH and are easily spotted due to their high C_β and low C_α. Glycine is the only residue having no C_β resonance. Identification of individual resonances using carbon chemical shifts as described above, combined with the knowledge of the amino acid sequence and sequential connectivities was sufficient to allow us to assign majority of the resonances on the ^{15}N-HSQC. Assignments were validated by comparing side-chain proton chemical shifts with the expected pattern for each residue, as shown in Fig. 5.3(B). The chemical shift of the side chain protons were obtained using H(CCO)NH and ^{15}N-HSQC-TOCSY spectra, which were used to correlate the HN and N of residue i with the side-chain protons of residue i-1 and residue i respectively.

In the case of the H(CCO)NH the magnetic energy is transferred from side chain protons to the attached carbon and then down the side chain to the H^N using the strong C-C scalar couplings, whereas in the ^{15}N-HSQC-TOCSY the magnetization is transferred via the weaker 3 bond H-H couplings. The H(CCO)NH is therefore a triple resonance experiment and requires a double-labelled sample, whereas the ^{15}N-HSQC-TOCSY requires only a ^{15}N-labelled sample.
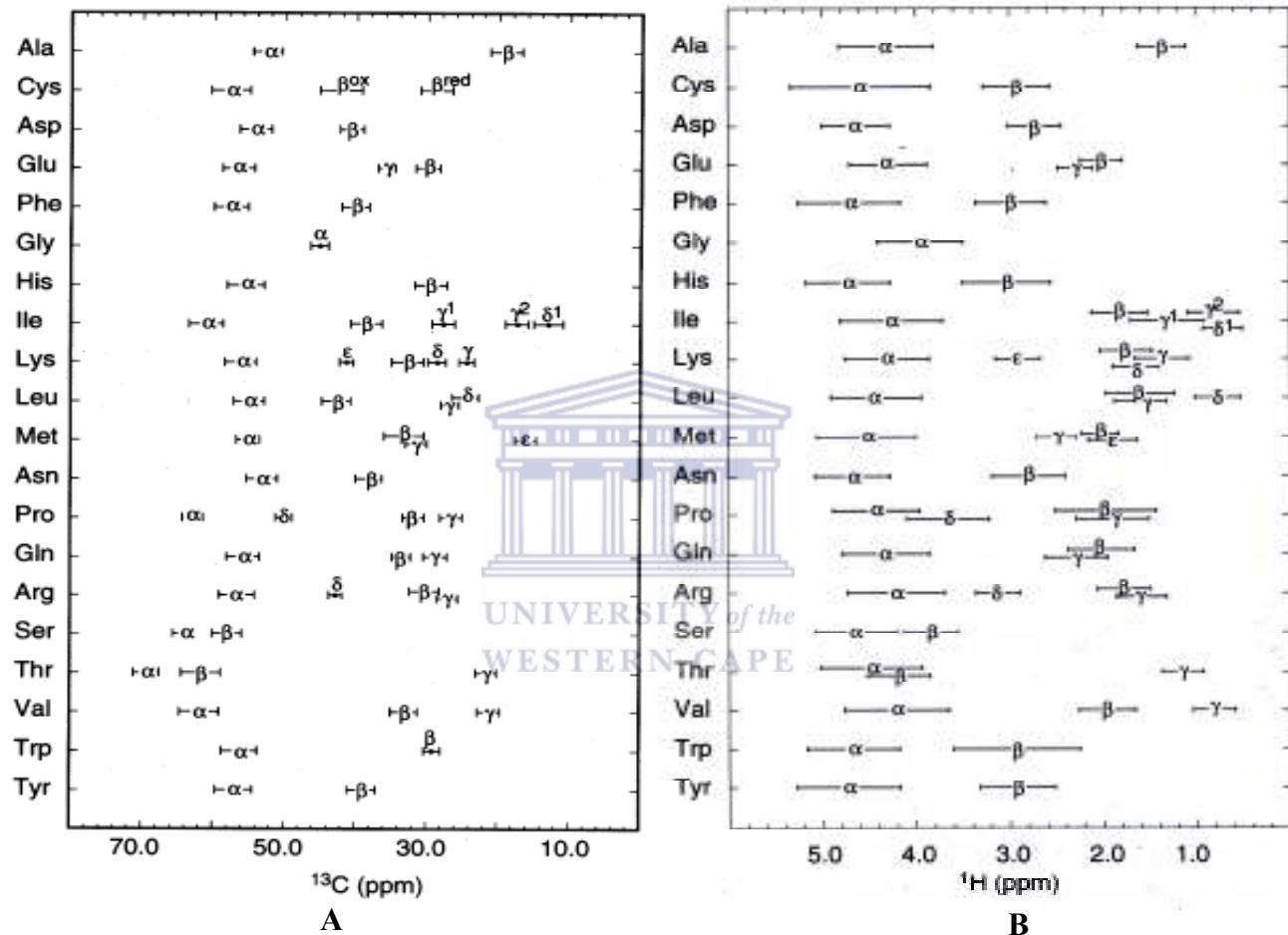
Fig. 5.3:(A) Average C$_\alpha$ and C$_\beta$ chemical shifts for all 20 commonly occurring residues. **(B)** Aliphatic side chain amide ^{1}H chemical shifts. These values were calculated using database of 13 proteins (Cavanagh 1996).
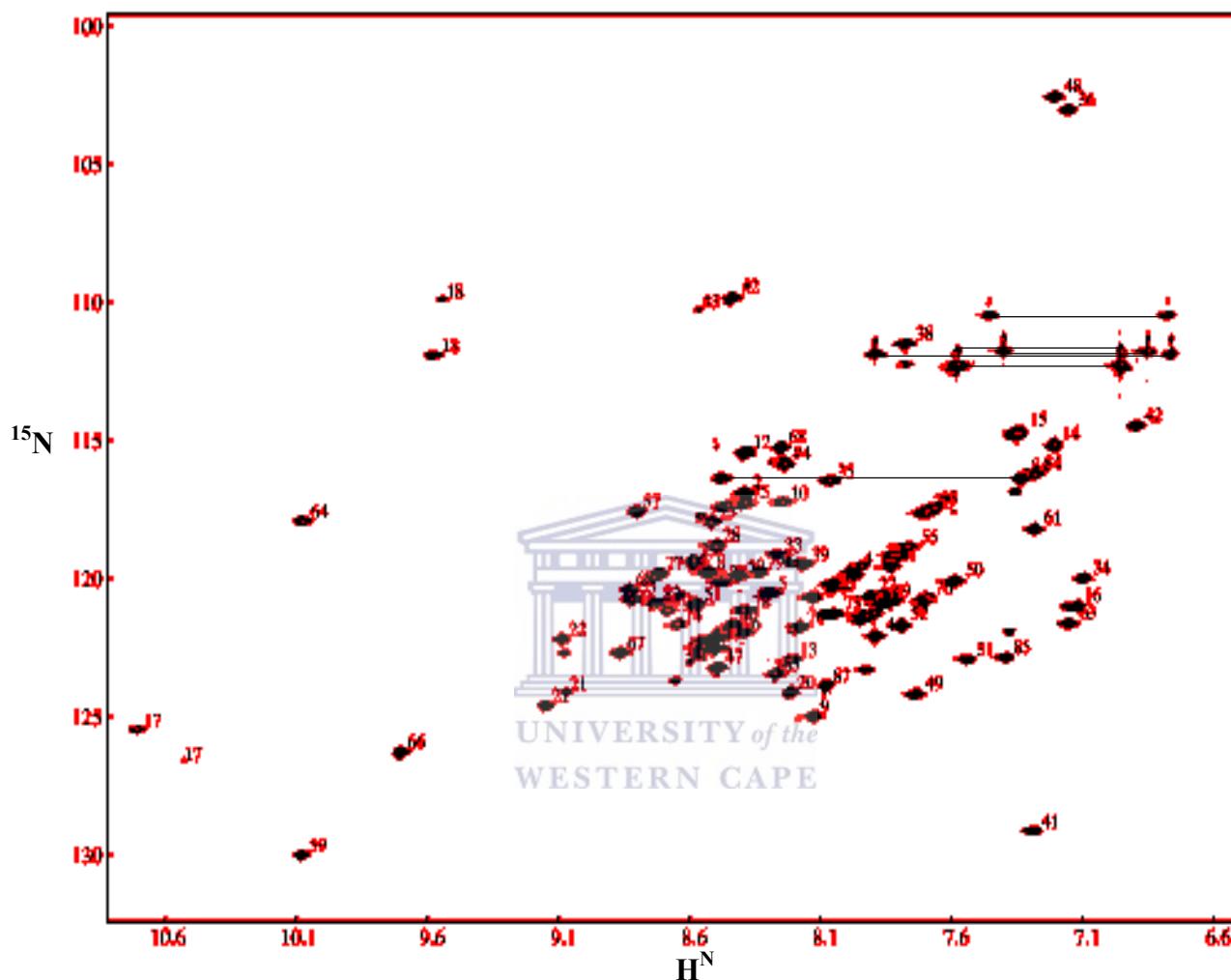
Fig. 5.4: ^{15}N-HSQC spectrum of endozepine recorded at pH 6.0, 25 ºC, 600 MHz. Each assigned peak is labelled with the corresponding residue number using a numbering system in which residues were numbered only from the initiation methionine (see Section 2.4). Six out of the seven expected NH$_2$ group side chains have been joined using horizontal lines. The final NH$_2$ group side chain, which is in the vicinity of 6ppm, is not shown. Residues indicated by " # " correspond to artifactual residues that precede the initiation methionine.

Table 5.1 Unassigned endozepine residues

A11
L26
Y29
S30
V20
Y32

Table 5.1 shows a list of residues whose resonances were not assigned. Resonances corresponding to these residues appeared to have experienced exchange broadening.

Using the above procedures we have managed to assign the backbone resonances of 82 of the 87 residues in endozepine (excluding the five artifactual at the N-terminus). An assigned ^{15}N-HSQC spectrum is shown in Fig. 5.4. Table 5.1 contains a list of residues whose corresponding resonances appeared to be 'missing' and therefore not assigned.

The five residues that we did not manage to assign appeared to be missing from the ^{15}N-HSQC, rather than it being a problem of overlap or ambiguity. Given that all of the residues are in the acyl-CoA binding pocket (Fig 5.9(A)), the most likely explanation is that they have low intensities due to broadening caused by on-off interactions with endogenous acyl-CoA-like molecules in *E. coli*.
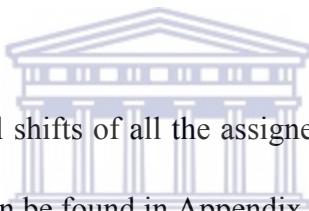
The HN, N, C$_\alpha$ and C$_\beta$ chemical shifts of all the assigned atoms were extracted from the spectra using NMRView, and can be found in Appendix III.

5.2 Endozepine model building and the mapping of the binding site to palmitoyl-CoA

5.2.1 Endozepine model building and evaluation

To gain insights into the site of binding of palmitoyl-CoA to endozepine, a model of endozepine was generated based on its homology to members of the ACBP family. Templates used for the model building were identified using mGenTHREADER (Jones *et al.* 1999). The template structures were the ACBP from *M. bovis* (PDB accession 2ABD) and *P. falciparum* (PDB accession 1HBK), with sequence identities of 52.3 and 29.2 % to endozepine respectively. An alignment of all three sequences is shown in Fig. 5.6. Model

Conf: ⊐■■■□■■■■■■■■■■■■■□■■■■■■■■■■■■■■■■■□⊏
Pred: ━━⬤▬▬▬▬▬▬▬⬤━━━━⬤▬▬▬▬▬▬▬▬
Pred: CCCHHHHHHHHHHHHHHHHHCCCCCCHHHHHHHHHHHHHH
  AA: GPLGSMSQVEFEMACASLKQLKGPVSDQEKLLVYSFYKQA
          10   20   30   40

Conf: ⊐□■■■■■■■■□□■■■■■■■■■■■□■■■■■■■■■■⊏
Pred: ▬━━━━━━━⬤▬▬▬▬⬤▬▬▬▬
Pred: HCCCCCCCCCCCCHHHHHHHHHHHHHCCCCHHHHHHHHH
  AA: TQGDCNIPVPPATDVRAKAKYEAWMVNKGMSKMDAMRIYI
          50   60   70   80

Conf: ⊐■■■■■□□□■■■⊏
Pred: ▬▬▬▬▬━━
Pred: HHHHHHHHHCCC
  AA: AKVEELKKKEPC
          90

Legend:
⬤▬▬▬▬▬ = helix   Conf: ⊐□■□⊏ = confidence of prediction

⇨ = strand   Pred: predicted secondary structure

──────── = coil   AA: target sequence

Fig. 5.5: The predicted secondary structure of endozepine generated using PSIPRED (McGuffin *et al.* 2000). This image was employed as a guide during the target-template alignment process to ensure that insertions or deletion were not introduced in the regions predicted to contain secondary structure elements in endozepine. This image suggests that endozepine is expected to contain only alpha helices and loop regions.
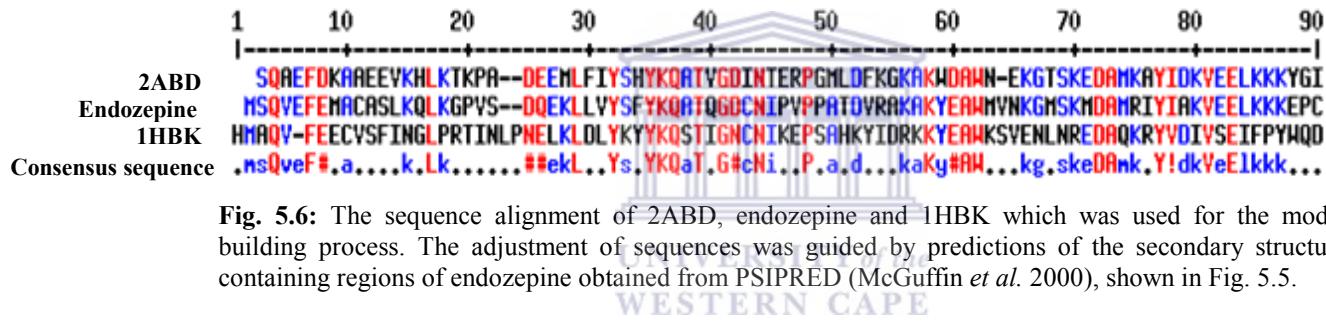
Fig. 5.6: The sequence alignment of 2ABD, endozepine and 1HBK which was used for the model building process. The adjustment of sequences was guided by predictions of the secondary structure containing regions of endozepine obtained from PSIPRED (McGuffin *et al.* 2000), shown in Fig. 5.5.

building was carried out in MODELLER (Sali and Blundell 1993). Structural alignment of the three sequences was generated, based on the sequences and on comparison of the secondary structures. The secondary structure of endozepine (see Fig 5.5) was generated using PSIPRED (McGuffin *et al.* 2000). Atom-atom distances and torsion angles were extracted from the template structures and used to construct into a Probability Density Function (PDF) for endozepine. Finally, an optimization procedure was used to find the structures with the smallest deviation from the PDF. A cartoon representation of the backbone structure of the final structure is shown in Fig. 5.7. As expected it is a 4-helix bundle, consistent with the template structures.

The final model was evaluated using RAMPAGE (Lovell *et al.* 2003), to check for possible errors in protein stereochemistry. A Ramachandran plot obtained from the model (see Fig. 5.8) showed that 98 % of the residues were in the sterically favoured regions, 2 % were in the sterically allowed regions and none were in the disallowed regions.

5.2.2 Mapping of the binding site of palmitoyl-CoA to endozepine

To gain insight into the spatial arrangement of the endozepine residues identified as being involved in the binding to palmitoyl-CoA (see Table 5.2), we mapped the identified residues onto the model, as shown in Fig. 5.9(A). The identified residues, which titrated on addition of palmitoyl-CoA, have been highlighted red in Fig. 5.9(A). In addition, the residues that appeared to be 'missing'(Table 5.1) have also been mapped onto the model and have been highlighted green (Fig. 5.9(A)). We note that both sets of residues cluster
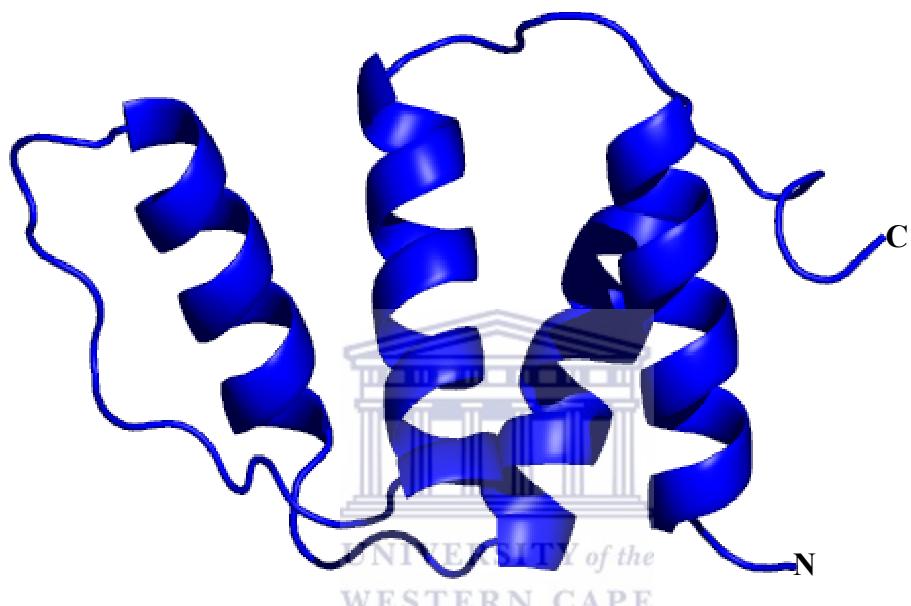
Fig. 5.7: A cartoon representation of the model of endozepine generated using MODELLER (Sali and Blundell 1993). The model suggests that endozepine is expected to contain 4 alpha helices, consistent with the PSIPRED (McGuffin *et al.* 2000) predictions (Fig. 5.6) and the solved ACBP structures. This figure was generated using PYMOL Molecular Graphics System (2003) Delano Scientific, San Carlos, CA, USA.
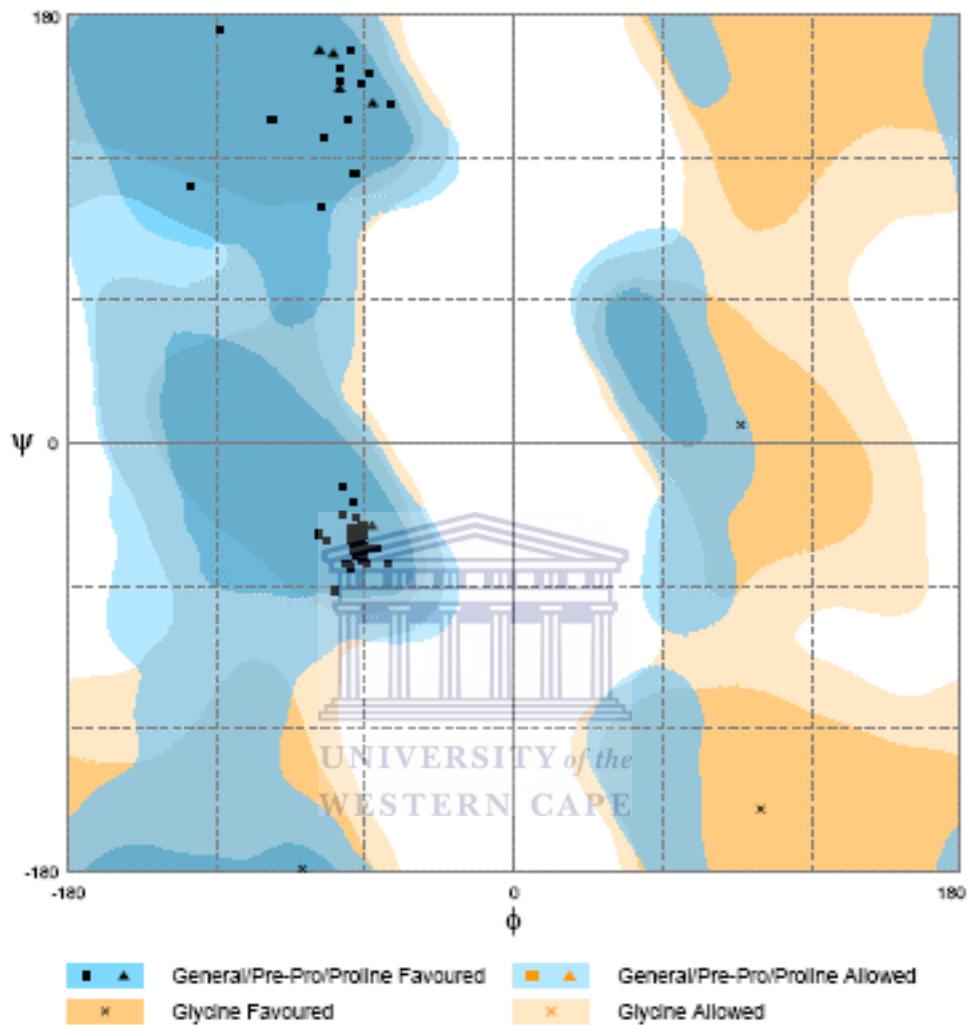
Fig. 5.8: The Ramachandran plot of the final endozepine model generated using RAMPAGE (Lovell *et al.* 2003). The area shaded blue represent the allowed and favoured regions on the plot. 98 % of our residues were predicted to be within the favoured region while 2 % of our residues were predicted to be within the allowed region. No residues were observed within the disallowed regions of the plot. The glycines have been represented by asterisks while the prolines have been represented by triangles. The plot is evidence that our model is reliable.

Table 5.2: Identified binding residues of Endozepine

K14
Q15
K17
G18
V20
D22
Q23
K25

Table 5.2 shows a list of endozepine residues which have been identified to be involved in binding to palmitoyl-CoA. These residues have been mapped (coloured red) onto the model of endozepine shown in Fig. 5.9 A
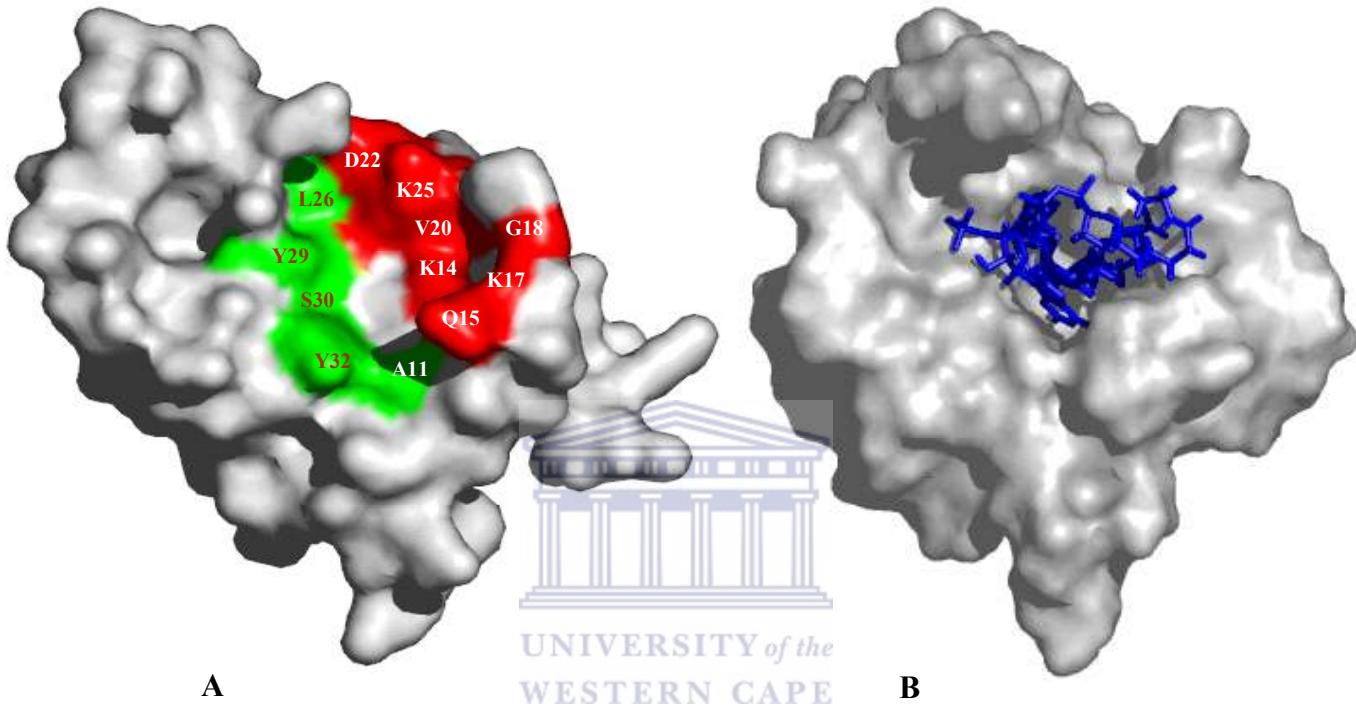
Fig. 5.9(A): Surface representation of the endozepine model generated using MODELLER (Sali and Blundell 1993), containing the identified binding residues (red patch) and the residues with no corresponding resonances ("missing" resonances) green patch. The image shows that the residues with no corresponding resonances and the binding residues converge into a pocket, which is consistent with the binding pocket of ACBP as can be seen in B. **(B)** Surface representation of ACBP structure (Kragelund *et al.* 1993), showing the binding pocket containing palmitoyl-CoA. These figures were generated using PYMOL Molecular Graphics System (2003) Delano Scientific, San Carlos, CA, USA.

into a pocket consistent with the ACBP binding pocket as shown in Fig. 5.9(B). This supports our hypothesis that the unassigned residues are not visible because they have low intensities due to broadening, possibly caused by on-off interactions with endogenous acyl-CoA-like molecules in *E. coli*.

Chapter 6: Summary and conclusions

6.1 Introduction

The main goal of the research described in this thesis was to investigate the role of endozepine in C_2-ceramide cell death signalling. We have investigated a model developed from studies, which showed that a 90 % reduction in endozepine expression correlated with the resistance to C_2-ceramide death signalling in CHO22 cells. We investigated two hypotheses for the involvement of endozepine with ceramide. The first is that endozepine contributes to apoptosis through the transport of palmitoyl-CoA, a substrate required for the *de novo* synthesis of ceramide. The second hypothesis is that endozepine interacts directly with ceramide, leading to interaction with the PBR and a subsequent opening of the mitochondria permeability transition pore, leading to apoptosis. The approach adopted involved using heteronuclear NMR to probe interaction between endozepine on the one hand, and C_2-ceramide, C_{16}-ceramide or palmitoyl-CoA on the other.

6.2 Recombinant expression and purification of endozepine

Endozepine was expressed as a GST fusion protein using the pGEX-6P-2 gene fusion system. Protein purification was carried out using a combination of affinity, anion exchange and size exclusion chromatography yielding samples in the range of 1 mM. ^{15}N-enriched and ^{15}N, ^{13}C-enriched samples for heteronuclear NMR were expressed in minimal media containing $^{15}NH_4Cl$ and ^{13}C-glucose as the sole nitrogen and carbon sources respectively.

6.3 Investigation of the binding of endozepine to palmitoyl-CoA, C16-ceramide and C2-ceramide and endozepine backbone assignment

NMR-based binding studies were carried out using ^{15}N-enriched samples of endozepine. ^{15}N-HSQC NMR spectra were used to monitor interactions between endozepine and palmitoyl-CoA, C_2-ceramide and C_{16}-ceramide respectively. Strong binding was observed between endozepine and palmitoyl-CoA while no significant binding was observed between endozepine and C_2-ceramide, or between endozepine and C_{16}-ceramide. Sequential assignment of the backbone resonances of endozepine were carried out using a combination of CBCA(CO)NH and HNCACB triple resonance experiments. A total of 82 out of 85 residues were successfully assigned. Backbone chemical shifts were extracted and can be found in Appendix II.

6.4 Endozepine model building

Using MODELLER, a 3-dimensional model of endozepine was generated based on its homology to ACBP from *M. bovis* and *P. falciparum*. As expected, the modelled structure is a four-helix bundle, consistent with the template structures. Evaluation of the model was carried out using RAMPAGE to check for possible errors in protein stereochemistry. 98 % of the residues fell within structurally favoured regions, and the remaining 2 % fell within allowed regions, indicating that the model is a good representation of the true structure of endozepine.

6.5 Mapping of experimentally identified residues onto the model

The assigned residues, which titrated on addition of palmitoyl-CoA to endozepine sample

were mapped onto the generated model of endozepine, and have been highlighted in red as shown in Fig. 5.9(A). The residues that we could not assign were also mapped onto the model, and have been highlighted green as shown in Fig. 5.9(A). We observe that the binding residues and the unassigned residues (residues that appeared to be "missing"), all clustered in a pocket, consistent with the ACBP binding pocket as can be seen in Fig. 5.9(B).

6.5 Conclusion

Our results show that endozepine does not interact directly with C_2 or C_{16}-ceramide. However, we have shown that endozepine binds very strongly to palmitoyl-CoA. Our results suggest that endozepine serves as a transport molecule for acyl-CoA esters. This lends support to our first hypothesis that endozepine is required for the *de novo* synthesis of ceramide. We observe though that ceramide synthesis occurs in the endoplasmic reticulum while endozepine is mostly expressed in the mitochondrion. It is possible therefore that endozepine functions in the *de novo* synthesis of ceramide only upon its release from the mitochondria, in response to death inducing signals and may therefore play a role in amplifying death inducing signals.

Future work will focus on the engineering of non-binding mutant proteins for re-introduction into the mutant CHO22 cells to determine whether the transduced mutant protein will sensitize the mutant CHO22 cells to undergo apoptosis in response to ceramide death signalling. Additionally, we hope to design siRNA constructs that will

target this gene and compare the results to the effects observed in the promoter-trapped mutant.

References

Alvarez-Vasquez F, Sims KJ, Cowart LA, Okamoto Y, Voit EO, Hannun YA (2005) Simulation and validation of modelled sphingolipid metabolism in Saccharomyces cerevisiae. *Nature* **433**, 425-30.

Andersen KV, Poulsen FM (1992) Three-dimensional structure in solution of acyl-coenzyme A binding protein from bovine liver. *J Mol Biol* **226**, 1131-41.

Birbes H, El Bawab S, Hannun YA, Obeid LM (2001) Selective hydrolysis of a mitochondrial pool of sphingomyelin induces apoptosis. *Faseb J* **15**, 2669-79.

Bovolin P, Schlichting J, Miyata M, Ferrarese C, Guidotti A, Alho H (1990) Distribution and characterization of diazepam binding inhibitor (DBI) in peripheral tissues of rat. *Regul Pept* **29**, 267-81.

Bradford MM (1976) A rapid and sensitive method for the quantitation of microgram quantities of protein utilizing the principle of protein-dye binding. *Anal Biochem* **72**, 248-54.

Burgi B, Lichtensteiger W, Lauber ME, Schlumpf M (1999) Ontogeny of diazepam binding inhibitor/acyl-CoA binding protein mRNA and peripheral benzodiazepine receptor mRNA expression in the rat. *J Neuroendocrinol* **11**, 85-100.

Casellas P, Galiegue S, Basile AS (2002) Peripheral benzodiazepine receptors and mitochondrial function. *Neurochem Int* **40**, 475-86.

Cavanagh J (1996) 'Protein NMR spectroscopy : principles and practice.' (Academic Press: San Diego)

Chye ML (1998) Arabidopsis cDNA encoding a membrane-associated protein with an acyl-CoA binding domain. *Plant Mol Biol* **38**, 827-38.

Chye ML, Huang BQ, Zee SY (1999) Isolation of a gene encoding Arabidopsis membrane-associated acyl-CoA binding protein and immunolocalization of its gene product. *Plant J* **18**, 205-14.

Chye ML, Li HY, Yung MH (2000) Single amino acid substitutions at the acyl-CoA-binding domain interrupt 14[C]palmitoyl-CoA binding of ACBP2, an Arabidopsis acyl-CoA-binding protein with ankyrin repeats. *Plant Mol Biol* **44**, 711-21.

Corda S, Laplace C, Vicaut E, Duranteau J (2001) Rapid reactive oxygen species production by mitochondria in endothelial cells exposed to tumor necrosis factor-alpha is mediated by ceramide. *Am J Respir Cell Mol Biol* **24**, 762-8.

Costa E, Guidotti A (1991) Diazepam binding inhibitor (DBI): a peptide with multiple biological actions. *Life Sci* **49**, 325-44.

Daugas E, Nochy D, Ravagnan L, Loeffler M, Susin SA, Zamzami N, Kroemer G (2000) Apoptosis-inducing factor (AIF): a ubiquitous mitochondrial oxidoreductase involved in apoptosis. *FEBS Lett* **476**, 118-23.

de Jong D, Prins FA, Mason DY, Reed JC, van Ommen GB, Kluin PM (1994) Subcellular localization of the bcl-2 protein in malignant and normal lymphoid cells. *Cancer Res* **54**, 256-60.

de Thonel A, Eriksson JE (2005) Regulation of death receptors-Relevance in cancer therapies. *Toxicol Appl Pharmacol* **207**, 123-32.

Decaudin D, Castedo M, Nemati F, Beurdeley-Thomas A, De Pinieux G, Caron A, Pouillart P, Wijdenes J, Rouillard D, Kroemer G, Poupon MF (2002) Peripheral benzodiazepine receptor ligands reverse apoptosis resistance of cancer cells in vitro and in vivo. *Cancer Res* **62,** 1388-93.

Delaglio F, Grzesiek S, Vuister GW, Zhu G, Pfeifer J, Bax A (1995) NMRPipe: a multidimensional spectral processing system based on UNIX pipes. *J Biomol NMR* **6**, 277-93.

Desai K, Sullards MC, Allegood J, Wang E, Schmelz EM, Hartl M, Humpf HU, Liotta DC, Peng Q, Merrill AH, Jr (2002) Fumonisins and fumonisin analogs as inhibitors of ceramide synthase and inducers of apoptosis. *Biochim Biophys Acta* **1585,** 188-92.

Donovan M, Cotter TG (2004) Control of mitochondrial integrity by Bcl-2 family members and caspase-independent cell death. *Biochim Biophys Acta* **1644**, 133-47.

Esquenet M, Swinnen JV, Heyns W, Verhoeven G (1997) LNCaP prostatic adenocarcinoma cells derived from low and high passage numbers display divergent responses not only to androgens but also to retinoids. *J Steroid Biochem Mol Biol* **62**, 391-9.

Faergeman NJ, Feddersen S, Christiansen JK, Larsen MK, Schneiter R, Ungermann C, Mutenda K, Roepstorff P, Knudsen J (2004) Acyl-CoA-binding protein, Acb1p, is required for normal vacuole function and ceramide synthesis in Saccharomyces cerevisiae. *Biochem J* **380**, 907-18.

Faergeman NJ, Knudsen J (1997) Role of long-chain fatty acyl-CoA esters in the regulation of metabolism and in cell signalling. *Biochem J* **323 (Pt 1)**, 1-12.

Faergeman NJ, Sigurskjold BW, Kragelund BB, Andersen KV, Knudsen J (1996) Thermodynamics of ligand binding to acyl-coenzyme A binding protein studied by titration calorimetry. *Biochemistry* **35**, 14118-26.

Ferrero P, Guidotti A, Conti-Tronconi B, Costa E (1984) A brain octadecaneuropeptide generated by tryptic digestion of DBI (diazepam binding inhibitor) functions as a proconflict ligand of benzodiazepine recognition sites. *Neuropharmacology* **23**, 1359-62.

Ferri KF, Jacotot E*, et al.* (2000) Apoptosis control in syncytia induced by the HIV type 1-envelope glycoprotein complex: role of mitochondria and caspases. *J Exp Med* **192**, 1081-92.

Fonfria E, Dare E, Benelli M, Sunol C, Ceccatelli S (2002) Translocation of apoptosis-inducing factor in cerebellar granule cells exposed to neurotoxic agents inducing oxidative stress. *Eur J Neurosci* **16**, 2013-6.

Gaigg B, Neergaard TB*, et al.* (2001) Depletion of acyl-coenzyme A-binding protein affects sphingolipid synthesis and causes vesicle accumulation and membrane defects in Saccharomyces cerevisiae. *Mol Biol Cell* **12**, 1147-60.

Gavish M, Katz Y, Bar-Ami S, Weizman R (1992) Biochemical, physiological, and pathological aspects of the peripheral benzodiazepine receptor. *J Neurochem* **58**, 1589-601.

Geisbrecht BV, Zhang D, Schulz H, Gould SJ (1999) Characterization of PECI, a novel monofunctional Delta(3), Delta(2)-enoyl-CoA isomerase of mammalian peroxisomes. *J Biol Chem* **274**, 21797-803.

Gudz TI, Tserng KY, Hoppel CL (1997) Direct inhibition of mitochondrial respiratory chain complex III by cell-permeable ceramide. *J Biol Chem* **272**, 24154-8.

Guidotti A, Corda MG, Costa E (1983) Strategies for the isolation and characterization of an endogenous effector of the benzodiazepine recognition sites. *Adv Biochem Psychopharmacol* **38**, 95-103.

Guillas I, Kirchman PA, Chuard R, Pfefferli M, Jiang JC, Jazwinski SM, Conzelmann A (2001) C26-CoA-dependent ceramide synthesis of Saccharomyces cerevisiae is operated by Lag1p and Lac1p. *Embo J* **20**, 2655-65.

Hannun YA (1996) Functions of ceramide in coordinating cellular responses to stress. *Science* **274**, 1855-9.

Hannun YA, Luberto C (2000) Ceramide in the eukaryotic stress response. *Trends Cell Biol* **10**, 73-80.

Hansen HO, Andreasen PH, Mandrup S, Kristiansen K, Knudsen J (1991) Induction of acyl-CoA-binding protein and its mRNA in 3T3-L1 cells by insulin during preadipocyte-to-adipocyte differentiation. *Biochem J* **277 (Pt 2)**, 341-4.

Hegde R, Srinivasula SM*, et al.* (2002) Identification of Omi/HtrA2 as a mitochondrial apoptotic serine protease that disrupts inhibitor of apoptosis protein-caspase interaction. *J Biol Chem* **277**, 432-8.

Heinrich M, Wickel M*, et al.* (1999) Cathepsin D targeted by acid sphingomyelinase-derived ceramide. *Embo J* **18**, 5252-63.

Hirsch T, Decaudin D, Susin SA, Marchetti P, Larochette N, Resche-Rigon M, Kroemer G (1998) PK11195, a ligand of the mitochondrial benzodiazepine receptor, facilitates the induction of apoptosis and reverses Bcl-2-mediated cytoprotection. *Exp Cell Res* **241**, 426-34.

Ivell R, Pusch W, Balvers M, Valentin M, Walther N, Weinbauer G (2000) Progressive inactivation of the haploid expressed gene for the sperm-specific endozepine-like peptide (ELP) through primate evolution. *Gene* **255**, 335-45.

Johnson BA (2004) Using NMRView to visualize and analyze the NMR spectra of macromolecules. *Methods Mol Biol* **278**, 313-52.

Jones DT, Tress M, Bryson K, Hadley C (1999) Successful recognition of protein folds using threading methods biased by sequence similarity and predicted secondary structure. *Proteins* **Suppl 3**, 104-11.

Kim CN, Wang X, Huang Y, Ibrado AM, Liu L, Fang G, Bhalla K (1997) Overexpression of Bcl-X(L) inhibits Ara-C-induced mitochondrial loss of cytochrome c and other perturbations that activate the molecular cascade of apoptosis. *Cancer Res* **57**, 3115-20.

Knudsen J, Mandrup S, Rasmussen JT, Andreasen PH, Poulsen F, Kristiansen K (1993) The function of acyl-CoA-binding protein (ACBP)/diazepam binding inhibitor (DBI). *Mol Cell Biochem* **123**, 129-38.

Knudsen J, Neergaard TB, Gaigg B, Jensen MV, Hansen JK (2000) Role of acyl-CoA binding protein in acyl-CoA metabolism and acyl-CoA-mediated cell signaling. *J Nutr* **130**, 294S-298S.

Kolmer M, Pelto-Huikko M, Parvinen M, Hoog C, Alho H (1997) The transcriptional and translational control of diazepam binding inhibitor expression in rat male germ-line cells. *DNA Cell Biol* **16**, 59-72.

Koybasi S, Senkal CE, Sundararaj K, Spassieva S, Bielawski J, Osta W, Day TA, Jiang JC, Jazwinski SM, Hannun YA, Obeid LM, Ogretmen B (2004) Defects in cell growth regulation by C18:0-ceramide and longevity assurance gene 1 in human head and neck squamous cell carcinomas. *J Biol Chem* **279,** 44311-9.

Kragelund BB, Andersen KV, Madsen JC, Knudsen J, Poulsen FM (1993) Three-dimensional structure of the complex between acyl-coenzyme A binding protein and palmitoyl-coenzyme A. *J Mol Biol* **230**, 1260-77.

Kragelund BB, Knudsen J, Poulsen FM (1999a) Acyl-coenzyme A binding protein (ACBP). *Biochim Biophys Acta* **1441**, 150-61.

Kragelund BB, Poulsen K, Andersen KV, Baldursson T, Kroll JB, Neergard TB, Jepsen J, Roepstorff P, Kristiansen K, Poulsen FM, Knudsen J (1999) Conserved residues and their role in the structure, function, and stability of acyl-coenzyme A binding protein. *Biochemistry* **38,** 2386-94.

Kroesen BJ, Pettus B, Luberto C, Busman M, Sietsma H, de Leij L, Hannun YA (2001) Induction of apoptosis through B-cell receptor cross-linking occurs via de novo generated C16-ceramide and involves mitochondria. *J Biol Chem* **276**, 13606-14.

Larsson G, Martinez G, Schleucher J, Wijmenga SS (2003) Detection of nano-second internal motion and determination of overall tumbling times independent of the time scale of internal motion in proteins from NMR relaxation data. *J Biomol NMR* **27**, 291-312.

Li LY, Luo X, Wang X (2001) Endonuclease G is an apoptotic DNase when released from mitochondria. *Nature* **412**, 95-9.

Li P, Nijhawan D, Budihardjo I, Srinivasula SM, Ahmad M, Alnemri ES, Wang X (1997) Cytochrome c and dATP-dependent formation of Apaf-1/caspase-9 complex initiates an apoptotic protease cascade. *Cell* **91**, 479-89.

Liao WC, Haimovitz-Friedman A, Persaud RS, McLoughlin M, Ehleiter D, Zhang N, Gatei M, Lavin M, Kolesnick R, Fuks Z (1999) Ataxia telangiectasia-mutated gene product inhibits DNA damage-induced apoptosis via ceramide synthase. *J Biol Chem* **274,** 17908-17.

Liu B, Andrieu-Abadie N, Levade T, Zhang P, Obeid LM, Hannun YA (1998) Glutathione regulation of neutral sphingomyelinase in tumor necrosis factor-alpha-induced cell death. *J Biol Chem* **273**, 11313-20.

Lovell SC, Davis IW, Arendall WB, 3rd, de Bakker PI, Word JM, Prisant MG, Richardson JS, Richardson DC (2003) Structure validation by Calpha geometry: phi,psi and Cbeta deviation. *Proteins* **50**, 437-50.

Mandrup S, Hummel R, Ravn S, Jensen G, Andreasen PH, Gregersen N, Knudsen J, Kristiansen K (1992) Acyl-CoA-binding protein/diazepam-binding inhibitor gene and pseudogenes. A typical housekeeping gene family. *J Mol Biol* **228**, 1011-22.

Martins LM, Iaccarino I, Tenev T, Gschmeissner S, Totty NF, Lemoine NR, Savopoulos J, Gray CW, Creasy CL, Dingwall C, Downward J (2002) The serine protease Omi/HtrA2 regulates apoptosis by binding XIAP through a reaper-like motif. *J Biol Chem* **277,** 439-44.

Matsumoto S, Yoshiga T, Yokoyama N, Iwanaga M, Koshiba S, Kigawa T, Hirota H, Yokoyama S, Okano K, Mita K, Shimada T, Tatsuki S (2001) Characterization of acyl-CoA-binding protein (ACBP) in the pheromone gland of the silkworm, Bombyx mori. *Insect Biochem Mol Biol* **31,** 603-9.

McGuffin LJ, Bryson K, Jones DT (2000) The PSIPRED protein structure prediction server. *Bioinformatics* **16**, 404-5.

Melloni E, Averna M, Salamino F, Sparatore B, Minafra R, Pontremoli S (2000) Acyl-CoA-binding protein is a potent m-calpain activator. *J Biol Chem* **275**, 82-6.

Metzner M, Ruecknagel KP, Knudsen J, Kuellertz G, Mueller-Uri F, Diettrich B (2000) Isolation and characterization of two acyl-CoA-binding proteins from proembryogenic masses of Digitalis lanata Ehrh. *Planta* **210**, 683-5.

Meyer M, (2003) Identification and characterisation of the role of endozepine in apoptosis induced by ceramide. *Ph.D. thesis, University of the Western Cape, South Africa*.

Milne KG, Ferguson MA (2000) Cloning, expression, and characterization of the acyl-CoA-binding protein in African trypanosomes. *J Biol Chem* **275**, 12503-8.

Miyazawa N, Hamel E, Diksic M (1998) Assessment of the peripheral benzodiazepine receptors in human gliomas by two methods. *J Neurooncol* **38**, 19-26.

Mogensen IB, Schulenberg H, Hansen HO, Spener F, Knudsen J (1987) A novel acyl-CoA-binding protein from bovine liver. Effect on fatty acid synthesis. *Biochem J* **241**, 189-92.

Nagata S, Golstein P (1995) The Fas death factor. *Science* **267**, 1449-56.

Nietlispach D, Mott HR, Stott KM, Nielsen PR, Thiru A, Laue ED (2004) Structure determination of protein complexes by NMR. *Methods Mol Biol* **278,** 255-88.

Owens GP, Sinha AK, Sikela JM, Hahn WE (1989) Sequence and expression of the murine diazepam binding inhibitor. *Brain Res Mol Brain Res* **6**, 101-8.

Parrish J, Li L, Klotz K, Ledwich D, Wang X, Xue D (2001) Mitochondrial endonuclease G is important for apoptosis in C. elegans. *Nature* **412**, 90-4.

Patterson SD, Spahr CS, Daugas E, Susin SA, Irinopoulou T, Koehler C, Kroemer G (2000) Mass spectrometric identification of proteins released from mitochondria undergoing permeability transition. *Cell Death Differ* **7**, 137-44.

Pellecchia M, Sem DS, Wuthrich K (2002) NMR in drug discovery. *Nat Rev Drug Discov* **1**, 211-9.

Perry DK, Carton J, Shah AK, Meredith F, Uhlinger DJ, Hannun YA (2000) Serine palmitoyltransferase regulates de novo ceramide generation during etoposide-induced apoptosis. *J Biol Chem* **275**, 9078-84.

Pettus BJ, Chalfant CE, Hannun YA (2002) Ceramide in apoptosis: an overview and current perspectives. *Biochim Biophys Acta* **1585**, 114-25.

Pusch W, Balvers M, Hunt N, Ivell R (1996) A novel endozepine-like peptide (ELP) is exclusively expressed in male germ cells. *Mol Cell Endocrinol* **122**, 69-80.

Pusch W, Balvers M, Weinbauer GF, Ivell R (2000) The rat endozepine-like peptide gene is highly expressed in late haploid stages of male germ cell development. *Biol Reprod* **63**, 763-8.

Pusch W, Jahner D, Spiess AN, Ivell R (1999) Rat endozepine-like peptide (ELP): cDNA cloning, genomic organization and tissue-specific expression. *Gene* **235**, 51-7.

Rasmussen JT, Rosendal J, Knudsen J (1993) Interaction of acyl-CoA binding protein (ACBP) on processes for which acyl-CoA is a substrate, product or inhibitor. *Biochem J* **292 (Pt 3)**, 907-13.

Rehm T, Huber R, Holak TA (2002) Application of NMR in structural proteomics: screening for proteins amenable to structural analysis. *Structure (Camb)* **10**, 1613-8.

Roberts DL, Merrison W, MacFarlane M, Cohen GM (2001) The inhibitor of apoptosis protein-binding domain of Smac is not essential for its proapoptotic activity. *J Cell Biol* **153**, 221-8.

Rose TM, Schultz ER, Sasaki GC, Kolattukudy PE, Shoyab M (1994) Nucleotide sequence and genomic structure of duck acyl-CoA binding protein/diazepam-binding inhibitor: co-localization with S-acyl fatty acid synthase thioesterase. *DNA Cell Biol* **13**, 669-78.

Sabri A, Bare G, Jacques P, Jabrane A, Ongena M, Van Heugen JC, Devreese B, Thonart P (2001) Influence of moderate temperatures on myristoyl-CoA metabolism and acyl-CoA thioesterase activity in the psychrophilic antarctic yeast Rhodotorula aurantiaca. *J Biol Chem* **276**, 12691-6.

Sakahira H, Enari M, Nagata S (1998) Cleavage of CAD inhibitor in CAD activation and DNA degradation during apoptosis. *Nature* **391**, 96-9.

Sali A, Blundell TL (1993) Comparative protein modelling by satisfaction of spatial restraints. *J Mol Biol* **234**, 779-815.

Sawada M, Nakashima S, Banno Y, Yamakawa H, Takenaka K, Shinoda J, Nishimura Y, Sakai N, Nozawa Y (2000) Influence of Bax or Bcl-2 overexpression on the ceramide-dependent apoptotic pathway in glioma cells. *Oncogene* **19**, 3508-20.

Schjerling CK, Hummel R, Hansen JK, Borsting C, Mikkelsen JM, Kristiansen K, Knudsen J (1996) Disruption of the gene encoding the acyl-CoA-binding protein (ACB1) perturbs acyl-CoA metabolism in Saccharomyces cerevisiae. *J Biol Chem* **271**, 22514-21.

Schmelz EM, Dombrink-Kurtzman MA, Roberts PC, Kozutsumi Y, Kawasaki T, Merrill AH, Jr. (1998) Induction of apoptosis by fumonisin B1 in HT29 cells is mediated by the accumulation of endogenous free sphingoid bases. *Toxicol Appl Pharmacol* **148**, 252-60.

Schorling S, Vallee B, Barz WP, Riezman H, Oesterhelt D (2001) Lag1p and Lac1p are essential for the Acyl-CoA-dependent ceramide synthase reaction in Saccharomyces cerevisae. *Mol Biol Cell* **12**, 3417-27.

Schutze S, Potthoff K, Machleidt T, Berkovic D, Wiegmann K, Kronke M (1992) TNF activates NF-kappa B by phosphatidylcholine-specific phospholipase C-induced "acidic" sphingomyelin breakdown. *Cell* **71**, 765-76.

Shirra MK, Patton-Vogt J, Ulrich A, Liuta-Tehlivets O, Kohlwein SD, Henry SA, Arndt KM (2001) Inhibition of acetyl coenzyme A carboxylase activity restores expression of the INO1 gene in a snf1 mutant strain of Saccharomyces cerevisiae. *Mol Cell Biol* **21**, 5710-22.

Spiess C, Beil A, Ehrmann M (1999) A temperature-dependent switch from chaperone to protease in a widely conserved heat shock protein. *Cell* **97**, 339-47.

Suk K, Kim YH, Hwang DY, Ihm SH, Yoo HJ, Lee MS (1999) Molecular cloning and expression of a novel human cDNA related to the diazepam binding inhibitor. *Biochim Biophys Acta* **1454**, 126-31.

Susin SA, Daugas E, Ravagnan L, Samejima K, Zamzami N, Loeffler M, Costantini P, Ferri KF, Irinopoulou T, Prevost MC, Brothers G, Mak TW, Penninger J, Earnshaw WC, Kroemer G (2000) Two distinct pathways leading to nuclear apoptosis. *J Exp Med* **192,** 571-80.

Susin SA, Lorenzo HK, Zamzami N, Marzo I, Snow BE, Brothers GM, Mangion J, Jacotot E, Costantini P, Loeffler M, Larochette N, Goodlett DR, Aebersold R, Siderovski

DP, Penninger JM, Kroemer G (1999) Molecular characterization of mitochondrial apoptosis-inducing factor. *Nature* **397,** 441-6.

Vadrevu R, Falzone CJ, Matthews CR (2003) Partial NMR assignments and secondary structure mapping of the isolated alpha subunit of Escherichia coli tryptophan synthase, a 29-kD TIM barrel protein. *Protein Sci* **12**, 185-91.

Valentin M, Balvers M, Pusch W, Weinbauer GF, Knudsen J, Ivell R (2000) Structure and expression of the mouse gene encoding the endozepine-like peptide from haploid male germ cells. *Eur J Biochem* **267**, 5438-49.

van Aalten DM, Milne KG, Zou JY, Kleywegt GJ, Bergfors T, Ferguson MA, Knudsen J, Jones TA (2001) Binding site differences revealed by crystal structures of Plasmodium falciparum and bovine acyl-CoA binding protein. *J Mol Biol* **309**, 181-92.

van Gurp M, Festjens N, van Loo G, Saelens X, Vandenabeele P (2003) Mitochondrial intermembrane proteins in cell death. *Biochem Biophys Res Commun* **304**, 487-97.

Van Loo G, Demol H, van Gurp M, Hoorelbeke B, Schotte P, Beyaert R, Zhivotovsky B, Gevaert K, Declercq W, Vandekerckhove J, Vandenabeele P (2002) A matrix-assisted laser desorption ionization post-source decay (MALDI-PSD) analysis of proteins released from isolated liver mitochondria treated with recombinant truncated Bid. *Cell Death Differ* **9,** 301-8.

van Loo G, Schotte P, van Gurp M, Demol H, Hoorelbeke B, Gevaert K, Rodriguez I, Ruiz-Carrillo A, Vandekerckhove J, Declercq W, Beyaert R, Vandenabeele P (2001) Endonuclease G: a mitochondrial protein released in apoptosis and involved in caspase-independent DNA degradation. *Cell Death Differ* **8,** 1136-42.

Venturini I, Zeneroli ML, Corsi L, Avallone R, Farina F, Alho H, Baraldi C, Ferrarese C, Pecora N, Frigo M, Ardizzone G, Arrigo A, Pellicci R, Baraldi M (1998) Up-regulation of peripheral benzodiazepine receptor system in hepatocellular carcinoma. *Life Sci* **63,** 1269-80.

Verhagen AM, Ekert PG, Pakusch M, Silke J, Connolly LM, Reid GE, Moritz RL, Simpson RJ, Vaux DL (2000) Identification of DIABLO, a mammalian protein that promotes apoptosis by binding to and antagonizing IAP proteins. *Cell* **102**, 43-53.

Wang KK (2000) Calpain and caspase: can you tell the difference? *Trends Neurosci* **23**, 20-6.

Wiegmann K, Schutze S, Machleidt T, Witte D, Kronke M (1994) Functional dichotomy of neutral and acidic sphingomyelinases in tumor necrosis factor signaling. *Cell* **78**, 1005-15.

Woestenenk EA, Hammarstrom M, Hard T, Berglund H (2003) Screening methods to determine biophysical properties of proteins in structural genomics. *Anal Biochem* **318**, 71-9.

Wüthrich K (1986) 'NMR of proteins and nucleic acids.' (Wiley: New York)

Appendix I: Derivation of Equation 3, Section 2.14

At equilibrium we have that

$$K_D = \frac{[P_{free}][L_{free}]}{[PL]}$$

where $[P_{free}]$, $[L_{free}]$, $[PL]$ and K_D are free protein concentration, free ligand concentration, concentration of the bound complex and the dissociation constant, respectively. Since

$$[P_{free}] = [P_{total}] - [PL]$$

and

$$[L_{free}] = [L_{total}] - [PL]$$

where $[P_{total}]$ and $[L_{total}]$ are total protein and ligand concentrations respectively,

$$\Rightarrow K_D[PL] = ([P_{total}] - [PL])([L_{total}] - [PL])$$

$$[PL]^2 - ([P_{total}] + [L_{total}] + K_D)[PL] + [P_{total}][L_{total}] = 0$$

since this is a quadratic equation in $[PL]$, we can use the well known formular:

$$[PL] = \frac{[P_{total}] + [L_{total}] + K_D \pm \sqrt{([P_{total}] + [L_{total}] + K_D)^2 - 4[P_{total}][L_{total}]}}{2}$$

where $[P_{total}]$ is the fixed protein concentration, $[L_{total}]$ is the variable ligand concentration. The expression above has two roots, only one of which is physical. In order to determine which of the two it is, we make use of the fact that the bound fraction θ_L must be zero when $[L_{total}] = 0$ implying that the negative root is the physical root. The expression is then written as

$$\theta_L \equiv \frac{[PL]}{[P_{total}]} = \frac{[P_{total}] + [L_{total}] + K_D - \sqrt{([P_{total}] + [L_{total}] + K_D)^2 - 4[P_{total}][L_{total}]}}{2[P_{total}]}$$

Appendix II: Titration data

K17 titration data

Palmitoyl-CoA concentrations (mM) [L]	Volume of unbound resonances (V_f)	Volume of bound resonances (V_b)	Bound fraction (θ)
0	0.412	0	0
0.114	0.440	0.030	0.067
0.223	0.486	0.075	0.134
0.377	0.409	0.142	0.257
0.600	0.272	0.304	0.526
0.821	0.258	0.359	0.581
1.039	0.015	0.559	0.973
1.183	0.002	0.570	0.995
1.397	0.006	0.644	0.990
2.025	0	0.654	1.000

G18 titration data

Palmitoyl-CoA concentrations (mM) [L]	Volume of unbound resonances (V_f)	Volume of bound resonances (V_b)	Bound fraction (θ)
0	0.679	0	0
0.114	0.757	0.077	0.093
0.223	0.623	0.121	0.162
0.377	0.600	0.180	0.230
0.600	0.278	0.311	0.528
0.821	0.214	0.366	0.631
1.039	0.082	0.492	0.857
1.183	0.006	0.496	0.890
1.397	0.004	0.374	0.988
2.025	0.007	0.539	0.987

Appendix III: Endozepine chemical shifts

Residue number	Residue name	Atom name	Chemical shift
1	M	N	122.16
1	M	C_α	56.00
1	M	C_β	32.85
2	S	N	116.92
2	S	HN	8.39
2	S	C_α	59.15
2	S	C_β	64.29
3	Q	N	122.53
3	Q	HN	8.50
3	Q	C_α	58.57
3	Q	C_β	28.27
4	V	N	119.83
4	V	HN	7.98
4	V	C_α	66.00
4	V	C_β	31.99
5	E	N	120.52
5	E	HN	8.29
5	E	C_α	60.00
5	E	C_β	29.70
6	F	N	121.96
6	F	HN	8.39
7	E	N	121.14
7	E	HN	8.68
7	E	C_α	60.29
7	E	C_β	29.13
8	M	N	119.78
8	M	HN	8.53
8	M	C_α	58.86
8	M	C_β	32.56
9	A	N	124.98
9	A	HN	8.13
9	A	C_α	55.43
9	A	C_β	19.12
10	C	N	117.23
10	C	HN	8.24
11	A	C_α	54.86
11	A	C_β	17.98
12	S	N	115.46
12	S	HN	8.39
13	L	N	122.92
13	L	HN	8.20
13	L	C_α	57.43
13	L	C_β	41.14
14	K	N	115.20
14	K	HN	7.21
14	K	C_α	58.29
14	K	C_β	32.27
15	Q	N	114.71
15	Q	HN	7.34
15	Q	C_α	54.86
15	Q	C_β	29.70
16	L	N	121.01
16	L	HN	7.12

Residue number	Residue name	Atom name	Chemical shift
16	L	C_α	56.15
16	L	C_β	41.04
17	K	N	126.08
17	K	HN	6.31
17	K	C_α	55.95
17	K	C_β	34.40
18	G	N	110.91
18	G	HN	9.56
18	G	C_α	44.15
19	P	C_α	62.68
19	P	C_β	31.70
20	V	N	124.13
20	V	HN	8.21
20	V	C_α	61.72
20	V	C_β	34.28
21	S	N	124.35
21	S	HN	9.10
21	S	C_α	58.00
21	S	C_β	65.15
22	D	N	122.20
22	D	HN	9.08
22	D	C_α	58.00
22	D	C_β	39.99
23	Q	N	117.95
23	Q	HN	8.51
23	Q	C_α	59.43
23	Q	C_β	28.27
24	E	N	121.28
24	E	HN	7.90
24	E	C_α	59.43
24	E	C_β	29.98
25	K	N	119.38
25	K	HN	8.59
25	K	C_α	60.58
25	K	C_β	32.56
26	L	C_α	57.72
26	L	C_β	42.28
27	L	N	120.67
27	L	HN	7.91
27	L	C_α	58.29
27	L	C_β	42.28
28	V	N	118.83
28	V	HN	8.50
28	V	C_α	68.29
28	V	C_β	31.70
31	F	N	122.93
31	F	HN	7.54
31	F	C_α	61.72
32	Y	C_α	54.85
32	Y	C_β	40.85
33	K	N	119.13
33	K	HN	8.26
33	K	C_α	56.00
33	K	C_β	25.98

Residue number	Residue name	Atom name	Chemical shift
34	Q	N	119.99
34	Q	HN	7.10
34	Q	C_α	57.72
34	Q	C_β	22.41
35	A	N	116.47
35	A	HN	8.06
35	A	C_α	54.57
35	A	C_β	18.55
36	T	N	103.03
36	T	HN	7.15
36	T	C_α	62.00
36	T	C_β	70.58
37	Q	N	120.14
37	Q	HN	8.48
37	Q	C_α	55.43
37	Q	C_β	31.13
38	G	N	111.50
38	G	HN	7.77
38	G	C_α	44.28
39	D	N	119.49
39	D	HN	8.16
39	D	C_α	54.57
39	D	C_β	41.71
40	C	N	121.68
40	C	HN	8.43
40	C	C_α	60.29
40	C	C_β	25.41
41	N	N	129.15
41	N	HN	7.29
41	N	C_α	52.29
41	N	C_β	37.99
42	I	HN	11.33
42	I	C_α	59.43
42	I	C_β	38.28
43	P	C_α	62.00
43	P	C_β	31.99
44	V	HN	7.88
44	V	C_α	62.58
44	V	C_β	32.27
46	P	C_α	62.58
46	P	C_β	32.27
47	A	N	123.23
47	A	HN	8.49
47	A	C_α	54.57
47	A	C_β	18.55
48	T	N	102.57
48	T	HN	7.21
48	T	C_α	62.00
48	T	C_β	68.87
49	D	N	124.20
49	D	HN	7.73
49	D	C_α	52.00
49	D	C_β	39.71
50	V	N	120.10
50	V	HN	7.59

Residue number	Residue name	Atom name	Chemical shift
50	V	C_α	66.29
50	V	C_β	31.99
51	R	N	120.93
51	R	HN	8.57
51	R	C_α	58.86
51	R	C_β	29.70
52	A	N	121.71
52	A	HN	7.79
52	A	C_α	54.86
52	A	C_β	18.84
53	K	N	120.74
53	K	HN	8.82
53	K	C_α	59.72
53	K	C_β	32.27
54	A	N	121.44
54	A	HN	7.94
54	A	C_α	55.43
54	A	C_β	18.27
55	K	N	118.83
55	K	HN	7.76
55	K	C_α	60.57
55	K	C_β	33.13
56	Y	N	120.69
56	Y	HN	8.13
56	Y	C_α	61.72
56	Y	C_β	39.14
57	E	N	117.58
57	E	HN	8.80
57	E	C_α	59.43
57	E	C_β	29.42
58	A	N	120.24
58	A	HN	8.05
58	A	C_α	55.14
58	A	C_β	18.84
59	W	N	119.91
59	W	HN	8.41
59	W	C_α	58.29
59	W	C_β	30.27
59	W	NE1	130.01
59	W	HE1	10.08
60	M	N	120.40
60	M	HN	8.83
60	M	C_α	57.43
60	M	C_β	31.13
61	V	N	118.23
61	V	HN	7.28
61	V	C_α	65.72
61	V	C_β	32.27
62	N	N	114.79
62	N	HN	7.35
62	N	C_α	52.86
62	N	C_β	38.56
63	K	N	121.65
63	K	HN	7.15
63	K	C_β	32.78

Residue number	Residue name	Atom name	Chemical shift
64	G	N	117.93
64	G	HN	10.08
64	G	C_α	51.89
65	M	N	123.46
65	M	HN	8.27
65	M	C_α	55.89
65	M	C_β	35.25
66	S	N	126.28
66	S	HN	9.70
66	S	C_α	58.00
66	S	C_β	64.58
67	K	N	122.70
67	K	HN	8.86
67	K	C_α	60.87
67	K	C_β	32.27
68	M	N	115.27
68	M	HN	8.25
68	M	C_α	58.57
68	M	C_β	32.27
69	M	N	120.90
69	D	HN	7.88
69	D	C_α	57.72
69	D	C_β	39.71
70	A	N	121.75
70	A	HN	8.18
70	A	C_α	55.43
70	A	C_β	17.98
71	M	N	117.40
71	M	HN	8.46
71	M	C_α	60.00
71	M	C_β	33.70
72	R	N	117.64
72	R	HN	7.71
72	R	C_α	59.72
72	R	C_β	29.99
73	I	N	121.29
73	I	HN	8.05
73	I	C_α	64.86
73	I	C_β	38.27
74	Y	N	121.67
74	Y	HN	8.64
74	Y	C_α	63.43
74	Y	C_β	39.14
75	I	N	117.27
75	I	HN	8.40
75	I	C_α	66.00
75	I	C_β	39.42
76	A	N	120.82
76	A	HN	7.70
76	A	C_α	55.14
76	A	C_β	18.27
77	K	N	119.83
77	K	HN	8.72
77	K	C_α	57.72
77	K	C_β	30.84

Residue number	Residue name	Atom name	Chemical shift
78	Y	N	121.16
78	Y	HN	8.39
78	Y	C_α	68.00
78	Y	C_β	31.13
79	E	N	119.77
79	E	HN	8.33
79	E	C_α	59.72
79	E	C_β	29.13
80	E	C_α	59.43
80	E	C_β	29.70
81	L	N	119.57
81	L	HN	7.83
81	L	C_α	57.72
81	L	C_β	41.42
82	K	N	120.88
82	K	HN	8.73
82	K	C_α	59.43
82	K	C_β	32.27
83	K	N	117.54
83	K	HN	7.68
83	K	C_α	58.29
83	K	C_β	32.56
84	K	N	116.31
84	K	HN	7.31
84	K	C_α	56.00
84	K	C_β	32.85
85	E	N	122.86
85	E	HN	7.39
85	E	C_α	54.57
85	E	C_β	30.56
86	P	C_α	63.15
86	P	C_β	31.99
87	C	N	121.88
87	C	HN	8.07
87	C	C_α	44.28